ANISOTROPIC DIFFUSION OF NEUTRAL PARTICLES IN STOCHASTIC MEDIA

by

Richard Vasques

A dissertation submitted in partial fulfillment
of the requirements for the degree of
Doctor of Philosophy
(Applied and Interdisciplinary Mathematics)
in The University of Michigan
2009

Doctoral Committee:

Professor Charles R. Doering, Co-Chair
Professor Edward W. Larsen, Co-Chair
Professor James Paul Holloway
Professor Peter S. Smereka

To my parents, Julio and Lourdes. For everything and forever.

ACKNOWLEDGEMENTS

I must first thank Marco Túllio Vilhena, for showing me the way to the fascinating subject of transport theory. I am fortunate to have had him as a teacher; I am proud to have him as a mentor; and I am delighted to have him as a friend.

I am immensely grateful to Ed Larsen, without whom I would probably have stayed in Brazil. As my "transcontinental" co-advisor during my Masters, he encouraged me to focus on the subject of transport in stochastic media, which has been a fabulous journey. He is the reason I came to work in the United States, and in every step of the way he has shown me what a monumentally wise decision that was. His patience, kindness, and dedication were always beyond the call of duty; I will be forever indebted to him for the confidence he has put in me. I should also mention that, thanks to him, Michigan Ice Hockey has gained another fervent fan.

I am deeply thankful to Charlie Doering, who has most kindly accepted me as a student and guided me through the tortuous ways of an interdisciplinary program. I have profited enormously from his classes and from our discussions, and will be forever grateful for his willingness to help every time I needed. One can hope that the future will arrive soon for the U.S., and that he will learn to love soccer as much as he loves (american) football.

Several Professors and friends have contributed to my personal and professional achievements. Amongst them, I must give special thanks to Professors Cynthia Segatto, Ricardo Barros, Mark Thompson, Ziya Akcasu, Robert Krasny, Smadar Karni, Peter Smereka, James Holloway, and Peter Miller - all of whom went out of their way to help me at key

points of my graduate studies.

Thanks and fireworks to the fantastic staff of the Department of Mathematics, filled with the most skilled professionals one could expect. Warren, Tara, Nathalie, Doreen, Carrie, Anjie, Bert and their team played the “lifeline” role more times than I can count, and certainly more times than I deserved.

For the financial and technical support over these 4 years, many thanks are due to the Brazilian government, specifically to CAPES (Coordenação de Aperfeiçoamento de Pessoal de Nível Superior); and to the U.S. government, specifically to the Fulbright Program and the IIE (Institute of International Education).

My dearest friends and colleagues - the ones I met here and the ones back home - I am blessed for knowing all of you and for having your support. These acknowledgements would be larger than the dissertation if I tried to name all of you; I am sure you all know how important you are to me.

My parents Julio and Lourdes Vasques, my brother Alexsander, his wife Fabiane, my Godson & nephew Christopher, my sister Fernanda; I can only hope you know how much I love all of you. Distance means nothing (although it is hard to bear sometimes) - your love and support means everything. I could never see this thing through without knowing you were always there by my side.

And to my beautiful wife, Laís, who has crossed a continent to be with me, I must admit that I will never be able to repay her for all the happiness she has brought me. But I promise I will try.

TABLE OF CONTENTS

LIST OF FIGURES

Figure

LIST OF TABLES

Table

CHAPTER I

Introduction

The term *Transport Theory* applies to the mathematical description of the transport of small particles (neutrons, electrons, photons, etc.) through a background material. The development of models for particle transport problems in stochastic mixtures consisting of two (or more) materials is of particular interest; here, the term "stochastic" means that the properties of the background material in which particles travel are known only in a statistical sense. This particular branch of research, known as *Stochastic Transport Theory*, is used in a vast range of applications: atmospheric physics [20, 21, 22, 23, 49, 50, 67, 75, 78, 81, 87, 94]; astrophysics [3, 9, 17]; reactor criticality problems [59, 61, 64, 88, 89]; nuclear medicine [56, 65, 66, 68, 69, 79]; etc.

The main goal in problems of this kind is to estimate the expected value of the particle intensity in phase space, and its higher moments (such as the variance) whenever necessary. A direct way to do this is to generate a large number of physical realizations of the problem, solve each realization deterministically, and then average the solutions [1, 12, 13, 24, 44, 57, 77, 84, 85, 93]. However, most problems have an infinite number of possible physical realizations, and to obtain a solution with zero statistical error one would need to perform these calculations an infinite number of times. In practice, a large number of such calculations is necessary to obtain an accurate estimate of the ensemble-averaged

intensity. The complexity and cost of constructing different random realizations of the system and solving the transport problem for each one of them makes this an undesirably expensive method.

Different mathematical models have been developed in an attempt to accurately predict the solution of such problems; the most notable (and widely used) one being the *Atomic Mix Model* [24, 27, 44, 63, 84, 85]. The term "atomic mix" applies to mixtures of two or more materials in which the "chunks" of the materials are so small that we can assume mixing at atomic level. This notion appears to have been used in chemistry over 200 years ago, to find rules for adding partial pressures of mixtures. Maxwell [52], in his attempt to treat molecular diffusion coefficients, modeled atomic mixtures of certain ideal gases in order to compute transport coefficients.

Nuclear engineering (as a distinct discipline of engineering) dates back to the 1940's. It is reasonable to assume that physicists who knew the concept of atomic mix adopted it to model neutron transport problems. Much of the work that was done from the 1940's to the 1960's regarding particle transport in mixtures used the atomic mix approximation. The atomic mix model is a widely-used homogenization technique, and is known to be accurate when the system's spatial heterogeneities occur on a length scale which is small compared to a typical mean free path. (This assumption, however, is physically very restrictive.) Moreover, if the locations of the scattering centers in the system are uncorrelated, then it can be accurately modeled by a "homogeneous" system with volume-averaged cross sections, with a vast gain in simplicity. As it happens, the atomix mix model inherently assumes the distribution of chord lengths between scattering centers to be exponential.

However, this feature is not present when we focus on the transport of particles in "nonclassical" systems. One way in which such an environment can occur was described in [46]: consider a single "clump" of randomly-spaced (uncorrelated) scattering centers,

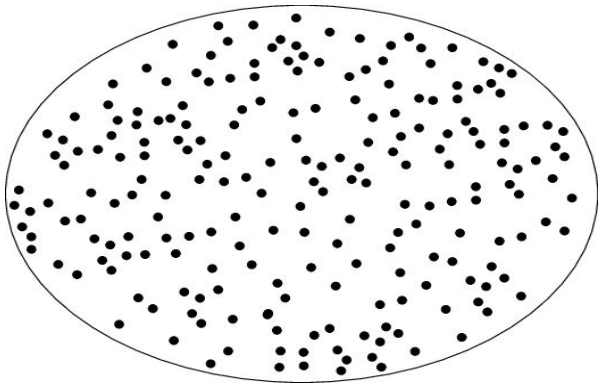

Figure 1.1: "Clump" of Randomly-Spaced (Uncorrelated) Scattering Centers

as shown in Figure 1.1. Particles in this clump will undergo many "classical" collisions before exiting. In a large system consisting of many clumps of the above type (separated by a "void"), particles leaking out of a clump will travel relatively long distances to their next collision, in a neighboring clump. Thus, relatively rare events (streaming between clumps) will significantly affect the particle transport, and the probability distribution function for distance-to-collision will *not* be exponential. In practice, the "nonclassical" system described above resembles the interior of a *Pebble-Bed Reactor* (PBR) core.

The PBR concept, which originated in Germany in the 1950's, is a graphite-moderated, helium-cooled, very-high-temperature (generation IV) reactor. Due to its highly desirable characteristics (convenient long-term waste storage, meltdown-proof passive safety, modular construction, on-line refueling, means to hydrogen production and desalination), several countries are currently addressing different possible PBR designs, such as China with the HTR-PM [92] (following the successful test reactor HTR-10 [91]), South Africa with the PBMR [36], and the United States with the MPBR [35].

The fundamental PBR design is based on the use of spherical, same-sized (60 mm diameter) fuel elements called *pebbles*. Each fuel pebble is made of pyrolytic graphite (the moderator), containing $\approx$10,000 microscopic fuel Tristructural-Isotropic (TRISO) particles. Each TRISO particle (Figure 1.2) has a diameter of $\approx$0.92 mm, and consists of a 0.5

mm kernel of fissile material (such as uranium dioxide) surrounded by porous carbon, pyrolitic carbon, and silicon carbide (SiC). The main functions of the various layers are: heat

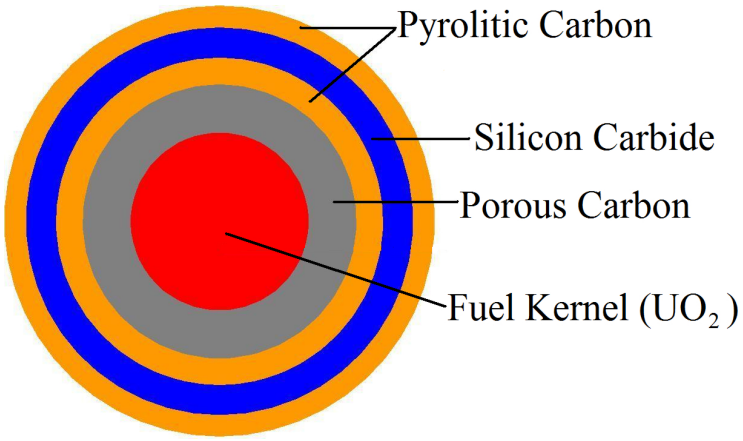

Figure 1.2: Layers of a TRISO Particle

generation in the kernel, fission product retention in the porous layer, structural integrity in both pyrolitic carbons, and fission product barrier in the SiC.

To achieve the desired reactivity, thousands of pebbles (≈500,000, varying according to the design) are piled on top of one another in a "random" manner (influenced by gravity) inside the cylindrical reactor core. They are dropped on top of this piling from charging tubes located at the top of the core, and move downward through the system in a dense granular flow. Once they reach the bottom of the core, they are discharged through another tube and examined for structure integrity and fuel content; if the burn-up target for fuel has not been reached, the pebble is re-circulated through the core. Due to this dynamic structuring, the exact locations of the pebbles inside the core at any given time are unknown. Some designs also have a dynamic central column of *moderator pebbles*, composed purely of graphite; this preserves passive safety and improves the power output. An example of such design is shown in Figure 1.3 [71].

Typically, the neutronic modeling of the geometrically "random" core is done by: (i) developing self-shielded multigroup cross sections for the pebbles, (ii) volume-averaging

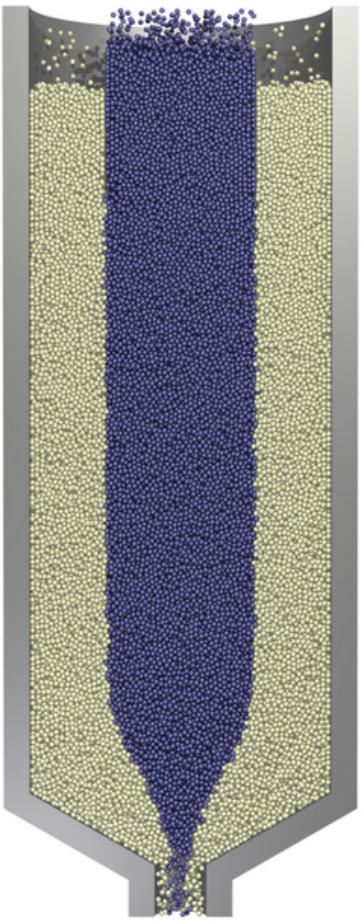

Figure 1.3: Vertical Cross Section of a PBR Core with Fuel (White) and Moderator (Blue) Pebbles

these cross sections over the entire core, including the helium-filled region between the pebbles (the *atomic mix* approximation), and (iii) introducing the spatially-homogenized cross sections into a diffusion code. This procedure leads to two questions that we consider in this work.

First, in the classic atomic mix model, the cross sections for a random heterogeneous medium are approximated by volume-averaging over the constituent materials, weighted by their respective volume fractions. This approximation is known [44, 85] to be accurate only when the chunk sizes of the constituent materials are *small* compared to a mean free path. However, the pebbles are O(1) mean free paths thick; this calls into question the validity of the atomic mix approximation. In fact, it has been observed that neutron

streaming in this type of system is strongly affected by the void spaces; to account for this effect, experimental and mathematical approaches were used to develop corrections for the diffusion coefficients obtained with atomic mix [5, 48].

The second question is related but subtly different: in a PBR core, does gravity affect the distance-to-collision in a direction-dependent (anisotropic) manner? In other words, the force of gravity (let us say it acts in the negative z direction) causes the pebbles to arrange themselves in a certain manner, which is affected by the direction of this force. If one considers a typical arrangement of pebbles in a PBR core, is the chord length probability distribution function different in the z direction than in the (x, y)-plane? If it is different, neutron transport and diffusion will be affected in a way that is not modeled.

Currently, PBR cores are modeled using a diffusion approximation with an *isotropic* diffusion tensor, in which neutrons diffuse equally in all spatial directions. However, if the chord length probability distribution function is different in the z direction than in the x and y directions, then the diffusion length in the z direction should be different than in the x and y directions, and in this case one has an anisotropic diffusion tensor. Previous research [51] has indicated that, for different 3-D crystal arrangements of a PBR core, anisotropic diffusion effects can be found; however, little is known about this effect in random structures. Moreover, although diffusion in the upper cavity of the reactor (between the top of the piling and the reflector) was addressed in previous work [29], very little has been done to formally address this issue close to the other boundaries. It stands to reason to assume that the diffusion of particles near the wall of the core will differ from the interior of the core, due to the differences in the orientations of the pebbles.

Bearing all of these issues in mind, this work extends an alternate theory for this kind of problem, first introduced by Larsen in [45]. By dropping the assumption that the scattering centers are uncorrelated, we have derived a *generalized theory* that accounts for the nonex-

ponential distribution of the distance-to-collision, and we have shown that this new theory reduces to the classic expressions under the appropriate circumstances. The basic idea behind this new theory is the use of a nonexponential ensemble-averaged probability distribution function to replace the true nonexponential probability distribution function for the distance-to-collision. To investigate the gain in accuracy, we have developed Monte Carlo simulations of both 2-D and 3-D model PBR cores, and compared the numerical results with those obtained with the diffusion approximations of both the atomic mix and the generalized theories. Overall, we find that the proposed generalized theory not only yields more accurate results than atomic mix, but it also predicts anisotropic diffusion in this kind of system - two highly desirable features.

The outline of this work is as follows:

• In Chapter II, we introduce the basic concepts needed to describe the interaction of particles with matter, and then we use particle conservation to formulate the classic linear Boltzmann equation in a nonstochastic medium. Next, we discuss the diffusion equation and several formulations that arise from it. We present a derivation of the atomic mix equation, and finish the chapter by introducing two correction models for the atomic mix diffusion coefficient.

• In Chapter III, we develop the proposed generalized theory, starting with a derivation for the generalized Boltzmann equation. We proceed to derive integral equations and a diffusion limit for this generalized theory, and to show that the resulting expressions reduce to the classic theory at the appropriate limits. We finish the chapter with a discussion about the nonexponential probability distribution function for distance-to-collision and how to obtain it.

• In Chapter IV, we consider the diffusion of particles in the interior of a model 2-D PBR core. We discuss the different packing structures (crystal and random), and

we obtain Monte Carlo estimates for both the diffusion coefficients and the k_D diffusion eigenvalue. We then compare these results with those obtained by the atomic mix model and the proposed generalized theory.

• In Chapter V, we discuss the different packing structures (crystal and random) in a model 3-D PBR core. To analyze the behavior of particles born in the interior of the core, we obtain Monte Carlo results for both the diffusion coefficients and the k_D diffusion eigenvalue. We then compare these results with those obtained by the proposed generalized theory and by the atomic mix model and its corrections. Then, we analyze the behavior of particles that are born close to a boundary, and we compare the Monte Carlo estimates for the mean square migration distances with theoretical approximations obtained with the atomic mix model and the generalized theory.

• Chapter VI presents our conclusions regarding the work developed. We discuss that the generalized theory yields results that are significantly more accurate than the ones obtained with the atomic mix approximation and its correction models. We argue that this result, as well as its ability of predicting anisotropic diffusion, makes the generalized theory a more suitable method to deal with problems of this type, even though it requires more work than atomic mix in order to be applied.

CHAPTER II

Background and Theoretical Considerations

2.1 Transport in a Known Medium

In this section, we introduce the basic concepts needed to describe the interaction of particles with matter. (We refer the reader to [15, 16, 25, 26, 40] for a more detailed description of these concepts.) We then proceed to use particle conservation to formulate the classic integro-differential transport equation in a nonstochastic medium (an example of integral formulation is also given, though we do not present its derivation here).

2.1.1 Basic Concepts

Let us consider neutral particles flowing through a background material and interacting with it. Assuming that no forces act on these particles, they will travel in a straight line at a constant speed between collisions. At any time t we use six variables to specify the position of any particle in phase space: three position variables denoted by the vector $\boldsymbol{x}$, the kinetic energy E, and a unit vector $\boldsymbol{\Omega}$, which indicates the direction in which the particle is traveling. With these variables we can define the distribution function $n(\boldsymbol{x}, E, \boldsymbol{\Omega}, t)$, such that

$$n(\boldsymbol{x}, E, \boldsymbol{\Omega}, t)dV\,dE\,d\Omega = \begin{array}{l}\text{the number of particles in a differential volume}\\ \text{element } dV \text{ at spatial point } \boldsymbol{x}\text{, with energy in } dE\\ \text{about } E\text{, traveling in a solid angle element } d\Omega\\ \text{about } \boldsymbol{\Omega}\text{, at time } t.\end{array} \tag{2.1}$$

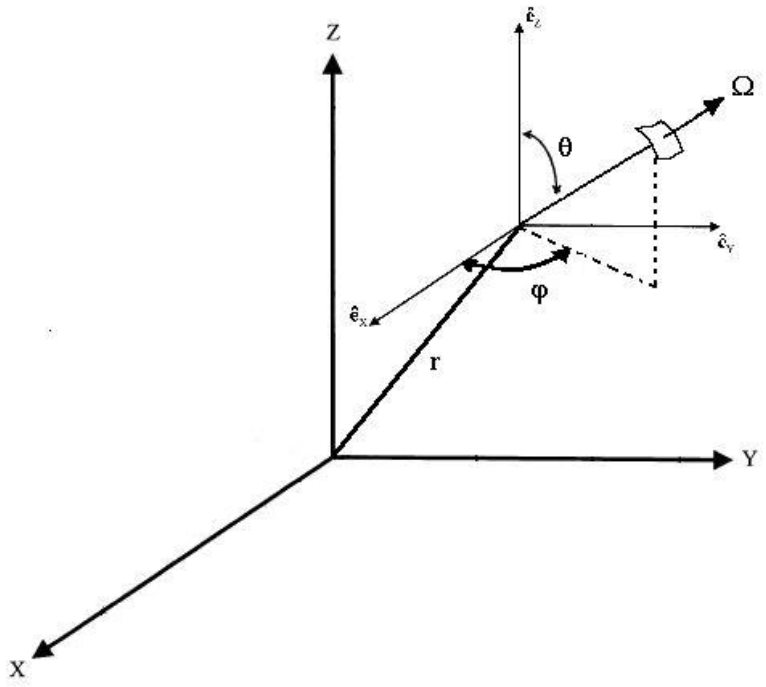

Figure 2.1: State of a Particle in a Coordinate System

Let the vector $\boldsymbol{x}$ be described by the Cartesian coordinates x, y, z, and the vector $\boldsymbol{\Omega}$ be described by a polar angle θ measured with respect to the z-axis and a corresponding azimuthal angle φ (Figure 2.1). If we introduce $\mu = \cos\theta$, then

(2.2a) $$dV = dxdydz\,,$$

(2.2b) $$d\Omega = \sin\theta d\theta d\varphi = d\mu d\varphi\,.$$

A minus sign was omitted from Eq. (2.2b), since μ runs from 1 to -1 when θ runs from 0 to π. If $\boldsymbol{v}$ is the velocity vector, then $\boldsymbol{\Omega} = \boldsymbol{v}/|\boldsymbol{v}|$, and it is easy to see that the components of the particle's velocity in the Cartesian coordinates are given by

(2.3a) $$\dot{x} = v\Omega_x\,,$$

(2.3b) $$\dot{y} = v\Omega_y\,,$$

(2.3c) $$\dot{z} = v\Omega_z\,,$$

where v is the particle's speed in the nonrelativistic case; that is, $v = \sqrt{2E/m_p}$, with m_p denoting the particle's mass. The particle density is obtained by integrating the distribution function over $\mathbf{\Omega}$ and E:

$$\tilde{n}(\boldsymbol{x}, t) = \int_0^\infty \int_{4\pi} n(\boldsymbol{x}, E, \mathbf{\Omega}, t) d\Omega dE. \tag{2.4}$$

It is conventional in linear transport theory to introduce a new function, the angular flux, given by

$$\psi(\boldsymbol{x}, E, \mathbf{\Omega}, t) = vn(\boldsymbol{x}, E, \mathbf{\Omega}, t). \tag{2.5}$$

Integrating ψ over E and $\mathbf{\Omega}$, we obtain the scalar flux Φ:

$$\Phi(\boldsymbol{x}, t) = \int_0^\infty \int_{4\pi} \psi(\boldsymbol{x}, E, \mathbf{\Omega}, t) d\Omega dE = v\tilde{n}(\boldsymbol{x}, t)\,. \tag{2.6}$$

Since particles are expected to interact with the background material through which they are flowing, we will introduce the concepts of the two basic interactions between particles and matter: absorption and scattering. As a particle travels through matter, there is a probability that it will not scatter when undergoing an interaction. In this case, the particle is said to have been absorbed. As examples of absorption we can mention radiative capture and nuclear fission, common processes in reactor theory.

A basic assumption in the absorption processes is that, in traveling a distance ds, the probability of absorption is proportional to ds, independent of the past history of the particle. The proportionality constant between the probability of absorption and the distance ds is called the macroscopic absorption cross section, denoted by $\Sigma_a(\boldsymbol{x}, E, \mathbf{\Omega}, t)$. In general, the absorption cross section depends upon the energy E of the particle as well as both space and time, since the background material properties are (in general) functions of $\boldsymbol{x}$ and t. Assuming that the matter is isotropic, the probability of absorption is independent

of the direction of travel of the particle:

(2.7a) $$\Sigma_a(\boldsymbol{x}, E, t)ds = \text{probability of absorption.}$$

Similarly to absorption, a particle can scatter when interacting with matter. In this case, the particle does not disappear as in absorption, but it continues to exist with, in general, a different energy and direction of travel. If there is no energy change upon scattering, the scattering event is said to be coherent. We define the macroscopic scattering cross section $\Sigma_s(\boldsymbol{x}, E, t)$ in analogy to the absorption cross section, such that for a particle at spatial point $\boldsymbol{x}$ with energy E traveling a distance ds, we have

(2.7b) $$\Sigma_s(\boldsymbol{x}, E, t)ds = \text{probability of scattering.}$$

The changing of the particle's energy and direction E and $\boldsymbol{\Omega}$ to a new energy and direction E' and $\boldsymbol{\Omega}'$ leads to the definition of the macroscopic differential scattering cross section $\Sigma_s(\boldsymbol{x}, E \rightarrow E', \boldsymbol{\Omega} \rightarrow \boldsymbol{\Omega}', t)$, such that the probability that a particle traveling a distance ds will scatter from E to dE' at E' and from $\boldsymbol{\Omega}$ to $d\Omega'$ at $\boldsymbol{\Omega}'$ is given by

(2.8) $$\Sigma_s(\boldsymbol{x}, E \rightarrow E', \boldsymbol{\Omega} \rightarrow \boldsymbol{\Omega}', t)dE'd\Omega'ds.$$

When the scattering process is rotationally invariant, the probability that a particle will scatter from direction $\boldsymbol{\Omega}$ to direction $\boldsymbol{\Omega}'$ depends only on the scattering angle (the angle between $\boldsymbol{\Omega}$ and $\boldsymbol{\Omega}'$), or on $\mu_0 = \boldsymbol{\Omega} \cdot \boldsymbol{\Omega}' =$ the cosine of this angle. In this case, Eq. (2.8) becomes

(2.9) $$\Sigma_s(\boldsymbol{x}, E \rightarrow E', \boldsymbol{\Omega} \cdot \boldsymbol{\Omega}', t)dE'd\Omega'ds,$$

and integrating this equation over all final energies and angles, we obtain the macroscopic scattering cross section at the initial energy, as defined by Eq. (2.7b) [26]:

(2.10) $$\Sigma_s(\boldsymbol{x}, E, t) = \int_0^\infty \int_{4\pi} \Sigma_s(\boldsymbol{x}, E \rightarrow E', \boldsymbol{\Omega} \cdot \boldsymbol{\Omega}', t)d\Omega'dE'.$$

If in Eq. (2.9) the differential scattering cross section is independent of $\mathbf{\Omega}\cdot\mathbf{\Omega}'$, the scattering process is said to be isotropic. In this case, when a particle with direction $\mathbf{\Omega}$ scatters, all outgoing directions $\mathbf{\Omega}'$ are equally probable.

Finally, the macroscopic total cross section is defined as

$$\Sigma_t(\boldsymbol{x}, E, t) = \Sigma_a(\boldsymbol{x}, E, t) + \Sigma_s(\boldsymbol{x}, E, t), \tag{2.11}$$

such that for a particle at spatial point $\boldsymbol{x}$ with energy E traveling a distance ds, $\Sigma_t(\boldsymbol{x}, E, t)ds =$ probability of undergoing an interaction.

At this point, it is important to remark that Eqs. (2.7) and (2.11) are based on the assumptions that the probability that a particle will undergo a collision when traveling a distance ds in the direction $\mathbf{\Omega}$ is: (i) proportional to ds, and (ii) independent of $\mathbf{\Omega}$. These assumptions carry with them the underlying premise that the positions of the scattering centers are uncorrelated and independent upon direction. This is valid for introducing the classical theory; in the subsequent chapters, however, it is dropped in order to better deal with the problem being studied.

Consider a homogeneous medium, and let $K(s)$ be the number of uncollided particles at position s in a directed beam of radiation. In traversing an additional element of path length ds along this beam, the value of $K(s)$ will be decreased by the number of particles that have interacted during this process. From the classical definition of the total cross section we have $-dK(s) = K(s)\Sigma_t ds$. This equation can be integrated with the result $K(s) = K_0 e^{-\Sigma_t s}$, which means that the K_0 particles initially in the beam will decrease exponentialy with distance. It should be noted that since $K(s)$ refers to those particles that have not interacted in traveling the distance s, the ratio $K(s)/K_0 = e^{-\Sigma_t s}$ is the probability that a particle will move through this distance without interacting. Now, let us define $p(s)ds$ as the probability that a particle will have its first interaction in ds in the neighborhood of s. This is equal to the probability that the particle reaches s without

interacting *times* the probability that it does interact in the additional distance ds:

$$p(s)ds = e^{-\Sigma_t s} \times \Sigma_t ds = \Sigma_t e^{-\Sigma_t s} ds. \tag{2.12}$$

The average distance between interactions is known as the *mean free path*, denoted by $\overline{s}$. This quantity is equal to the average distance of s (the distance traversed by a particle without interaction):

$$\overline{s} = \int_0^\infty s p(s) ds = \Sigma_t \int_0^\infty s e^{-\Sigma_t s} ds = \frac{1}{\Sigma_t}. \tag{2.13}$$

Therefore, in a classical homogeneous medium, the mean free path is just the inverse of the total cross section. If the material properties are functions of space and time, the mean free path will depend upon these variables. In this situation, Eq. (2.13) is taken as a definition of the mean free path:

$$\overline{s} = \overline{s}(\boldsymbol{x}, E, t) = \frac{1}{\Sigma_t(\boldsymbol{x}, E, t)}. \tag{2.14a}$$

By analogy, we can define absorption and scattering mean free paths as

$$\overline{s}_a(\boldsymbol{x}, E, t) = \frac{1}{\Sigma_a(\boldsymbol{x}, E, t)}, \tag{2.14b}$$

$$\overline{s}_s(\boldsymbol{x}, E, t) = \frac{1}{\Sigma_s(\boldsymbol{x}, E, t)}, \tag{2.14c}$$

and by Eq. (2.11), the inverse addition rule is satisfied:

$$\frac{1}{\overline{s}} = \frac{1}{\overline{s}_a} + \frac{1}{\overline{s}_s}. \tag{2.15}$$

2.1.2 The Classic Linear Boltzmann Equation

The transport equation was first introduced by Boltzmann in 1872, in the kinetic theory of gases [10]. This equation describes the relationship between the mechanisms of loss and gain of particles in any given volume of a phase space. Much neutral particle transport work is based on this equation, or equations derived from it.

Using [63] as a guide, let the vectors $\boldsymbol{x}$ and $\boldsymbol{\Omega}$ be described by the representation introduced earlier, in such way that Eqs. (2.2) and Figure 2.1 are satisfied. We consider a six-dimensional volume (as a six-dimensional cube) fixed in space, of dimensions $\triangle x$, $\triangle y$, $\triangle z$, $\triangle E$, $\triangle \mu$, $\triangle \varphi$. Then, by Eq. (2.1), the number of particles within this volume at time t is

$$n(\boldsymbol{x}, E, \boldsymbol{\Omega}, t)\triangle x\triangle y\triangle z\triangle E\triangle \mu\triangle \varphi = n(\boldsymbol{x}, E, \boldsymbol{\Omega}, t)\triangle \beta, \tag{2.16}$$

where all arguments of n are "average" arguments in the increment of six-dimensional phase space $\triangle\beta$. The number of particles in this cube changes with time:

$$\triangle\beta\frac{\partial}{\partial t}n(\boldsymbol{x}, E, \boldsymbol{\Omega}, t) = \begin{array}{l}\text{time rate of change of the number of}\\ \text{particles in the six-dimensional cube } \triangle\beta.\end{array} \tag{2.17}$$

This time rate of change is due to five separate processes. One is the rate of streaming of particles out of the volume through the boundaries. The others occur within the six-dimensional "cube": the rate of absorption; the rate of scattering from E, $\boldsymbol{\Omega}$ to all other energies and directions, known as outscattering; the rate of scattering into E, $\boldsymbol{\Omega}$ from all other energies and directions, known as inscattering; and the rate of production of particles due to an internal source.

Now, let us consider the surfaces of the cube perpendicular to the x-axis. For the net rate of particles leaving the cube through these two surfaces, we have

$$(\text{Streaming})_x = \dot{x}n(\boldsymbol{x}, E, \boldsymbol{\Omega}, t)\,|_x^{x+\triangle x}\ \triangle y\triangle z\triangle E\triangle\mu\triangle\varphi, \tag{2.18}$$

where $\dot{x}$ is the x component of the particle velocity as defined by Eq. (2.3a), and $\triangle y\triangle z\triangle E\triangle\mu\triangle\varphi$ is the surface area. Letting $\triangle x$ go to the differential dx, we rewrite Eq. (2.18) as

$$(\text{Streaming})_x = \triangle\beta\frac{\partial}{\partial x}\big[\dot{x}n(\boldsymbol{x}, E, \boldsymbol{\Omega}, t)\big]. \tag{2.19}$$

Using the same procedure for the flow from the cube in the other five "directions", we obtain

$$\text{Streaming} = \left[\frac{\partial}{\partial x}(\dot{x}n)+\frac{\partial}{\partial y}(\dot{y}n) + \frac{\partial}{\partial z}(\dot{z}n) + \frac{\partial}{\partial E}(\dot{E}n) + \frac{\partial}{\partial \mu}(\dot{\mu}n) + \frac{\partial}{\partial \varphi}(\dot{\varphi}n)\right]\triangle\beta, \tag{2.20}$$

where $n = n(\boldsymbol{x}, E, \boldsymbol{\Omega}, t)$.

The rate of absorption within the cube is the product of the number of particles in the cube and the probability of absorption per particle per unit of time. This probability is given by the product of the absorption cross section and the particle speed v. That is,

$$\text{Absorption} = v\Sigma_a(\boldsymbol{x}, E, t)n(\boldsymbol{x}, E, \boldsymbol{\Omega}, t)\triangle\beta. \tag{2.21}$$

Using similar arguments and the fact that we need to sum the scattering from (to) E, $\boldsymbol{\Omega}$ to (from) all other energies and directions E', $\boldsymbol{\Omega}'$, we find

$$\text{Outscattering} = \triangle\beta \int_0^\infty \int_{4\pi} v\Sigma_s(\boldsymbol{x}, E \rightarrow E', \boldsymbol{\Omega}\cdot\boldsymbol{\Omega}', t)n(\boldsymbol{x}, E, \boldsymbol{\Omega}, t)d\Omega' dE', \tag{2.22a}$$

$$\text{Inscattering} = \triangle\beta \int_0^\infty \int_{4\pi} v'\Sigma_s(\boldsymbol{x}, E' \rightarrow E, \boldsymbol{\Omega}'\cdot\boldsymbol{\Omega}, t)n(\boldsymbol{x}, E', \boldsymbol{\Omega}', t)d\Omega' dE', \tag{2.22b}$$

where $\Sigma_s(\boldsymbol{x}, E' \rightarrow E, \boldsymbol{\Omega}'\cdot\boldsymbol{\Omega}, t)$ is the macroscopic differential scattering cross section as defined earlier. Since the distribution function in the integrand of Eq. (2.22a) is independent of the integration variables, using Eq. (2.10) we can rewrite Outscattering as $\triangle\beta v\Sigma_s(\boldsymbol{x}, E, t)n(\boldsymbol{x}, E, \boldsymbol{\Omega}, t)$. Finally, we need to consider the internal source of particles. We quantify this source by introducing the function $Q(\boldsymbol{x}, E, \boldsymbol{\Omega}, t)$ such that the rate of introduction of particles into the cube is given by

$$\text{Source} = Q(\boldsymbol{x}, E, \boldsymbol{\Omega}, t)\triangle\beta. \tag{2.23}$$

In order to build the transport equation, we sum Eqs. (2.20-2.23), with appropriate signs for loss and gain, to the overall rate given by Eq. (2.17). Letting $\triangle\beta$ approach a differential

element and canceling it, we obtain

$$\begin{aligned}(2.24)\quad \frac{\partial n}{\partial t} = &-\left[\frac{\partial(\dot{x}n)}{\partial x}+\frac{\partial(\dot{y}n)}{\partial y}+\frac{\partial(\dot{z}n)}{\partial z}+\frac{\partial(\dot{E}n)}{\partial E}+\frac{\partial(\dot{\mu}n)}{\partial \mu}+\frac{\partial(\dot{\varphi}n)}{\partial \varphi}\right]\\ &- v\Sigma_a(\boldsymbol{x},E,t)n\\ &+\int_0^\infty\int_{4\pi} v'\Sigma_s(\boldsymbol{x},E'\to E,\boldsymbol{\Omega}'\cdot\boldsymbol{\Omega},t)n(\boldsymbol{x},E',\boldsymbol{\Omega}',t)d\Omega' dE'\\ &-\int_0^\infty\int_{4\pi} v\Sigma_s(\boldsymbol{x},E\to E',\boldsymbol{\Omega}\cdot\boldsymbol{\Omega}',t)n(\boldsymbol{x},E,\boldsymbol{\Omega},t)d\Omega' dE'\\ &+Q(\boldsymbol{x},E,\boldsymbol{\Omega},t),\end{aligned}$$

where $n = n(\boldsymbol{x},E,\boldsymbol{\Omega},t)$. Since particles travel in a straight line between collisions, $\dot{\mu} = \dot{\varphi} = 0$. Furthermore, $\dot{E} = 0$ because particles stream with no change in energy. Finally, performing the outscattering integral and using Eqs. (2.3) and (2.5), Eq. (2.24) becomes

$$\begin{aligned}(2.25)\quad &\frac{1}{v}\frac{\partial\psi}{\partial t}(\boldsymbol{x},E,\boldsymbol{\Omega},t)+\boldsymbol{\Omega}\cdot\boldsymbol{\nabla}\psi(\boldsymbol{x},E,\boldsymbol{\Omega},t)+\Sigma_t(\boldsymbol{x},E,t)\psi(\boldsymbol{x},E,\boldsymbol{\Omega},t)\\ &\quad=\int_0^\infty\int_{4\pi}\Sigma_s(\boldsymbol{x},E'\to E,\boldsymbol{\Omega}'\cdot\boldsymbol{\Omega},t)\psi(\boldsymbol{x},E',\boldsymbol{\Omega}',t)d\Omega' dE'+Q(\boldsymbol{x},E,\boldsymbol{\Omega},t).\end{aligned}$$

Following [25], we can easily generalize this equation to include nuclear fission. To do that, we must revisit our treatment of Σ_a; as we have mentioned, there are two main processes responsible for the absorption of particles in the system: *radiative capture* and *nuclear fission*. Now, we define

$$(2.26a)\qquad \Sigma_\gamma(\boldsymbol{x},E,t)ds = \text{probability of capture}$$

and

$$(2.26b)\qquad \Sigma_f(\boldsymbol{x},E,t)ds = \text{probability of a fission event,}$$

such that

$$(2.27)\qquad \Sigma_a(\boldsymbol{x},E,t) = \Sigma_\gamma(\boldsymbol{x},E,t)+\Sigma_f(\boldsymbol{x},E,t)\,.$$

While a captured neutron is simply removed from the system, a neutron with energy E that induces a fission event causes the target nucleus to split into two smaller daughter nuclei, and

(2.28) $\nu(E) =$ the mean number of fission neutrons that are released .

Of this number, $\nu(E)[1 - M(E)]$ are *prompt* fission neutrons (being emitted within 10^{-15} seconds of the fission event). These fission neutrons are emitted isotropically, with an energy distribution given by the fission spectrum $\chi_p(E)$. Also, $\nu(E)M(E)$ *delayed* fission neutrons (being released roughly 0.1 to 60 seconds after the fission event) are created; a delayed neutron is produced when a radioactive daughter nucleus undergoes a radioactive decay process in which a neutron is emitted.

Assuming (for simplicity) that the number of delayed neutrons emitted by fission is very small [$M(E) << 1$], we can neglect the delayed neutron terms and rewrite Eq. (2.25) as

$$\begin{aligned}(2.29)\qquad \frac{1}{v}\frac{\partial\psi}{\partial t}(\boldsymbol{x},E,\boldsymbol{\Omega},t) + \boldsymbol{\Omega}\cdot\boldsymbol{\nabla}\psi(\boldsymbol{x},E,\boldsymbol{\Omega},t) + \Sigma_t(\boldsymbol{x},E,t)\psi(\boldsymbol{x},E,\boldsymbol{\Omega},t)\\ = \int_0^\infty\int_{4\pi}\Sigma_s(\boldsymbol{x},E'\to E,\boldsymbol{\Omega}'\cdot\boldsymbol{\Omega},t)\psi(\boldsymbol{x},E',\boldsymbol{\Omega}',t)d\Omega' dE'\\ + \frac{\chi_p(E)}{4\pi}\int_0^\infty\int_{4\pi}\nu(E')\Sigma_f(\boldsymbol{x},E',t)\psi(\boldsymbol{x},E',\boldsymbol{\Omega}',t)d\Omega' dE'\\ + Q(\boldsymbol{x},E,\boldsymbol{\Omega},t).\end{aligned}$$

Equation (2.29) [as well as Eq. (2.25)] requires both spatial and temporal boundary conditions. Assuming that the physical system of interest is nonreentrant (convex) and characterized by a volume V, it is sufficient to specify the flux of particles at all points of the bounding surface of the system in the incoming directions. This implies

(2.30a) $$\psi(\boldsymbol{x}_s,E,\boldsymbol{\Omega},t) = \psi_b(\boldsymbol{x}_s,E,\boldsymbol{\Omega},t)\,, \quad \mathbf{n}\cdot\boldsymbol{\Omega} < 0,$$

where ψ_b is a specified function at the boundary, $\boldsymbol{x}_s$ is a point on the surface, and $\mathbf{n}$ is the unit outward normal vector at this point. In the time variable, we assume the range of interest $0 \leq t < \infty$ and specify the initial condition at $t = 0$, such that

$$\psi(\boldsymbol{x}, E, \boldsymbol{\Omega}, 0) = \psi_i(\boldsymbol{x}, E, \boldsymbol{\Omega}), \tag{2.30b}$$

where ψ_i is a specified function. In particular, Eqs. (2.29) and (2.30) completely specify the linear particle transport problem (without delayed fission neutrons).

It is common to make extra assumptions in order to obtain a simpler version of these equations. For instance, in the case of time-independent, monoenergetic particle transport in a homogeneous medium with a known interior isotropic source, Eq. (2.25) becomes

$$\boldsymbol{\Omega} \cdot \boldsymbol{\nabla}\psi(\boldsymbol{x}, \boldsymbol{\Omega}) + \Sigma_t \psi(\boldsymbol{x}, \boldsymbol{\Omega}) = \int_{4\pi} \Sigma_s(\boldsymbol{\Omega}' \cdot \boldsymbol{\Omega})\psi(\boldsymbol{x}, \boldsymbol{\Omega}')d\Omega' + \frac{Q(\boldsymbol{x})}{4\pi}\,, \tag{2.31}$$

and Eq. (2.29) becomes

$$\begin{aligned}\boldsymbol{\Omega} \cdot \boldsymbol{\nabla}\psi(\boldsymbol{x}, \boldsymbol{\Omega}) + \Sigma_t \psi(\boldsymbol{x}, \boldsymbol{\Omega}) = &\int_{4\pi} \Sigma_s(\boldsymbol{\Omega}' \cdot \boldsymbol{\Omega})\psi(\boldsymbol{x}, \boldsymbol{\Omega}')d\Omega' \\ &+ \frac{\nu\Sigma_f}{4\pi}\int_{4\pi} \psi(\boldsymbol{x}, \boldsymbol{\Omega}')d\Omega' + \frac{Q(\boldsymbol{x})}{4\pi}\,.\end{aligned} \tag{2.32}$$

Both the equations above need a spatial boundary condition, which is given by

$$\psi(\boldsymbol{x}_s, \boldsymbol{\Omega}) = \psi_b(\boldsymbol{x}_s, \boldsymbol{\Omega})\,, \quad \mathbf{n} \cdot \boldsymbol{\Omega} < 0\,. \tag{2.33}$$

In steady-state reactor calculations, one often sees [25, 26, 40] a version of Eqs. (2.61b) and (2.33) in which the inhomogeneous source $Q(\boldsymbol{x})$ and the boundary source $\psi_b(\boldsymbol{x}_s, \boldsymbol{\Omega})$ are set to zero, and the fission source is modified by a constant factor $1/k$:

$$\begin{aligned}\boldsymbol{\Omega} \cdot \boldsymbol{\nabla}\psi(\boldsymbol{x}, \boldsymbol{\Omega}) + \Sigma_t \psi(\boldsymbol{x}, \boldsymbol{\Omega}) = &\int_{4\pi} \Sigma_s(\boldsymbol{\Omega}' \cdot \boldsymbol{\Omega})\psi(\boldsymbol{x}, \boldsymbol{\Omega}')d\Omega' \\ &+ \frac{\nu\Sigma_f}{4\pi k}\int_{4\pi} \psi(\boldsymbol{x}, \boldsymbol{\Omega}')d\Omega'\,,\end{aligned} \tag{2.34a}$$

$$\psi(\boldsymbol{x}_s, \boldsymbol{\Omega}) = 0, \quad \mathbf{n} \cdot \boldsymbol{\Omega} < 0\,. \tag{2.34b}$$

These equations always have the zero solution $\psi = 0$; the goal is to find the largest value of k such that a nonzero solution ψ exists. The resulting k is called the *criticality* (or *criticality eigenvalue*) of the system. If a system has a fissile region, it can be shown that k always exists, and the corresponding (eigenfunction) ψ in unique and positive.

The eigenvalue k is a measure of the ability of a reactor to regenerate neutrons by fission; namely, it is the average number of neutrons from one fission that cause another fission. If $k = 1$, capture and leakage exactly balance fission, and a nonzero, steady-state neutron flux is possible. In this case, the reactor is said to be *critical*. If $k < 1$, then capture and leakage dominate fission, and the reactor is *subcritical*. On the other hand, if $k > 1$, fission dominates capture and leakage, and the reactor is *supercritical*.

Finally, it is important to remark that an integral formulation for the Boltzmann equation can also be obtained. For instance, defining the inscattering rate density $g(\boldsymbol{x}, \boldsymbol{\Omega})$ as

$$g(\boldsymbol{x}, \boldsymbol{\Omega}) = \int_{4\pi} \Sigma_s(\boldsymbol{\Omega}' \cdot \boldsymbol{\Omega}) \psi(\boldsymbol{x}, \boldsymbol{\Omega}') d\Omega' \tag{2.35}$$

and solving the integral equation

$$\begin{aligned} g(\boldsymbol{x}, \boldsymbol{\Omega}) &= \iiint \Sigma_s \left(\frac{\boldsymbol{x} - \boldsymbol{x}'}{|\boldsymbol{x} - \boldsymbol{x}'|} \cdot \boldsymbol{\Omega} \right) \left[g\left(\boldsymbol{x}', \frac{\boldsymbol{x} - \boldsymbol{x}'}{|\boldsymbol{x} - \boldsymbol{x}'|} \right) + \frac{Q(\boldsymbol{x}')}{4\pi} \right] \frac{e^{-\Sigma_t |\boldsymbol{x} - \boldsymbol{x}'|}}{|\boldsymbol{x} - \boldsymbol{x}'|^2} \, dV' \end{aligned} \tag{2.36a}$$

allows us to write an integral expression for the classic angular flux in terms of $g(\boldsymbol{x}, \boldsymbol{\Omega})$:

$$\psi(\boldsymbol{x}, \boldsymbol{\Omega}) = \int_0^\infty \left[g(\boldsymbol{x} - s\boldsymbol{\Omega}, \boldsymbol{\Omega}) + \frac{Q\big(\boldsymbol{x} - s\boldsymbol{\Omega}\big)}{4\pi} \right] e^{-\Sigma_t s} \, ds \, . \tag{2.36b}$$

Equations (2.36) are the classic integral transport equations for the case modeled by Eqs. (2.31) and (2.33). We refer to [16, 26, 63] for more details on this formulation.

2.2 The Diffusion Equation

The *diffusion approximation* is a classic model for particle transport in a physical system in which absorption and sources are weak and the solution varies slowly over the

distance of a mean free path. The diffusion equation has long been known to be an asymptotic limit of the transport equation [31, 42, 43].

For instance, in the case of time-independent, monoenergetic particle transport in a homogeneous medium with a known interior isotropic source, Eqs. (2.31) and (2.61b) become respectively [25]:

$$-\mathrm{D}\nabla^2\Phi(\boldsymbol{x}) + \Sigma_a\Phi(\boldsymbol{x}) = Q(\boldsymbol{x})\,, \tag{2.37}$$

and

$$-\mathrm{D}\nabla^2\Phi(\boldsymbol{x}) + \Sigma_a\Phi(\boldsymbol{x}) = \nu\Sigma_f\Phi(\boldsymbol{x}) + Q(\boldsymbol{x})\,; \tag{2.38}$$

where

$$\mathrm{D} = \frac{1}{3(\Sigma_t - \overline{\mu}_0\Sigma_s)} \tag{2.39}$$

is the *neutron diffusion coefficient*, with $\overline{\mu}_0$ representing the mean scattering cosine. These equations share the boundary condition

$$\frac{\mathrm{D}}{2}\mathbf{n}\cdot\boldsymbol{\nabla}\Phi(\boldsymbol{x}) + \frac{1}{2}\Phi(\boldsymbol{x}) = \int_{\mathbf{n}\cdot\boldsymbol{\Omega}<0} |\mathbf{n}\cdot\boldsymbol{\Omega}|\psi(\boldsymbol{x}_s,\boldsymbol{\Omega})d\Omega\,, \tag{2.40}$$

where $\boldsymbol{x}_s$ is a point on the surface and $\mathbf{n}$ is the unit outward normal vector at this point.

2.2.1 On the k_D Diffusion Eigenvalue

As mentioned in Section 2.1.2, one of the most important quantities in reactor physics is the criticality eigenvalue k. The value of k determines how a nuclear chain reaction proceeds, and even a very small difference on its estimate has a significant impact on the overall problem, such that errors in the estimate of k on the order of 0.1% are significant.

Let $\boldsymbol{x} = (x, y, z)$, where $x \in [0, X]$, $y \in [0, Y]$, and $z \in [0, Z]$, and consider the following eigenvalue problem based on a diffusion equation with a fission source [see

Eq. (2.34a)]:

$$-\mathrm{D}_x\frac{\partial^2}{\partial x^2}\Phi(\boldsymbol{x})-\mathrm{D}_y\frac{\partial^2}{\partial y^2}\Phi(\boldsymbol{x})-\mathrm{D}_z\frac{\partial^2}{\partial z^2}\Phi(\boldsymbol{x})+\Sigma_a\Phi(\boldsymbol{x})=\frac{\nu\Sigma_f\Phi(\boldsymbol{x})}{k_D}\,, \tag{2.41a}$$

$$\Phi(0,y,z)=\Phi(X,y,z)=0\,,\ \forall\ y\in[0,Y]\,,\ z\in[0,Z]\,, \tag{2.41b}$$

$$\Phi(x,0,z)=\Phi(x,Y,z)=0\,,\ \forall\ x\in[0,X]\,,\ z\in[0,Z]\,, \tag{2.41c}$$

$$\Phi(x,y,0)=\Phi(x,y,Z)=0\,,\ \forall\ x\in[0,X]\,,\ y\in[0,Y]\,; \tag{2.41d}$$

where $\nu\Sigma_f$ is the thermal neutron cross section [40]. Let

$$\Phi(\boldsymbol{x})=\sin\left(\frac{\pi x}{X}\right)\sin\left(\frac{\pi y}{Y}\right)\sin\left(\frac{\pi z}{Z}\right) \tag{2.42}$$

satisfy Eqs. (2.41); then the *diffusion* eigenvalue k_D must be given by:

$$k_D=\frac{\nu\Sigma_f}{\Sigma_a+\pi^2\left(\frac{\mathrm{D}_x}{X^2}+\frac{\mathrm{D}_y}{Y^2}+\frac{\mathrm{D}_z}{Z^2}\right)}. \tag{2.43}$$

We wish to emphasize that the formula in Eq. (2.43) for the *diffusion* eigenvalue k_D applies to the *diffusion* problem defined by Eqs. (2.41). It does not apply to the eigenvalue k defined by Eq. (2.34a), unless the transport problem is so diffusive in its nature that the differences between transport and diffusion theory can be ignored.

It is clear from Eq. (2.43) that different estimates for the diffusion coefficients will generate different results for k_D. This fact will play an important role later in this work.

2.2.2 Theoretical Predictions of Σ_a and Mean Square Distances from Point of Birth

Consider the diffusion equation below, taking place in an infinite system with a point source at the origin:

$$-\mathrm{D}_x\frac{\partial^2}{\partial x^2}\Phi(\boldsymbol{x})-\mathrm{D}_y\frac{\partial^2}{\partial y^2}\Phi(\boldsymbol{x})-\mathrm{D}_z\frac{\partial^2}{\partial z^2}\Phi(\boldsymbol{x})+\Sigma_a\Phi(\boldsymbol{x})=Q(\boldsymbol{x})\delta(x)\delta(y)\delta(z)\,. \tag{2.44}$$

Bearing in mind that $\Phi(\boldsymbol{x})\to 0$ and $\nabla\Phi(\boldsymbol{x})\to 0$ as $|\boldsymbol{x}|\to\infty$, we can manipulate this equation to obtain exact formulas for Σ_a and for the mean square distances of particles from point of birth.

Operating on Eq. (2.44) by

$$\int_{-\infty}^{\infty}\int_{-\infty}^{\infty}\int_{-\infty}^{\infty}(.)dxdydz\,, \tag{2.45}$$

we obtain the exact expression

$$\Sigma_a\int_{-\infty}^{\infty}\int_{-\infty}^{\infty}\int_{-\infty}^{\infty}\Phi(\boldsymbol{x})dxdydz = Q(0)\,. \tag{2.46}$$

Using Eq. (2.6), we have:

$$\begin{aligned}\Phi dVdt = v(\tilde{n}dV)dt &= (vdt)(\tilde{n}dV)\\ &= \begin{array}{l}\text{[path length traveled by one neutron in time } dt\text{]}\\ \times\text{ [number of neutrons in } dV \text{ about } \boldsymbol{x}\text{]}\end{array}\\ &= \begin{array}{l}\text{total path length traveled by neutrons}\\ \text{in } dV \text{ about } \boldsymbol{x} \text{ during time increment } dt\,,\end{array}\end{aligned} \tag{2.47}$$

and dividing by dt we obtain a volume-based interpretation for Φ:

$$\Phi dV = \text{rate at which path length is generated by neutrons in } dV \text{ about } \boldsymbol{x}\,. \tag{2.48}$$

Operating on this equation by Eq. (2.45), we get:

$$\begin{aligned}\int_{-\infty}^{\infty}\int_{-\infty}^{\infty}\int_{-\infty}^{\infty}\Phi(\boldsymbol{x})dxdydz &= \begin{array}{l}\text{rate at which path length is}\\ \text{generated by neutrons in the system}\end{array}\\ &= \begin{array}{l}\text{[number of neutrons in the system]}\\ \times\text{[mean path length generated by one neutron]}\end{array}\\ &= \begin{array}{l}\text{[number of neutrons in the system]}\\ \times\text{[mean number of collisions of a neutron]}\\ \times\text{[mean free path of a neutron]}\end{array}\\ &= [Q(0)]\left[\frac{1}{1-c}\right][\overline{s}]\,.\end{aligned} \tag{2.49}$$

Introducing this result into Eq. (2.46) we obtain the *exact* expression

$$\Sigma_a = \frac{1-c}{\overline{s}}\,. \tag{2.50}$$

Notice that for the classic case (in which $\Sigma_t = 1/\overline{s}$) this expression reduces to the classic expression $\Sigma_a = (1-c)\Sigma_t$.

Next, multiplying Eq. (2.44) by x^2 and operating on it by Eq. (2.45), we obtain:

$$-\mathrm{D}_x \int_{-\infty}^{\infty}\int_{-\infty}^{\infty}\int_{-\infty}^{\infty} x^2 \frac{\partial^2}{\partial x^2}\Phi(\boldsymbol{x})dxdydz + \Sigma_a \int_{-\infty}^{\infty}\int_{-\infty}^{\infty}\int_{-\infty}^{\infty} x^2\Phi(\boldsymbol{x})dxdydz = 0\,. \tag{2.51}$$

Integrating the first term on this equation by parts we get

$$\int_{-\infty}^{\infty}\int_{-\infty}^{\infty}\int_{-\infty}^{\infty} x^2 \frac{\partial^2}{\partial x^2}\Phi(\boldsymbol{x})dxdydz = 2\int_{-\infty}^{\infty}\int_{-\infty}^{\infty}\int_{-\infty}^{\infty} \Phi(\boldsymbol{x})dxdydz\,. \tag{2.52}$$

Therefore, Eq. (2.51) can be rewritten as

$$\overline{x^2} = \frac{\int_{-\infty}^{\infty}\int_{-\infty}^{\infty}\int_{-\infty}^{\infty} x^2\Phi(\boldsymbol{x})dxdydz}{\int_{-\infty}^{\infty}\int_{-\infty}^{\infty}\int_{-\infty}^{\infty} \Phi(\boldsymbol{x})dxdydz} = 2\frac{\mathrm{D}_x}{\Sigma_a}\,, \tag{2.53a}$$

where $\overline{x^2}$ represents the mean square distance of a particle to its point of birth *in the x-direction*. Similarly, the mean square distance of a particle to its point of birth *in the y-direction* is given by:

$$\overline{y^2} = \frac{\int_{-\infty}^{\infty}\int_{-\infty}^{\infty}\int_{-\infty}^{\infty} y^2\Phi(\boldsymbol{x})dxdydz}{\int_{-\infty}^{\infty}\int_{-\infty}^{\infty}\int_{-\infty}^{\infty} \Phi(\boldsymbol{x})dxdydz} = 2\frac{\mathrm{D}_y}{\Sigma_a}\,; \tag{2.53b}$$

the mean square distance of a particle to its point of birth *in the z-direction* is given by:

$$\overline{z^2} = \frac{\int_{-\infty}^{\infty}\int_{-\infty}^{\infty}\int_{-\infty}^{\infty} z^2\Phi(\boldsymbol{x})dxdydz}{\int_{-\infty}^{\infty}\int_{-\infty}^{\infty}\int_{-\infty}^{\infty} \Phi(\boldsymbol{x})dxdydz} = 2\frac{\mathrm{D}_z}{\Sigma_a}\,; \tag{2.53c}$$

and therefore, the *total* mean square distance of a particle to its point of birth is given by:

$$\overline{\rho^2} = \frac{\int_{-\infty}^{\infty}\int_{-\infty}^{\infty}\int_{-\infty}^{\infty}(x^2+y^2+z^2)\Phi(\boldsymbol{x})dxdydz}{\int_{-\infty}^{\infty}\int_{-\infty}^{\infty}\int_{-\infty}^{\infty} \Phi(\boldsymbol{x})dxdydz} = \frac{2}{\Sigma_a}(\mathrm{D}_x+\mathrm{D}_y+\mathrm{D}_z)\,. \tag{2.53d}$$

Finally, we define the notation:

(2.54a) $\overline{x} = \overline{|x|}$ = mean distance of a particle to its point of birth in the x-direction;

(2.54b) $\overline{y} = \overline{|y|}$ = mean distance of a particle to its point of birth in the y-direction;

(2.54c) $\overline{z} = \overline{|z|}$ = mean distance of a particle to its point of birth in the z-direction;

(2.54d) $\overline{\rho} = \overline{\left(\sqrt{x^2+y^2+z^2}\right)}$ = total mean distance of a particle to its point of birth.

2.3 The Atomic Mix Equation

Let us consider the integro-differential transport equation given by Eq. (2.25). In a deterministic medium, the total cross section Σ_t, the scattering kernel Σ_s, and the source Q are known functions of their arguments. In order to find the angular flux ψ, one must solve this equation subject to the boundary and initial conditions given by Eqs. (2.30).

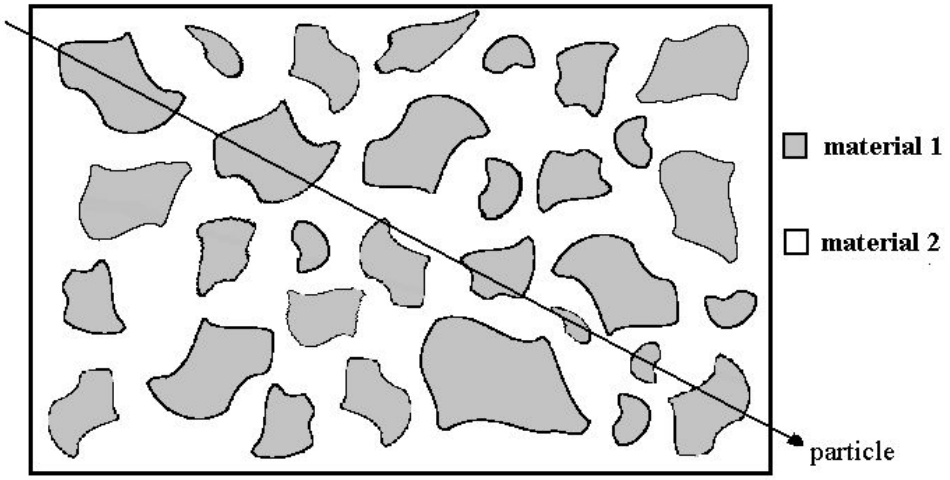

Figure 2.2: Particle Traversing the Mixture Along a Random Path

Now, we consider neutron transport in a heterogeneous volume V such that the boundary ∂V of V is specified, but the interior structure of V is not. Specifically, we restrict our attention to the case in which V consists of two random immiscible materials denoted by an index i, with $i \in \{1, 2\}$. We can imagine V as a heterogeneous volume consisting of randomly distributed chunks of random sizes and shapes of material 1 imbedded in material 2. If we consider a particle traversing the mixture along a random path, it will pass through alternating segments of these two materials, as shown in Figure 2.2.

The quantities Σ_t, Σ_s and Q are considered as discrete random variables. That is, in the ith material these elements are denoted by $\Sigma_{ti}(\boldsymbol{x}, E, t)$, $\Sigma_{si}(\boldsymbol{x}, E' \rightarrow E, \boldsymbol{\Omega}' \cdot \boldsymbol{\Omega}, t)$, and $Q_i(\boldsymbol{x}, E, \boldsymbol{\Omega}, t)$. The stochasticity of the problem is that we have only probabilistic

knowledge about which material occupies the space point $\boldsymbol{x}$ at a time t. Therefore, since we are considering Σ_t, Σ_s and Q as random variables, we must also consider the angular flux ψ as a random variable. We want to find an expression for $\langle\psi\rangle$, the ensemble-averaged angular flux (expected value) of ψ.

For convenience, let us consider the case of transport in a nonscattering medium. Thinking about $\boldsymbol{\Omega}\cdot\boldsymbol{\nabla}$ in Eq. (2.25) as a directional derivative, we can rewrite this equation as

$$\frac{1}{v}\frac{\partial\psi(\eta,t)}{\partial t}+\frac{\partial\psi(\eta,t)}{\partial\eta}+\Sigma_t(\eta,t)\psi(\eta,t)=Q(\eta,t), \tag{2.55}$$

where η denotes the spatial variable in the direction $\boldsymbol{\Omega}$. One must notice that Eq. (2.55) describes particle transport at each energy E and direction $\boldsymbol{\Omega}$, which are omitted since they are only parameters. We let $\langle W\rangle$ denote the ensemble average of any random variable W, and define $\tilde{W}$ as the deviation of W from $\langle W\rangle$. Then $\langle\tilde{W}\rangle=0$, and $W=\langle W\rangle+\tilde{W}$. Using this notation and following the work in [63], we ensemble-average Eq. (2.55) to obtain

$$\frac{1}{v}\frac{\partial\langle\psi\rangle}{\partial t}+\frac{\partial\langle\psi\rangle}{\partial\eta}+\langle\Sigma_t\rangle\langle\psi\rangle+\langle\tilde{\Sigma}_t\tilde{\psi}\rangle=\langle Q\rangle. \tag{2.56}$$

The values of $\langle\Sigma_t\rangle$ and $\langle Q\rangle$ in this equation are defined in terms of the properties of materials 1 and 2. Defining $\hat{p}_i(\eta,t)$ as the probability of presence of the material i at position η at time t, then $\hat{p}_1(\eta,t)+\hat{p}_2(\eta,t)=1$, and we can write

$$\langle\Sigma_t(\eta,t)\rangle=\hat{p}_1(\eta,t)\Sigma_{t1}(\eta,t)+\hat{p}_2(\eta,t)\Sigma_{t2}(\eta,t), \tag{2.57a}$$

$$\langle Q(\eta,t)\rangle=\hat{p}_1(\eta,t)Q_1(\eta,t)+\hat{p}_2(\eta,t)Q_2(\eta,t). \tag{2.57b}$$

Let us define the characteristic chord length for the chunks of material i as Λ_i. Assuming that

$$\Sigma_{ti}\Lambda_i\ll 1,\quad i=1,2, \tag{2.58}$$

a particle between collisions is likely to travel a distance that spans many chunks of materials 1 and 2. Recalling the relationship given by Eq. (2.14a), Eq. (2.58) means that Λ_i is very small when compared with the mean free path $\overline{s}_i$. On physical grounds, this assumption appropriately describes vanishingly small chunks in the mixture, which can be understood as if the two components of the system were mixed at the atomic level. When Eq. (2.58) is satisfied, it is physically intuitive that the transport process will be well-approximated by the process that holds when the chunk sizes are close to zero (the atomic mix limit). Moreover, when the chunk sizes shrink the deviations in the angular flux should also shrink, and $\tilde{\psi}$ will go to zero. Hence, the cross correlation term $\langle\tilde{\Sigma}_t\tilde{\psi}\rangle$ in Eq. (2.56) can be neglected, and Eq. (2.56) becomes

$$\frac{1}{v}\frac{\partial\langle\psi\rangle}{\partial t} + \frac{\partial\langle\psi\rangle}{\partial\eta} + \langle\Sigma_t\rangle\langle\psi\rangle = \langle Q\rangle, \tag{2.59}$$

which is closed for the ensemble-averaged angular flux $\langle\psi\rangle$. This equation represents the atomic mix description of Eq. (2.55).

For instance, applying the same arguments above on Eq. (2.25), the atomic mix description of stochastic transport including scattering is given by

$$\begin{aligned}\frac{1}{v}\frac{\partial\langle\psi(\boldsymbol{x},E,\boldsymbol{\Omega},t)\rangle}{\partial t} + \boldsymbol{\Omega}\cdot\boldsymbol{\nabla}\langle\psi(\boldsymbol{x},E,\boldsymbol{\Omega},t)\rangle + \langle\Sigma_t(\boldsymbol{x},E,t)\rangle\langle\psi(\boldsymbol{x},E,\boldsymbol{\Omega},t)\rangle \\ = \int_0^\infty\int_{4\pi}\langle\Sigma_s(\boldsymbol{x},E'\to E,\boldsymbol{\Omega}'\cdot\boldsymbol{\Omega},t)\rangle\langle\psi(\boldsymbol{x},E',\boldsymbol{\Omega}',t)\rangle d\Omega' dE' \\ + \langle Q(\boldsymbol{x},E,\boldsymbol{\Omega},t)\rangle,\end{aligned} \tag{2.60a}$$

with boundary condition

$$\langle\psi(\boldsymbol{x}_s,E,\boldsymbol{\Omega},t)\rangle = \psi_b(\boldsymbol{x}_s,E,\boldsymbol{\Omega},t), \quad \mathbf{n}\cdot\boldsymbol{\Omega} < 0 \tag{2.60b}$$

and initial condition

$$\langle\psi(\boldsymbol{x},E,\boldsymbol{\Omega},0)\rangle = \psi_i(\boldsymbol{x},E,\boldsymbol{\Omega}). \tag{2.60c}$$

Here, $\langle W\rangle = \hat{p}_1(\boldsymbol{x},t)W_1 + \hat{p}_2(\boldsymbol{x},t)W_2$, where W stands for Σ_t, Σ_s and Q. The neglected cross correlation terms are $\langle\tilde{\Sigma}_t\tilde{\psi}\rangle$ and $\langle\tilde{\Sigma}_s\tilde{\psi}\rangle$.

Similarly, the atomic mix description of Eqs. (2.31-2.33) is given by

$$\text{(2.61a)}\quad \boldsymbol{\Omega}\cdot\boldsymbol{\nabla}\langle\psi(\boldsymbol{x},\boldsymbol{\Omega})\rangle + \langle\Sigma_t\rangle\langle\psi(\boldsymbol{x},\boldsymbol{\Omega})\rangle = \int_{4\pi}\langle\Sigma_s(\boldsymbol{\Omega}'\cdot\boldsymbol{\Omega})\rangle\langle\psi(\boldsymbol{x},\boldsymbol{\Omega}')\rangle d\Omega' + \frac{\langle Q(\boldsymbol{x})\rangle}{4\pi}\,,$$

$$\text{(2.61b)}\quad \boldsymbol{\Omega}\cdot\boldsymbol{\nabla}\langle\psi(\boldsymbol{x},\boldsymbol{\Omega})\rangle + \langle\Sigma_t\rangle\langle\psi(\boldsymbol{x},\boldsymbol{\Omega})\rangle = \int_{4\pi}\langle\Sigma_s(\boldsymbol{\Omega}'\cdot\boldsymbol{\Omega})\rangle\langle\psi(\boldsymbol{x},\boldsymbol{\Omega}')\rangle d\Omega' + \frac{\langle\nu\Sigma_f\rangle}{4\pi}\int_{4\pi}\langle\psi(\boldsymbol{x},\boldsymbol{\Omega}')\rangle d\Omega' + \frac{\langle Q(\boldsymbol{x})\rangle}{4\pi}\,.$$

$$\text{(2.61c)}\quad \langle\psi(\boldsymbol{x}_s,\boldsymbol{\Omega})\rangle = \psi_b(\boldsymbol{x}_s,\boldsymbol{\Omega})\,,\qquad \mathbf{n}\cdot\boldsymbol{\Omega} < 0\,.$$

For a formal derivation of this result using the multiscale expansion technique, we refer the reader to the work in [27], or to a particular case of this work presented in [85].

Finally, applying this theory on Eqs. (2.37) and (2.38), we obtain the *atomic mix diffusion equations*

$$-\mathrm{D}^{am}\nabla^2\langle\Phi(\boldsymbol{x})\rangle + \langle\Sigma_a\rangle\langle\Phi(\boldsymbol{x})\rangle = \langle Q(\boldsymbol{x})\rangle \tag{2.62}$$

and

$$-\mathrm{D}^{am}\nabla^2\langle\Phi(\boldsymbol{x})\rangle + \langle\Sigma_a\rangle\langle\Phi(\boldsymbol{x})\rangle = \langle\nu\Sigma_f\rangle\langle\Phi(\boldsymbol{x})\rangle + \langle Q(\boldsymbol{x})\rangle\,, \tag{2.63}$$

where the *atomic mix diffusion coefficient* is simply given by

$$\mathrm{D}^{am} = \frac{1}{3(\langle\Sigma_t\rangle - \overline{\mu}_0\langle\Sigma_s\rangle)}\,. \tag{2.64}$$

2.4 Corrections for the Atomic Mix Diffusion Coefficient

In 1949, Behrens investigated the increase in the migration length of neutrons in a reactor caused by the presence of "holes" in the reactor [5]. In that work, "holes" are

primarily understood to be the coolant spaces, due to the low density of the substances used as coolants. He also noticed that a small anisotropic effect occurred depending on the shape of the holes. For the case of pebble beds in which $r\Sigma_t << 1$, he proposed that the isotropic diffusion coefficient D^B be given by

$$\mathrm{D}^B = \left(1 + \frac{2}{3}\frac{\phi^2}{(1+\phi)^2} r\Sigma_t \mathrm{Q}_B\right) \mathrm{D}^{am}\,, \tag{2.65}$$

where Σ_t is the total cross section of the solid material, r is the radius of a pebble, ϕ is the hole/material volume ratio of the system, D^{am} is the diffusion constant in a homogeneous model (the atomic mix diffusion coefficient), and Q_B is the quotient of the mean square path length through the hole divided by the square of the mean path length through the hole, estimated by

$$\mathrm{Q}_B = 1 + \frac{1}{8\phi^2}\,. \tag{2.66}$$

Later work [58, 73] emphasized the general validity of these equations for pebble-bed problems, but although Eq. (2.65) was mostly applied for a long time, in his work Behrens rather recommended the expression

$$\mathrm{D}^B = \left[1 + \frac{\phi^2}{(1+\phi)^2}\left(\frac{2}{3} r\Sigma_t \mathrm{Q}_B + \frac{\frac{4}{3} r\Sigma_t}{\exp\left[\frac{4}{3} r\Sigma_t\right] - 1} - 1\right)\right] \mathrm{D}^{am} \tag{2.67}$$

for holes of any kind.

In 1980, Lieberoth & Stojadinović [48] revisited this theory. They developed a mock-up model of a pebble-bed using steel balls and measured the coordinates of 3,024 sphere centers so that Monte Carlo games for neutron diffusion could be established. Using these results (as well as Monte Carlo calculations for crystal structures), they proposed an improved expression for Q_B:

$$\mathrm{Q}_L = 1.956 + \frac{1}{260\phi^2}\,, \tag{2.68}$$

which also more closely relates to the theoretical value Q = 2 obtained for randomly overlapping spheres [76]. Moreover, under the assumption that no correlation exists between the passage lengths in the holes and in the balls, they developed the following formula for the diffusion lengths:

$$\mathrm{D}^L = \left\{1+\frac{\phi^2}{(1+\phi)^2}\left[\frac{2}{3}r\Sigma_t \mathrm{Q}_L + \frac{4}{3}r\Sigma_t\left(\frac{2r^2\Sigma_t^2}{2r^2\Sigma_t^2-1+(1+2r\Sigma_t)e^{-2r\Sigma_t}}-1\right)-1\right]\right\}\mathrm{D}^{am}\,. \tag{2.69}$$

This correction is still used when more accurate estimates of neutron streaming in pebble-bed type reactors are required [7, 90].

CHAPTER III

The Proposed Generalized Theory

In the classical theory of time-independent linear particle transport, the incremental probability dp that a particle at point $\boldsymbol{x}$ with energy E will experience an interaction while traveling an incremental distance ds is given by $dp = \Sigma_t(\boldsymbol{x}, E)ds$, where Σ_t (the cross section) is independent of $\boldsymbol{\Omega}$ and:

(3.1) $$s = \begin{array}{l}\text{the path length traveled by the particle since} \\ \text{its previous interaction (birth or scattering) .}\end{array}$$

The assumption that Σ_t is independent of $\boldsymbol{\Omega}$ and s is valid when the locations of the scattering centers in the system are uncorrelated. Moreover, for homogeneous media, $\Sigma_t(\boldsymbol{x}, E) = \Sigma_t(E)$ is independent of space, and the probability distribution function for distance-to-collision is an exponential [as described in Eq. (2.12)].

In an inhomogeneous medium, Σ_t being independent of space holds only locally; that is, if $\boldsymbol{x_i} \in$ material i, then $\Sigma_t(\boldsymbol{x_i}, E) = \Sigma_{ti}(E)$. However, during their flight paths, particles travel through different materials with randomly-located interfaces. Hence, Σ_t will depend upon space, and the probability distribution function for distance-to-collision will *not* be an exponential.

For inhomogeneous systems such as a pebble-bed reactor (or an atmospheric cloud), the physically correct mathematical theory for the transport of neutrons in the reactor (or of photons in the cloud) is given by the linear Boltzmann equation (2.25), with highly

space-dependent cross sections. Unfortunately, due to the statistical distribution of the materials, it is impossible to specify the cross sections at any given point in these systems. Thus, it is necessary to develop models that describe transport problems in this situation.

One such model is the atomic mix approximation, as described in section 2.3. It homogenizes the system by volume-averaging the parameters of the different materials (such as the cross sections), which leads to an exponential probability ditribution function for the distance-to-collision. Furthermore, the pebbles in a pebble-bed reactor are O(1) mean free paths thick, and the atomic mix approximation can [84, 85] be inaccurate when the chunk sizes of the constituent materials are not small when compared to a mean free path (with very particular exceptions [44]).

Here, we present a new model to describe this type of transport problem. *In a random medium, where the material interfaces are unknown, we propose to replace the true non-exponential probability distribution function for the distance-to-collision by its ensemble-average.* This ensemble-averaged probability distribution function is used at all points to determine how far particles travel between collisions. When collisions between the particles and the scattering centers occur, the changes in energy and direction are determined by the physically correct probability distribution functions.

The concept of a generalized Boltzmann equation was first introduced by Larsen [45], with the assumption that the positions of the scattering centers are correlated but independent of direction $\mathbf{\Omega}$; that is, Σ_t is independent of $\mathbf{\Omega}$ but not s. Since then, we have extended this approach to the case in which the incremental probability dp that a particle at point $\boldsymbol{x}$ with energy E will experience an interaction while traveling an incremental distance ds in a direction $\mathbf{\Omega}$ is given by $dp = \Sigma_t(\boldsymbol{x}, \mathbf{\Omega}, s, E)ds$ [86]. This implies that Σ_t must depend upon both s and $\mathbf{\Omega}$, since the locations of the scattering centers in the system are not only correlated, but dependent upon direction as well.

We will not consider the most general problem, but will instead follow the assumptions presented in [45, 86] for simplicity. Namely, we will assume that

- The physical system is infinite and statistically homogeneous.
- Particle transport is monoenergetic. (However, the inclusion of energy-dependence is straightforward.)
- Particle transport is driven by a known interior isotropic source $Q(\boldsymbol{x})$ satisfying $Q \to 0$ as $|\boldsymbol{x}| \to \infty$.
- $\Sigma_t(\boldsymbol{\Omega}, s)$ is known. (We discuss how to obtain it in Section 3.6.)
- The distribution function $P(\boldsymbol{\Omega} \cdot \boldsymbol{\Omega}')$ for scattering from $\boldsymbol{\Omega}'$ to $\boldsymbol{\Omega}$ is independent of s. (The correlation in positions of the scattering centers affects the probability of collision, but not the scattering properties when scattering events occur.)

Based on these assumptions we shall now proceed to a formal derivation of the generalized Boltzmann equation.

3.1 Derivation of the Generalized Boltzmann Equation

Using the notation $\boldsymbol{x} = (x, y, z) =$ position and $\boldsymbol{\Omega} = (\Omega_x, \Omega_y, \Omega_z) =$ direction of flight (with $|\boldsymbol{\Omega}| = 1$), and using Eq. (3.1) for s, we define:

(3.2a) $\hat{n}(\boldsymbol{x}, \boldsymbol{\Omega}, s) dV d\Omega ds =$ the number of particles in $dV d\Omega ds$ about $(\boldsymbol{x}, \boldsymbol{\Omega}, s)$,

(3.2b) $$v = \frac{ds}{dt} = \text{ the particle speed ,}$$

(3.2c) $$\hat{\psi}(\boldsymbol{x}, \boldsymbol{\Omega}, s) = v\hat{n}(\boldsymbol{x}, \boldsymbol{\Omega}, s) = \text{ the angular flux ,}$$

(3.2d) $\Sigma_t(\boldsymbol{\Omega}, s) ds =$ the probability that a particle that has traveled a distance s in the direction $\boldsymbol{\Omega}$ since its previous interaction (birth as a source particle or scattering) will experience its next interaction while traveling a further distance ds,

(3.2e) $c =$ the probability that when a particle experiences a collision, it will scatter (c is independent of s and $\boldsymbol{\Omega}$),

(3.2f) $P(\boldsymbol{\Omega}' \cdot \boldsymbol{\Omega})d\Omega =$ the probability that when a particle with direction of flight $\boldsymbol{\Omega}'$ scatters, its outgoing direction of flight will lie in $d\Omega$ about $\boldsymbol{\Omega}$ (P is independent of s),

(3.2g) $Q(\boldsymbol{x})dV =$ the rate at which source particles are isotropically emitted by an internal source $Q(\boldsymbol{x})$ in dV about $\boldsymbol{x}$.

Classic manipulations directly lead to:

(3.3a) $$\begin{aligned}\frac{\partial}{\partial s}\hat{\psi}(\boldsymbol{x},\boldsymbol{\Omega},s)dVd\Omega ds =& \frac{\partial}{v\partial t}v\hat{n}(\boldsymbol{x},\boldsymbol{\Omega},s)dVd\Omega ds \\ =& \frac{\partial}{\partial t}\hat{n}(\boldsymbol{x},\boldsymbol{\Omega},s)dVd\Omega ds \\ =& \text{ the rate of change of the number of particles in } dVd\Omega ds \text{ about } (\boldsymbol{x},\boldsymbol{\Omega},s)\,,\end{aligned}$$

(3.3b) $|\boldsymbol{\Omega}\cdot\mathbf{n}|\hat{\psi}(\boldsymbol{x},\boldsymbol{\Omega},s)dSd\Omega ds =$ the rate at which particles in $d\Omega ds$ about $(\boldsymbol{\Omega},s)$ flow through an incremental surface area dS with unit normal vector $\mathbf{n}$,

(3.3c) $\boldsymbol{\Omega}\cdot\boldsymbol{\nabla}\hat{\psi}(\boldsymbol{x},\boldsymbol{\Omega},s)dVd\Omega ds =$ the net rate at which particles in $d\Omega ds$ about $(\boldsymbol{\Omega},s)$ flow (leak) out of dV about $\boldsymbol{x}$,

(3.3d) $$\begin{aligned}\Sigma_t(\boldsymbol{\Omega},s)\hat{\psi}(\boldsymbol{x},\boldsymbol{\Omega},s)dVd\Omega ds =& \Sigma_t(\boldsymbol{\Omega},s)\frac{ds}{dt}\hat{n}(\boldsymbol{x},\boldsymbol{\Omega},s)dVd\Omega ds \\ =& \frac{1}{dt}[\Sigma_t(\boldsymbol{\Omega},s)ds][\hat{n}(\boldsymbol{x},\boldsymbol{\Omega},s)dVd\Omega ds] \\ =& \text{ the rate at which particles in } dVd\Omega ds \text{ about } (\boldsymbol{x},\boldsymbol{\Omega},s) \text{ experience collisions.}\end{aligned}$$

The treatment of the inscattering and source terms requires extra care. From Eq. (3.3d),

$$\left[\int_0^\infty \Sigma_t(\boldsymbol{\Omega}',s')\hat{\psi}(\boldsymbol{x},\boldsymbol{\Omega}',s')ds'\right]dVd\Omega' = \text{ the rate at which particles in } dVd\Omega' \text{ about } (\boldsymbol{x},\boldsymbol{\Omega}') \text{ experience collisions.}$$

Multiplying this expression by $cP(\boldsymbol{\Omega}\cdot\boldsymbol{\Omega}')d\Omega$, we obtain:

$$cP(\boldsymbol{\Omega}\cdot\boldsymbol{\Omega}')\left[\int_0^\infty \Sigma_t(\boldsymbol{\Omega}',s')\hat{\psi}(\boldsymbol{x},\boldsymbol{\Omega}',s')ds'\right]dVd\Omega' d\Omega =$$

$$= \text{ the rate at which particles in } dVd\Omega' \text{ about } (\boldsymbol{x},\boldsymbol{\Omega}') \text{ scatter into } dVd\Omega \text{ about } (\boldsymbol{x},\boldsymbol{\Omega}).$$

Integrating this expression over $\mathbf{\Omega}' \in 4\pi$, we get:

$$\left[c \int_{4\pi} \int_0^\infty P(\mathbf{\Omega}' \cdot \mathbf{\Omega}) \Sigma_t(\mathbf{\Omega}', s') \hat{\psi}(\boldsymbol{x}, \mathbf{\Omega}', s')\, ds' d\Omega'\right] dV d\Omega$$

$$= \text{the rate at which particles scatter into } dV d\Omega \text{ about } (\boldsymbol{x}, \mathbf{\Omega}) \ .$$

Finally, when particles emerge from a scattering event their value of s is "reset" to $s = 0$. Therefore, the path length spectrum of particles that emerge from scattering events is the delta function $\delta(s)$. Multiplying the previous expression by $\delta(s)ds$, we obtain:

$$\text{(3.3e)} \quad \left[\delta(s) c \int_{4\pi} \int_0^\infty P(\mathbf{\Omega}' \cdot \mathbf{\Omega}) \Sigma_t(\mathbf{\Omega}', s') \hat{\psi}(\boldsymbol{x}, \mathbf{\Omega}', s')\, ds' d\Omega'\right] dV d\Omega ds$$

$$= \text{the rate at which particles scatter into } dV d\Omega ds \text{ about } (\boldsymbol{x}, \mathbf{\Omega}, s) \ .$$

Also,

$$\text{(3.3f)} \qquad \delta(s) \frac{Q(\boldsymbol{x})}{4\pi} dV d\Omega ds = \begin{array}{l}\text{the rate at which source particles are} \\ \text{emitted into } dV d\Omega ds \text{ about } (\boldsymbol{x}, \mathbf{\Omega}, s).\end{array}$$

We now use the familiar conservation equation (in each of the following terms, the phrase "of particles in $dV d\Omega ds$ about $(\boldsymbol{x}, \mathbf{\Omega}, s)$" is omitted):

$$\text{(3.4)} \qquad \text{Rate of change} = \text{Rate of gain} - \text{Rate of loss}$$

$$= \begin{array}{l}(\text{Inscatter rate} + \text{Source rate}) \\ -(\text{Net leakage rate} + \text{Collision rate}).\end{array}$$

Introducing Eqs. (3.3) into this expression and dividing by $dV d\Omega ds$, we obtain the *generalized Boltzmann equation* (GBE) for $\hat{\psi}(\boldsymbol{x}, \mathbf{\Omega}, s)$:

$$\text{(3.5)} \qquad \frac{\partial \hat{\psi}}{\partial s}(\boldsymbol{x}, \mathbf{\Omega}, s) + \mathbf{\Omega} \cdot \boldsymbol{\nabla} \hat{\psi}(\boldsymbol{x}, \mathbf{\Omega}, s) + \Sigma_t(\mathbf{\Omega}, s) \hat{\psi}(\boldsymbol{x}, \mathbf{\Omega}, s)$$

$$= \delta(s)\, c \int_{4\pi} \int_0^\infty P(\mathbf{\Omega}' \cdot \mathbf{\Omega}) \Sigma_t(\mathbf{\Omega}', s') \hat{\psi}(\boldsymbol{x}, \mathbf{\Omega}', s')\, ds' d\Omega' + \delta(s) \frac{Q(\boldsymbol{x})}{4\pi} \, .$$

To repeat, we have for simplicity assumed an infinite homogeneous system with a "local" source $Q(\boldsymbol{x})$; and we take $\hat{\psi}(\boldsymbol{x}, \mathbf{\Omega}, s) \to 0$ as $|\boldsymbol{x}| \to \infty$.

Equation (3.5) can be written in a mathematically equivalent way in which the delta function is not present. We write Eq. (3.5) for $s > 0$:

$$\frac{\partial\hat{\psi}}{\partial s}(\boldsymbol{x},\boldsymbol{\Omega},s) + \boldsymbol{\Omega}\cdot\boldsymbol{\nabla}\hat{\psi}(\boldsymbol{x},\boldsymbol{\Omega},s) + \Sigma_t(\boldsymbol{\Omega},s)\hat{\psi}(\boldsymbol{x},\boldsymbol{\Omega},s) = 0\,. \tag{3.6a}$$

Then we operate on Eq. (3.5) by $\lim_{\varepsilon\to 0}\int_{-\varepsilon}^{\varepsilon}(\cdot)\,ds$ and use $\hat{\psi} = 0$ for $s < 0$ to obtain:

$$\hat{\psi}(\boldsymbol{x},\boldsymbol{\Omega},0) = c\int_{4\pi}\int_0^\infty P(\boldsymbol{\Omega}'\cdot\boldsymbol{\Omega})\Sigma_t(\boldsymbol{\Omega}',s')\hat{\psi}(\boldsymbol{x},\boldsymbol{\Omega}',s')\,ds'd\Omega' + \frac{Q(\boldsymbol{x})}{4\pi}\,. \tag{3.6b}$$

Equations (3.6) are mathematically equivalent to Eq. (3.5).

To establish the relationship between the present work and the classic number density and angular flux, we integrate Eq. (3.2a) over s and obtain:

$$\left[\int_0^\infty \hat{n}(\boldsymbol{x},\boldsymbol{\Omega},s)\,ds\right] dVd\Omega = \begin{array}{l}\text{the total number of particles}\\ \text{in } dVd\Omega \text{ about } (\boldsymbol{x},\boldsymbol{\Omega})\end{array}\,. \tag{3.7}$$

Therefore,

$$n(\boldsymbol{x},\boldsymbol{\Omega}) = \int_0^\infty \hat{n}(\boldsymbol{x},\boldsymbol{\Omega},s)\,ds = \text{ classic number density,} \tag{3.8}$$

and

$$\psi(\boldsymbol{x},\boldsymbol{\Omega}) = vn(\boldsymbol{x},\boldsymbol{\Omega}) = \int_0^\infty \hat{\psi}(\boldsymbol{x},\boldsymbol{\Omega},s)\,ds = \text{ classic angular flux,} \tag{3.9}$$

as defined in Chapter II.

3.2 The Angular-Dependent Path Length and Equilibrium Path Lengh Distributions

Without loss of generality, let us consider a single particle released from an interaction site at $x = 0$ in the direction $\boldsymbol{\Omega} = \boldsymbol{i}$ = direction of the positive x-axis. Eq. (3.6a) for this particle becomes:

$$\frac{\partial\hat{\psi}}{\partial s}(x,\boldsymbol{\Omega}=\boldsymbol{i},s) + \frac{\partial\hat{\psi}}{\partial x}(x,\boldsymbol{\Omega}=\boldsymbol{i},s) + \Sigma_t(\boldsymbol{\Omega}=\boldsymbol{i},s)\hat{\psi}(x,\boldsymbol{\Omega}=\boldsymbol{i},s) = 0\,. \tag{3.10}$$

For this particle, we have $x(s) = s$ and $\hat{\psi}(x(s), \boldsymbol{i}, s) \equiv F(\boldsymbol{i}, s)$. Therefore,

$$\frac{dF}{ds}(\boldsymbol{i}, s) = \frac{\partial \hat{\psi}}{\partial x}(x(s), \boldsymbol{i}, s)\left(\frac{dx}{ds}\right) + \frac{\partial \hat{\psi}}{\partial s}(x(s), \boldsymbol{i}, s) = \frac{\partial \hat{\psi}}{\partial x} + \frac{\partial \hat{\psi}}{\partial s} \ . \tag{3.11}$$

Equation (3.10) will then simplify to:

$$\frac{dF}{ds}(\boldsymbol{i}, s) + \Sigma_t(\boldsymbol{i}, s)F(\boldsymbol{i}, s) = 0 \ . \tag{3.12a}$$

We apply the initial condition

$$F(\boldsymbol{i}, 0) = 1 \ , \tag{3.12b}$$

since we are considering a single particle. The solution of Eqs. (3.12) is:

$$F(\boldsymbol{\Omega} = \boldsymbol{i}, s) = e^{-\int_0^s \Sigma_t(\boldsymbol{\Omega}=\boldsymbol{i}, s')\, ds'} \tag{3.13}$$

$$= \text{the probability that the particle will travel the distance } s \text{ in the given direction } \boldsymbol{\Omega} = \boldsymbol{i} \text{ without interacting .}$$

We can generalize this equation for all directions, which gives

$$F(\boldsymbol{\Omega}, s) = e^{-\int_0^s \Sigma_t(\boldsymbol{\Omega}, s')\, ds'} \tag{3.14}$$

$$= \text{the probability that the particle will travel the distance } s \text{ in a given direction } \boldsymbol{\Omega} \text{ without interacting.}$$

The probability of a collision between s and $s + ds$ in a given direction $\boldsymbol{\Omega}$ is:

$$\Sigma_t(\boldsymbol{\Omega}, s)F(\boldsymbol{\Omega}, s)ds = p_{s|\boldsymbol{\Omega}}(s|\boldsymbol{\Omega})ds \ , \tag{3.15}$$

and therefore:

$$p_{s|\boldsymbol{\Omega}}(s|\boldsymbol{\Omega}) = \Sigma_t(\boldsymbol{\Omega}, s)e^{-\int_0^s \Sigma_t(\boldsymbol{\Omega}, s')\, ds'} \tag{3.16}$$

$$= \text{conditional distribution function for the distance-to-collision in a given direction } \boldsymbol{\Omega}.$$

Let us define

(3.17) $p_{\mathbf{\Omega}}(\mathbf{\Omega})d\Omega =$ probability that a particle is traveling in $d\Omega$ about $\mathbf{\Omega}$;

and

(3.18) $p(\mathbf{\Omega}, s)d\Omega ds =$ probability that a particle traveling in $d\Omega$ about $\mathbf{\Omega}$ will experience a collision between s and $s + ds$.

Then

(3.19) $p(\mathbf{\Omega}, s)d\Omega ds =$ (prob. that a particle is traveling in $d\Omega$ about $\mathbf{\Omega}$)$\times$(prob. of a collision between s and $s + ds$ in a given direction $\mathbf{\Omega}$)

$$= (p_{\mathbf{\Omega}}(\mathbf{\Omega})d\Omega)(p_{s|\mathbf{\Omega}}(s|\mathbf{\Omega})ds);$$

that is, $p(\mathbf{\Omega}, s)$ is a joint distribution function [30].

Equation (3.16) expresses $p_{s|\mathbf{\Omega}}(s|\mathbf{\Omega})$ in terms of $\Sigma_t(\mathbf{\Omega}, s)$. To express $\Sigma_t(\mathbf{\Omega}, s)$ in terms of $p_{s|\mathbf{\Omega}}(s|\mathbf{\Omega})$, we operate on Eq. (3.16) by $\int_0^s(\cdot)ds'$ and get:

(3.20a) $$\int_0^s p_{s|\mathbf{\Omega}}(s|\mathbf{\Omega})ds' = 1 - e^{-\int_0^s \Sigma_t(\mathbf{\Omega},s')\,ds'} \quad ,$$

or

(3.20b) $$e^{-\int_0^s \Sigma_t(\mathbf{\Omega},s')\,ds'} = 1 - \int_0^s p_{s|\mathbf{\Omega}}(s|\mathbf{\Omega})ds' \quad .$$

Hence,

(3.20c) $$\int_0^s \Sigma_t(\mathbf{\Omega}, s')\,ds' = -\ln\left(1 - \int_0^s p_{s|\mathbf{\Omega}}(s|\mathbf{\Omega})ds'\right) \quad .$$

Differentiating with respect to s, we obtain:

(3.21) $$\Sigma_t(\mathbf{\Omega}, s) = \frac{p_{s|\mathbf{\Omega}}(s|\mathbf{\Omega})}{1 - \int_0^s p_{s|\mathbf{\Omega}}(s|\mathbf{\Omega})ds'} \, .$$

Equations (3.16) and (3.21) show that $p_{s|\mathbf{\Omega}}(s|\mathbf{\Omega})$ is exponential if and only if $\Sigma_t(\mathbf{\Omega}, s)$ is independent of s.

Moreover, for the case of an infinite medium with an "equilibrium" intensity having no space dependence (but dependent on direction), Eq. (3.6a) for $s > 0$ reduces to:

$$\frac{\partial \hat{\psi}}{\partial s}(\mathbf{\Omega}, s) + \Sigma_t(\mathbf{\Omega}, s)\hat{\psi}(\mathbf{\Omega}, s) = 0\,, \tag{3.22}$$

which has the solution

$$\hat{\psi}(\mathbf{\Omega}, s) = \hat{\psi}(\mathbf{\Omega}, 0)e^{-\int_0^s \Sigma_t(\mathbf{\Omega}, s')\, ds'}\,. \tag{3.23}$$

Normalizing this solution to have integral = unity, we obtain:

$$\begin{aligned} \hat{\chi}(\mathbf{\Omega}, s) &= \frac{e^{-\int_0^s \Sigma_t(\mathbf{\Omega}, s')\, ds'}}{\int_0^\infty e^{-\int_0^{s'} \Sigma_t(\mathbf{\Omega}, s'')ds''} ds'} \\ &= \text{ "equilibrium" spectrum of path length } s \text{ in a given direction } \mathbf{\Omega}\,. \end{aligned} \tag{3.24}$$

From Eq. (3.16), the mean distance-to-collision (mean free path) in a given direction $\mathbf{\Omega}$ is:

$$\begin{aligned} \overline{s_{\mathbf{\Omega}}}(\mathbf{\Omega}) &= \int_0^\infty s p_{s|\mathbf{\Omega}}(s|\mathbf{\Omega})\, ds \\ &= \int_0^\infty s \left[\Sigma_t(\mathbf{\Omega}, s)e^{-\int_0^s \Sigma_t(\mathbf{\Omega}, s')ds'}\right] ds \\ &= s\left[-e^{-\int_0^s \Sigma_t(\mathbf{\Omega}, s')ds'}\right]_0^\infty - \int_0^\infty \left[-e^{-\int_0^s \Sigma_t(\mathbf{\Omega}, s')ds'}\right] ds \\ &= \int_0^\infty e^{-\int_0^s \Sigma_t(\mathbf{\Omega}, s')ds'}\, ds\,. \end{aligned} \tag{3.25}$$

Equation (3.24) can then be written:

$$\hat{\chi}(\mathbf{\Omega}, s) = \frac{e^{-\int_0^s \Sigma_t(\mathbf{\Omega}, s')ds'}}{\overline{s_{\mathbf{\Omega}}}(\mathbf{\Omega})}\,, \tag{3.26}$$

and by the Law of Total Expectation [8], the mean free path $\overline{s}$ is given by

$$\overline{s} = \int_{4\pi}\int_0^\infty s p(\mathbf{\Omega}, s) ds d\Omega = \int_{4\pi} p_{\mathbf{\Omega}}(\mathbf{\Omega})\overline{s_{\mathbf{\Omega}}}(\mathbf{\Omega}) d\Omega\,. \tag{3.27}$$

Note: from now on we will assume that $\overline{s_{\mathbf{\Omega}}}(\mathbf{\Omega})$ is an *even* function of the direction of flight $\mathbf{\Omega}$. This makes sense since, from the physical point of view, the mean free path of

a particle traveling in the direction $\boldsymbol{\Omega}$ *must* be equal to the mean free path of a particle traveling in the direction $-\boldsymbol{\Omega}$.

3.3 Integral Equation Formulations of the Generalized Boltzmann Equation

Using the work in [45] as a guide, let us define:

$$\hat{f}(\boldsymbol{x},\boldsymbol{\Omega}) = \int_0^\infty \Sigma_t(\boldsymbol{\Omega},s)\hat{\psi}(\boldsymbol{x},\boldsymbol{\Omega},s)\,ds = \text{ collision rate density,} \tag{3.28}$$

and

$$\hat{g}(\boldsymbol{x},\boldsymbol{\Omega}) = c\int_{4\pi} P(\boldsymbol{\Omega}'\cdot\boldsymbol{\Omega})\hat{f}(\boldsymbol{x},\boldsymbol{\Omega}')\,d\Omega' = \text{ inscattering rate density.} \tag{3.29}$$

The definition (3.28) allows us to rewrite Eqs. (3.6) as:

$$\frac{\partial\hat{\psi}}{\partial s}(\boldsymbol{x},\boldsymbol{\Omega},s) + \boldsymbol{\Omega}\cdot\boldsymbol{\nabla}\hat{\psi}(\boldsymbol{x},\boldsymbol{\Omega},s) + \Sigma_t(\boldsymbol{\Omega},s)\hat{\psi}(\boldsymbol{x},\boldsymbol{\Omega},s) = 0\,, \tag{3.30a}$$

$$\hat{\psi}(\boldsymbol{x},\boldsymbol{\Omega},0) = c\int_{4\pi} P(\boldsymbol{\Omega}'\cdot\boldsymbol{\Omega})\hat{f}(\boldsymbol{x},\boldsymbol{\Omega}')\,d\Omega' + \frac{Q(\boldsymbol{x})}{4\pi}\,. \tag{3.30b}$$

Solving Eq. (3.30a) and using Eq. (3.30b), we obtain for $s > 0$

$$\begin{aligned}\hat{\psi}(\boldsymbol{x},\boldsymbol{\Omega},s) &= \hat{\psi}(\boldsymbol{x}-s\boldsymbol{\Omega},\boldsymbol{\Omega},0)e^{-\int_0^s \Sigma_t(\boldsymbol{\Omega},s')ds'} \\ &= \left[c\int_{4\pi} P(\boldsymbol{\Omega}'\cdot\boldsymbol{\Omega})\hat{f}(\boldsymbol{x}-s\boldsymbol{\Omega},\boldsymbol{\Omega}')\,d\Omega' + \frac{Q(\boldsymbol{x}-s\boldsymbol{\Omega})}{4\pi}\right] e^{-\int_0^s \Sigma_t(\boldsymbol{\Omega},s')ds'}\,.\end{aligned} \tag{3.31}$$

Operating on this equation by $\int_0^\infty \Sigma_t(\boldsymbol{\Omega},s)(\cdot)ds$ and using Eqs. (3.28) and (3.16), we get:

$$\begin{aligned}&\hat{f}(\boldsymbol{x},\boldsymbol{\Omega}) \\ &\quad= \int_0^\infty \left[c\int_{4\pi} P(\boldsymbol{\Omega}'\cdot\boldsymbol{\Omega})\hat{f}(\boldsymbol{x}-s\boldsymbol{\Omega},\boldsymbol{\Omega}')\,d\Omega' + \frac{Q(\boldsymbol{x}-s\boldsymbol{\Omega})}{4\pi}\right] p_{s|\boldsymbol{\Omega}}(s|\boldsymbol{\Omega})\,ds\,.\end{aligned} \tag{3.32a}$$

Also, operating on Eq. (3.31) by $\int_0^\infty(\cdot)ds$ and using Eq. (3.9), we obtain:

$$\begin{aligned}&\psi(\boldsymbol{x},\boldsymbol{\Omega}) \\ &\quad= \int_0^\infty \left[c\int_{4\pi} P(\boldsymbol{\Omega}'\cdot\boldsymbol{\Omega})\hat{f}(\boldsymbol{x}-s\boldsymbol{\Omega},\boldsymbol{\Omega}')\,d\Omega' + \frac{Q(\boldsymbol{x}-s\boldsymbol{\Omega})}{4\pi}\right] e^{-\int_0^s \Sigma_t(\boldsymbol{\Omega},s')ds'}\,ds\,.\end{aligned} \tag{3.32b}$$

Using definition (3.29), we can rewrite Eq. (3.32a) as:

$$\hat{f}(\boldsymbol{x},\boldsymbol{\Omega}) = \int_0^\infty \left[\hat{g}(\boldsymbol{x}-s\boldsymbol{\Omega},\boldsymbol{\Omega}) + \frac{Q(\boldsymbol{x}-s\boldsymbol{\Omega})}{4\pi}\right] p_{s|\boldsymbol{\Omega}}(s|\boldsymbol{\Omega})ds\,, \tag{3.33}$$

and operating on this result by $c\int_{4\pi} P(\boldsymbol{\Omega}\cdot\boldsymbol{\Omega}')(\cdot)d\Omega$ we obtain:

$$\hat{g}(\boldsymbol{x},\boldsymbol{\Omega}') = c\int_{4\pi} P(\boldsymbol{\Omega}\cdot\boldsymbol{\Omega}')\int_0^\infty \left[\hat{g}(\boldsymbol{x}-s\boldsymbol{\Omega},\boldsymbol{\Omega}) + \frac{Q(\boldsymbol{x}-s\boldsymbol{\Omega})}{4\pi}\right] p_{s|\boldsymbol{\Omega}}(s|\boldsymbol{\Omega})\,dsd\Omega\,. \tag{3.34}$$

Changing the spatial variables from the 3-D spherical $(\boldsymbol{\Omega}, s)$ to the 3-D Cartesian $\boldsymbol{x}'$ defined by

$$\boldsymbol{x}' = \boldsymbol{x} - s\boldsymbol{\Omega}\,, \tag{3.35}$$

we obtain

$$s = |\boldsymbol{x}-\boldsymbol{x}'|\,, \tag{3.36a}$$

$$\boldsymbol{\Omega} = \frac{\boldsymbol{x}-\boldsymbol{x}'}{|\boldsymbol{x}-\boldsymbol{x}'|}\,, \tag{3.36b}$$

$$s^2 dsd\Omega = dV'\,. \tag{3.36c}$$

Now, we can rewrite Eq. (3.34) as:

$$\begin{aligned}\hat{g}(\boldsymbol{x},\boldsymbol{\Omega}) &= c\iiint P\left(\frac{\boldsymbol{x}-\boldsymbol{x}'}{|\boldsymbol{x}-\boldsymbol{x}'|}\cdot\boldsymbol{\Omega}\right)\left[\hat{g}\left(\boldsymbol{x}',\frac{\boldsymbol{x}-\boldsymbol{x}'}{|\boldsymbol{x}-\boldsymbol{x}'|}\right) + \frac{Q(\boldsymbol{x}')}{4\pi}\right]\frac{\tilde{p}(|\boldsymbol{x}-\boldsymbol{x}'|)}{|\boldsymbol{x}-\boldsymbol{x}'|^2}\,dV'\,,\end{aligned} \tag{3.37a}$$

where $\tilde{p}(|\boldsymbol{x}-\boldsymbol{x}'|)dV'$ is the conditional probability that, given the direction defined by $\boldsymbol{x}-\boldsymbol{x}'$, a particle moving from a point $\boldsymbol{x}$ to a point lying in dV' about $\boldsymbol{x}'$ will experience a collision. Definition (3.29) allows us to rewrite Eq. (3.32b) as well:

$$\psi(\boldsymbol{x},\boldsymbol{\Omega}) = \int_0^\infty \left[\hat{g}(\boldsymbol{x}-s\boldsymbol{\Omega},\boldsymbol{\Omega}) + \frac{Q(\boldsymbol{x}-s\boldsymbol{\Omega})}{4\pi}\right] e^{-\int_0^s \Sigma_t(\boldsymbol{\Omega},s')ds'}\,ds\,. \tag{3.37b}$$

Finally, for the case of isotropic scattering (in which $P(\boldsymbol{\Omega}'\cdot\boldsymbol{\Omega}) = 1/4\pi$), $\hat{g}(\boldsymbol{x},\boldsymbol{\Omega})$ in Eq. (3.29) becomes isotropic:

$$\hat{g}(\boldsymbol{x}) = \frac{c}{4\pi}\int_{4\pi}\hat{f}(\boldsymbol{x},\boldsymbol{\Omega}')d\Omega' \equiv \frac{c}{4\pi}\hat{F}(\boldsymbol{x})\,, \tag{3.38a}$$

where

$$\hat{F}(\boldsymbol{x}) = \int_{4\pi} \hat{f}(\boldsymbol{x}, \boldsymbol{\Omega}')d\Omega' = \text{ scalar collision rate density.} \tag{3.38b}$$

Equation (3.37a) will then be reduced to

$$\hat{F}(\boldsymbol{x}) = \iiint \left[c\hat{F}(\boldsymbol{x}') + Q(\boldsymbol{x}')\right] \frac{\tilde{p}(|\boldsymbol{x} - \boldsymbol{x}'|)}{4\pi|\boldsymbol{x} - \boldsymbol{x}'|^2}\, dV'\,; \tag{3.39a}$$

and using Eq. (3.38a), we write Eq. (3.37b) as:

$$\psi(\boldsymbol{x}, \boldsymbol{\Omega}) = \frac{1}{4\pi} \int_0^\infty \left[c\hat{F}(\boldsymbol{x} - s\boldsymbol{\Omega}) + Q(\boldsymbol{x} - s\boldsymbol{\Omega})\right] e^{-\int_0^s \Sigma_t(\boldsymbol{\Omega}, s')ds'} ds\,. \tag{3.39b}$$

Operating on this equation by $\int_{4\pi}(\cdot)d\Omega$ and using Eqs. (3.35) and (3.36), we obtain the classic scalar flux $\Phi(\boldsymbol{x})$:

$$\Phi(\boldsymbol{x}) = \iiint \left[c\hat{F}(\boldsymbol{x}') + Q(\boldsymbol{x}')\right] \frac{e^{-\int_0^{|\boldsymbol{x}-\boldsymbol{x}'|} \Sigma_t\left(\frac{\boldsymbol{x}-\boldsymbol{x}'}{|\boldsymbol{x}-\boldsymbol{x}'|}, s'\right)ds'}}{4\pi|\boldsymbol{x} - \boldsymbol{x}'|^2} dV'\,. \tag{3.39c}$$

To summarize: for general anisotropic scattering, Eq. (3.32b) yields the classic angular flux $\psi(\boldsymbol{x}, \boldsymbol{\Omega})$ in terms of $\hat{f}(\boldsymbol{x}, \boldsymbol{\Omega})$, which is obtained by solving Eq. (3.32a). Moreover, one can write an integral equation formulation of the GBE [Eqs. (3.37)] that does not contain the pathlength variable s as an independent variable. Finally, if scattering is isotropic, then the classic scalar flux can be obtained using Eqs. (3.39a) and (3.39c), in which the direction variable $\boldsymbol{\Omega}$ also does not occur as an independent variable.

3.4 Asymptotic Diffusion Limit of the Generalized Boltzmann Equation

To begin this discussion, we must first consider the Legendre polynomial expansion of the distribution function $P(\boldsymbol{\Omega} \cdot \boldsymbol{\Omega}') = P(\mu_0)$ defined by Eq. (3.2f) [47]:

$$P(\mu_0) = \sum_{n=0}^{\infty} \frac{2n+1}{4\pi} a_n P_n(\mu_0)\,, \tag{3.40}$$

where $a_0 = 1$ and $a_1 = \overline{\mu}_0$ = mean scattering cosine. We define $P^*(\mu_0)$ by:

$$P^*(\mu_0) = cP(\mu_0) + \frac{1-c}{4\pi}\,, \tag{3.41}$$

which has the Legendre polynomial expansion:

$$P^*(\mu_0) = \sum_{n=0}^{\infty} \frac{2n+1}{4\pi} a_n^* P_n(\mu_0)\,, \tag{3.42a}$$

$$a_n^* = \begin{cases} 1 & , \quad n = 0 \\ ca_n & , \quad n \geq 1 \end{cases}\,. \tag{3.42b}$$

Using the work in [41] as a guide, we scale $\Sigma_t = O(\varepsilon^{-1})$, $1 - c = O(\varepsilon^2)$, $Q = O(\varepsilon)$, $P^*(\mu_0)$ is independent of ε, and $\partial\hat{\psi}/\partial s = O(\varepsilon^{-1})$, with $\varepsilon \ll 1$. Equations (3.5) and (3.41) yield, in this scaling,

$$\begin{aligned} \frac{1}{\varepsilon}\frac{\partial\hat{\psi}}{\partial s}(\boldsymbol{x},\boldsymbol{\Omega},s) + \boldsymbol{\Omega}\cdot\boldsymbol{\nabla}\hat{\psi}(\boldsymbol{x},\boldsymbol{\Omega},s) + \frac{\Sigma_t(\boldsymbol{\Omega},s)}{\varepsilon}\hat{\psi}(\boldsymbol{x},\boldsymbol{\Omega},s) \\ = \delta(s)\int_{4\pi}\int_0^{\infty}\left[P^*(\boldsymbol{\Omega}\cdot\boldsymbol{\Omega}') - \varepsilon^2\frac{1-c}{4\pi}\right]\frac{\Sigma_t(\boldsymbol{\Omega}',s')}{\varepsilon}\hat{\psi}(\boldsymbol{x},\boldsymbol{\Omega}',s')\,ds'd\Omega' \\ + \varepsilon\delta(s)\frac{Q(\boldsymbol{x})}{4\pi}\,. \end{aligned} \tag{3.43}$$

Let us define $\Psi(\boldsymbol{x},\boldsymbol{\Omega},s)$ by:

$$\hat{\psi}(\boldsymbol{x},\boldsymbol{\Omega},s) \equiv \Psi(\boldsymbol{x},\boldsymbol{\Omega},s)\frac{e^{-\int_0^s \Sigma_t(\boldsymbol{\Omega},s')ds'}}{\overline{s}}\,. \tag{3.44}$$

Then, using Eq. (3.16), Eq. (3.43) for $\hat{\psi}(\boldsymbol{x},\boldsymbol{\Omega},s)$ becomes the following equation for $\Psi(\boldsymbol{x},\boldsymbol{\Omega},s)$:

$$\begin{aligned} \frac{\partial\Psi}{\partial s}(\boldsymbol{x},\boldsymbol{\Omega},s) + \varepsilon\boldsymbol{\Omega}\cdot\boldsymbol{\nabla}\Psi(\boldsymbol{x},\boldsymbol{\Omega},s) \\ = \delta(s)\int_{4\pi}\int_0^{\infty}\left[P^*(\boldsymbol{\Omega}\cdot\boldsymbol{\Omega}') - \varepsilon^2\frac{1-c}{4\pi}\right]p_{s|\boldsymbol{\Omega}}(s'|\boldsymbol{\Omega}')\Psi(\boldsymbol{x},\boldsymbol{\Omega}',s')\,ds'd\Omega' \\ + \varepsilon^2\delta(s)\overline{s}\frac{Q(\boldsymbol{x})}{4\pi}\,. \end{aligned} \tag{3.45}$$

This equation is mathematically equivalent to:

$$\frac{\partial\Psi}{\partial s}(\boldsymbol{x},\boldsymbol{\Omega},s) + \varepsilon\boldsymbol{\Omega}\cdot\boldsymbol{\nabla}\Psi(\boldsymbol{x},\boldsymbol{\Omega},s) = 0 \quad , \quad s > 0\,, \tag{3.46a}$$

$$\begin{aligned} \Psi(\boldsymbol{x},\boldsymbol{\Omega},0) = \int_{4\pi}\left[P^*(\boldsymbol{\Omega}\cdot\boldsymbol{\Omega}') - \varepsilon^2\frac{1-c}{4\pi}\right]\int_0^{\infty} p_{s|\boldsymbol{\Omega}}(s'|\boldsymbol{\Omega}')\Psi(\boldsymbol{x},\boldsymbol{\Omega}',s')ds'd\Omega' \\ + \varepsilon^2\overline{s}\frac{Q(\boldsymbol{x})}{4\pi}\,. \end{aligned} \tag{3.46b}$$

Integrating Eq. (3.46a) over $0 < s' < s$, we obtain:

$$\begin{aligned}(3.47)\quad \Psi(\boldsymbol{x},\boldsymbol{\Omega},s) &= \Psi(\boldsymbol{x},\boldsymbol{\Omega},0) - \varepsilon\boldsymbol{\Omega}\cdot\boldsymbol{\nabla}\int_0^s \Psi(\boldsymbol{x},\boldsymbol{\Omega},s')\,ds' \\ &= \int_{4\pi}\left[P^*(\boldsymbol{\Omega}\cdot\boldsymbol{\Omega}') - \varepsilon^2\frac{1-c}{4\pi}\right]\int_0^\infty p_{s|\boldsymbol{\Omega}}(s'|\boldsymbol{\Omega}')\Psi(\boldsymbol{x},\boldsymbol{\Omega}',s')ds'd\Omega' \\ &\quad + \varepsilon^2\overline{s}\frac{Q(\boldsymbol{x})}{4\pi} - \varepsilon\boldsymbol{\Omega}\cdot\boldsymbol{\nabla}\int_0^s \Psi(\boldsymbol{x},\boldsymbol{\Omega},s')\,ds'\,.\end{aligned}$$

Introducing into this equation the ansatz

$$(3.48)\qquad \Psi(\boldsymbol{x},\boldsymbol{\Omega},s) = \sum_{n=0}^{\infty}\varepsilon^n\Psi^{(n)}(\boldsymbol{x},\boldsymbol{\Omega},s)$$

and equating the coefficients of different powers of ε, we obtain for $n \geq 0$:

$$\begin{aligned}(3.49)\quad \Psi^{(n)}(\boldsymbol{x},\boldsymbol{\Omega},s) &= \int_{4\pi} P^*(\boldsymbol{\Omega}\cdot\boldsymbol{\Omega}')\int_0^\infty p_{s|\boldsymbol{\Omega}}(s'|\boldsymbol{\Omega}')\Psi^{(n)}(\boldsymbol{x},\boldsymbol{\Omega}',s')ds'd\Omega' \\ &\quad - \boldsymbol{\Omega}\cdot\boldsymbol{\nabla}\int_0^s \Psi^{(n-1)}(\boldsymbol{x},\boldsymbol{\Omega},s')\,ds' \\ &\quad - \frac{1-c}{4\pi}\int_{4\pi}\int_0^\infty p_{s|\boldsymbol{\Omega}}(s'|\boldsymbol{\Omega}')\Psi^{(n-2)}(\boldsymbol{x},\boldsymbol{\Omega}',s')ds'd\Omega' \\ &\quad + \delta_{n,2}\overline{s}\frac{Q(\boldsymbol{x})}{4\pi}\,.\end{aligned}$$

We shall solve these equations recursively, using the Legendre polynomial expansion (3.42) of $P^*(\mu_0)$.

Equation (3.49) with $n = 0$ is:

$$(3.50)\qquad \Psi^{(0)}(\boldsymbol{x},\boldsymbol{\Omega},s) = \int_{4\pi} P^*(\boldsymbol{\Omega}\cdot\boldsymbol{\Omega}')\int_0^\infty p_{s|\boldsymbol{\Omega}}(s'|\boldsymbol{\Omega}')\Psi^{(0)}(\boldsymbol{x},\boldsymbol{\Omega}',s')ds'd\Omega'\,.$$

The general solution of this equation is:

$$(3.51)\qquad \Psi^{(0)}(\boldsymbol{x},\boldsymbol{\Omega},s) = \frac{\Phi^{(0)}(\boldsymbol{x})}{4\pi}\,,$$

where $\Phi^{(0)}(\boldsymbol{x})$ is, at this point, undetermined.

Next, Eq. (3.49) with $n = 1$ is:

$$\begin{aligned}(3.52)\quad \Psi^{(1)}(\boldsymbol{x},\boldsymbol{\Omega},s) &= \int_{4\pi} P^*(\boldsymbol{\Omega}\cdot\boldsymbol{\Omega}')\int_0^\infty p_{s|\boldsymbol{\Omega}}(s'|\boldsymbol{\Omega}')\Psi^{(1)}(\boldsymbol{x},\boldsymbol{\Omega}',s')ds'd\Omega' \\ &\quad - s\boldsymbol{\Omega}\cdot\boldsymbol{\nabla}\frac{\Phi^{(0)}(\boldsymbol{x})}{4\pi}\quad .\end{aligned}$$

This equation has a particular solution of the form:

$$\Psi^{(1)}_{part}(\boldsymbol{x},\boldsymbol{\Omega},s) = [\boldsymbol{\tau}(\boldsymbol{\Omega}) - s\boldsymbol{\Omega}]\cdot\boldsymbol{\nabla}\frac{\Phi^{(0)}(\boldsymbol{x})}{4\pi}\,, \tag{3.53}$$

where

$$\boldsymbol{\tau}(\boldsymbol{\Omega}) = \int_{4\pi} P^*(\boldsymbol{\Omega}\cdot\boldsymbol{\Omega}')\boldsymbol{\tau}(\boldsymbol{\Omega}')d\Omega' + \hat{\boldsymbol{S}}(\boldsymbol{\Omega})\,, \tag{3.54a}$$

$$\hat{\boldsymbol{S}}(\boldsymbol{\Omega}) = -\int_{4\pi} \boldsymbol{\Omega}' P^*(\boldsymbol{\Omega}\cdot\boldsymbol{\Omega}')\overline{s_{\boldsymbol{\Omega}}}(\boldsymbol{\Omega}')d\Omega'\,. \tag{3.54b}$$

As a Fredholm integral equation of the second kind, Eq. (3.54a) has the Liouville-Neumann series solution [2]:

$$\boldsymbol{\tau}(\boldsymbol{\Omega}) = \lim_{N\to\infty}\sum_{n=0}^{N}\boldsymbol{\tau}_n(\boldsymbol{\Omega})\,, \tag{3.55}$$

where

$$\boldsymbol{\tau}_0(\boldsymbol{\Omega}) = \hat{\boldsymbol{S}}(\boldsymbol{\Omega})\,, \tag{3.56a}$$

$$\boldsymbol{\tau}_1(\boldsymbol{\Omega}) = \int_{4\pi} P^*(\boldsymbol{\Omega}\cdot\boldsymbol{\Omega}_1)\hat{\boldsymbol{S}}(\boldsymbol{\Omega}_1)d\Omega_1\,, \tag{3.56b}$$

$$\boldsymbol{\tau}_2(\boldsymbol{\Omega}) = \int_{4\pi}\int_{4\pi} P^*(\boldsymbol{\Omega}\cdot\boldsymbol{\Omega}_1)P^*(\boldsymbol{\Omega}_1\cdot\boldsymbol{\Omega}_2)\hat{\boldsymbol{S}}(\boldsymbol{\Omega}_2)d\Omega_2 d\Omega_1\,, \tag{3.56c}$$

$$\vdots$$

$$\boldsymbol{\tau}_n(\boldsymbol{\Omega}) = \int_{4\pi}\int_{4\pi}\ldots\int_{4\pi} P^*(\boldsymbol{\Omega}\cdot\boldsymbol{\Omega}_1)P^*(\boldsymbol{\Omega}_1\cdot\boldsymbol{\Omega}_2)\ldots \ldots P^*(\boldsymbol{\Omega}_{n-1}\cdot\boldsymbol{\Omega}_n)\hat{\boldsymbol{S}}(\boldsymbol{\Omega}_n)d\Omega_n\ldots d\Omega_2 d\Omega_1\,. \tag{3.56d}$$

Since $\overline{s_{\boldsymbol{\Omega}}}(\boldsymbol{\Omega})$ is an even function of $\boldsymbol{\Omega}$, we note that $\hat{\boldsymbol{S}}(\boldsymbol{\Omega})$ and $\boldsymbol{\tau}(\boldsymbol{\Omega})$ are odd functions of $\boldsymbol{\Omega}$:

$$\hat{\boldsymbol{S}}(-\boldsymbol{\Omega}) = -\int_{4\pi} \boldsymbol{\Omega}' P^*(-\boldsymbol{\Omega}\cdot\boldsymbol{\Omega}')\overline{s_{\boldsymbol{\Omega}}}(\boldsymbol{\Omega}')d\Omega' \tag{3.57}$$
$$= -\int_{4\pi} -\boldsymbol{\Omega}' P^*(-\boldsymbol{\Omega}\cdot -\boldsymbol{\Omega}')\overline{s_{\boldsymbol{\Omega}}}(-\boldsymbol{\Omega}')d\Omega'$$
$$= \int_{4\pi} \boldsymbol{\Omega}' P^*(\boldsymbol{\Omega}\cdot\boldsymbol{\Omega}')\overline{s_{\boldsymbol{\Omega}}}(\boldsymbol{\Omega}')d\Omega'$$
$$= -\hat{\boldsymbol{S}}(\boldsymbol{\Omega})\,,$$

and $\boldsymbol{\tau}_n(-\boldsymbol{\Omega}) = -\boldsymbol{\tau}_n(\boldsymbol{\Omega})\ \forall\ n \geq 0$ follows with the same argument, by Eqs. (3.56). The general solution of Eq. (3.52) is given by:

$$\Psi^{(1)}(\boldsymbol{x},\boldsymbol{\Omega},s) = \frac{\Phi^{(1)}(\boldsymbol{x})}{4\pi} + [\boldsymbol{\tau}(\boldsymbol{\Omega}) - s\boldsymbol{\Omega}]\cdot\boldsymbol{\nabla}\frac{\Phi^{(0)}(\boldsymbol{x})}{4\pi}\,, \tag{3.58}$$

where $\Phi^{(1)}(\boldsymbol{x})$ is undetermined.

Equation (3.49) with $n = 2$ has a solvability condition, which is obtained by operating on it by $\int_{4\pi}\int_0^\infty p_{s|\boldsymbol{\Omega}}(s|\boldsymbol{\Omega})(\cdot)dsd\Omega$. Using Eqs. (3.51) and (3.58) to obtain:

$$\int_{4\pi}\int_0^\infty p_{s|\boldsymbol{\Omega}}(s'|\boldsymbol{\Omega}')\Psi^{(0)}(\boldsymbol{x},\boldsymbol{\Omega}',s')\,ds'd\Omega' = \Phi^{(0)}(\boldsymbol{x})\,, \tag{3.59a}$$

and:

$$\int_0^s \Psi^{(1)}(\boldsymbol{x},\boldsymbol{\Omega},s')\,ds' = s\frac{\Phi^{(1)}(\boldsymbol{x})}{4\pi} + \left(s\boldsymbol{\tau}(\boldsymbol{\Omega}) - \frac{s^2}{2}\boldsymbol{\Omega}\right)\cdot\boldsymbol{\nabla}\frac{\Phi^{(0)}(\boldsymbol{x})}{4\pi}\,, \tag{3.59b}$$

the solvability condition becomes:

$$0 = \frac{1}{4\pi}\int_{4\pi}\int_0^\infty p_{s|\boldsymbol{\Omega}}(s|\boldsymbol{\Omega})\left(\frac{s^2}{2}[\boldsymbol{\Omega}\cdot\boldsymbol{\nabla}]^2 - s[\boldsymbol{\tau}(\boldsymbol{\Omega})\cdot\boldsymbol{\nabla}][\boldsymbol{\Omega}\cdot\boldsymbol{\nabla}]\right)\Phi^{(0)}(\boldsymbol{x})dsd\Omega \tag{3.60}$$
$$- \frac{(1-c)}{4\pi}\int_{4\pi}\int_0^\infty p_{s|\boldsymbol{\Omega}}(s|\boldsymbol{\Omega})\Phi^{(0)}(\boldsymbol{x})\,dsd\Omega + \overline{s}Q(\boldsymbol{x})\,.$$

Thus, using the fact that $\int_0^\infty p_{s|\boldsymbol{\Omega}}(s|\boldsymbol{\Omega})ds = 1$ and $\int_0^\infty s^m p_{s|\boldsymbol{\Omega}}(s|\boldsymbol{\Omega})ds = \overline{s^m_{\boldsymbol{\Omega}}}(\boldsymbol{\Omega})$, we can rewrite Eq. (3.60) as:

$$\frac{1}{4\pi\overline{s}}\int_{4\pi}\left(\frac{\overline{s^2_{\boldsymbol{\Omega}}}(\boldsymbol{\Omega})}{2}[\boldsymbol{\Omega}\cdot\boldsymbol{\nabla}]^2 - \overline{s_{\boldsymbol{\Omega}}}(\boldsymbol{\Omega})[\boldsymbol{\tau}(\boldsymbol{\Omega})\cdot\boldsymbol{\nabla}][\boldsymbol{\Omega}\cdot\boldsymbol{\nabla}]\right)\Phi^{(0)}(\boldsymbol{x})\,d\Omega \tag{3.61}$$
$$- \frac{(1-c)}{\overline{s}}\Phi^{(0)}(\boldsymbol{x}) + Q(\boldsymbol{x}) = 0\,.$$

If we write $\boldsymbol{\tau}(\boldsymbol{\Omega}) = \big(\tau_x(\boldsymbol{\Omega}), \tau_y(\boldsymbol{\Omega}), \tau_z(\boldsymbol{\Omega})\big)$, this equation is equivalent to:

$$-\Bigg[\mathrm{D}^{gt}_{xx}\frac{\partial^2}{\partial x^2} + \mathrm{D}^{gt}_{yy}\frac{\partial^2}{\partial y^2} + \mathrm{D}^{gt}_{zz}\frac{\partial^2}{\partial z^2} + \mathrm{D}^{gt}_{xy}\frac{\partial^2}{\partial x\partial y} + \mathrm{D}^{gt}_{xz}\frac{\partial^2}{\partial x\partial z} + \mathrm{D}^{gt}_{yz}\frac{\partial^2}{\partial y\partial z}\Bigg]\Phi^{(0)}(\boldsymbol{x}) + \frac{1-c}{\overline{s}}\Phi^{(0)}(\boldsymbol{x}) = Q(\boldsymbol{x})\,, \tag{3.62}$$

where D^{gt}_{xx}, D^{gt}_{yy}, D^{gt}_{zz}, D^{gt}_{xy}, D^{gt}_{xz}, and D^{gt}_{yz} are the diffusion coefficients given by

$$\mathrm{D}^{gt}_{xx} = \frac{1}{4\pi\overline{s}}\int_{4\pi}\left(\frac{\overline{s^2_{\boldsymbol{\Omega}}}(\boldsymbol{\Omega})}{2}\Omega_x - \overline{s_{\boldsymbol{\Omega}}}(\boldsymbol{\Omega})\tau_x(\boldsymbol{\Omega})\right)\Omega_x d\Omega, \tag{3.63a}$$

$$\mathrm{D}^{gt}_{yy} = \frac{1}{4\pi\overline{s}}\int_{4\pi}\left(\frac{\overline{s^2_{\boldsymbol{\Omega}}}(\boldsymbol{\Omega})}{2}\Omega_y - \overline{s_{\boldsymbol{\Omega}}}(\boldsymbol{\Omega})\tau_y(\boldsymbol{\Omega})\right)\Omega_y d\Omega, \tag{3.63b}$$

$$\mathrm{D}^{gt}_{zz} = \frac{1}{4\pi\overline{s}}\int_{4\pi}\left(\frac{\overline{s^2_{\boldsymbol{\Omega}}}(\boldsymbol{\Omega})}{2}\Omega_z - \overline{s_{\boldsymbol{\Omega}}}(\boldsymbol{\Omega})\tau_z(\boldsymbol{\Omega})\right)\Omega_z d\Omega, \tag{3.63c}$$

$$\mathrm{D}^{gt}_{xy} = \frac{1}{4\pi\overline{s}}\int_{4\pi}\Big(\overline{s^2_{\boldsymbol{\Omega}}}(\boldsymbol{\Omega})\Omega_x\Omega_y - \overline{s_{\boldsymbol{\Omega}}}(\boldsymbol{\Omega})[\tau_x(\boldsymbol{\Omega})\Omega_y + \tau_y(\boldsymbol{\Omega})\Omega_x]\Big)\, d\Omega, \tag{3.63d}$$

$$\mathrm{D}^{gt}_{xz} = \frac{1}{4\pi\overline{s}}\int_{4\pi}\Big(\overline{s^2_{\boldsymbol{\Omega}}}(\boldsymbol{\Omega})\Omega_x\Omega_z - \overline{s_{\boldsymbol{\Omega}}}(\boldsymbol{\Omega})[\tau_x(\boldsymbol{\Omega})\Omega_z + \tau_z(\boldsymbol{\Omega})\Omega_x]\Big)\, d\Omega, \tag{3.63e}$$

$$\mathrm{D}^{gt}_{yz} = \frac{1}{4\pi\overline{s}}\int_{4\pi}\Big(\overline{s^2_{\boldsymbol{\Omega}}}(\boldsymbol{\Omega})\Omega_y\Omega_z - \overline{s_{\boldsymbol{\Omega}}}(\boldsymbol{\Omega})[\tau_y(\boldsymbol{\Omega})\Omega_z + \tau_z(\boldsymbol{\Omega})\Omega_y]\Big)\, d\Omega. \tag{3.63f}$$

Summarizing: the solution $\hat{\psi}(\boldsymbol{x}, \boldsymbol{\Omega}, s)$ of Eq. (3.43) satisfies:

$$\hat{\psi}(\boldsymbol{x}, \boldsymbol{\Omega}, s) = \frac{\Phi^{(0)}(\boldsymbol{x})}{4\pi}\frac{e^{-\int_0^s \Sigma_t(\boldsymbol{\Omega}, s')ds'}}{\overline{s}} + O(\varepsilon)\,, \tag{3.64}$$

where $\Phi^{(0)}(\boldsymbol{x})$ satisfies Eq. (3.62). Integrating Eq. (3.64) over $0 < s < \infty$ and using equation (3.25), we obtain an expression to the classic angular flux (to leading order):

$$\psi(\boldsymbol{x}, \boldsymbol{\Omega}) = \Phi^{(0)}(\boldsymbol{x})\frac{\overline{s_{\boldsymbol{\Omega}}}(\boldsymbol{\Omega})}{4\pi\overline{s}}\,. \tag{3.65}$$

Special Case 1

Let us now examine what happens when the locations of the scattering centers are correlated but independent upon direction. In this case, we can write $\Sigma_t(\boldsymbol{\Omega}, s) = \Sigma_t(s)$, and Eq. (3.16) yields $p_{s|\boldsymbol{\Omega}}(s|\boldsymbol{\Omega}) = \Sigma_t(s)e^{-\int_0^s \Sigma_t(s')ds'}$. Introducing this result into Eq.

(3.25), we see that $\overline{s_{\mathbf{\Omega}}}(\mathbf{\Omega}) = \overline{s_{\mathbf{\Omega}}}$ is now independent of $\mathbf{\Omega}$, and we can use Eq. (3.27) to obtain $\overline{s} = \overline{s_{\mathbf{\Omega}}}$. $\big($Similarly, $\overline{s^2_{\mathbf{\Omega}}}(\mathbf{\Omega}) = \overline{s^2_{\mathbf{\Omega}}} = \overline{s^2}.\big)$ Therefore, operating on Eq. (3.65) by $\int_{4\pi}(\cdot)d\Omega$, we obtain

$$\int_{4\pi} \psi(\boldsymbol{x}, \mathbf{\Omega}) d\Omega = \Phi^{(0)}(\boldsymbol{x})\,; \tag{3.66}$$

that is, the solution $\Phi^{(0)}(\boldsymbol{x})$ of Eq. (3.62) is the classic scalar flux (to leading order). Furthermore, we notice that we can write

$$\hat{\boldsymbol{S}}(\mathbf{\Omega}) = -\int_{4\pi} \mathbf{\Omega}' P^*(\mathbf{\Omega}\cdot\mathbf{\Omega}')\overline{s_{\mathbf{\Omega}}}(\mathbf{\Omega}')d\Omega' = -\overline{s}\int_{4\pi} \mathbf{\Omega}' P^*(\mathbf{\Omega}\cdot\mathbf{\Omega}')d\Omega'. \tag{3.67a}$$

To evaluate this integral, let us choose our system of coordinates such that $\mathbf{\Omega} = (0,0,1) = \vec{\boldsymbol{k}}$. Then, $\mathbf{\Omega}\cdot\mathbf{\Omega}' = \mu'$ and

$$\int_{4\pi} \mathbf{\Omega}' P^*(\mathbf{\Omega}\cdot\mathbf{\Omega}')d\Omega' = 2\pi\vec{\boldsymbol{k}}\int_{-1}^{1} \mu' P^*(\mu')d\mu' = 2\pi\mathbf{\Omega}\int_{-1}^{1} \mu' P^*(\mu')d\mu'. \tag{3.67b}$$

We know [47] that $P_1(\mu') = \mu'$; thus, using Eqs. (3.42):

$$\int_{-1}^{1} \mu' P^*(\mu')d\mu' = \int_{-1}^{1} \frac{3}{4\pi} a_1^* \mu'^2 d\mu' = \frac{a_1^*}{2\pi} = \frac{c a_1}{2\pi}, \tag{3.67c}$$

due to the orthogonality of the Legendre polynomials. Since $a_1 = \overline{\mu}_0$ (the mean scattering cosine), Eqs. (3.67) yield the explicit expression

$$\hat{\boldsymbol{S}}(\mathbf{\Omega}) = -\overline{s}\left(2\pi\mathbf{\Omega}\frac{c\overline{\mu}_0}{2\pi}\right) = -\overline{s}\,\mathbf{\Omega}[c\overline{\mu}_0]\,. \tag{3.68}$$

Introducing this equation into Eqs. (3.56), we obtain $\boldsymbol{\tau}_n(\mathbf{\Omega}) = -\overline{s}\,\mathbf{\Omega}[c\overline{\mu}_0]^{n+1}\;\forall\; n \geq 0$; and using Eq. (3.55):

$$\boldsymbol{\tau}(\mathbf{\Omega}) = -\frac{c\overline{\mu}_0}{1 - c\overline{\mu}_0}\,\overline{s}\,\mathbf{\Omega}\,. \tag{3.69}$$

In this case, the angular integrals in Eqs. (3.63) yield:

$$\mathrm{D}^{iso} = \mathrm{D}^{gt}_{xx} = \mathrm{D}^{gt}_{yy} = \mathrm{D}^{gt}_{zz} = \frac{1}{3}\left(\frac{\overline{s^2}}{2\overline{s}} + \frac{c\overline{\mu}_0}{1 - c\overline{\mu}_0}\overline{s}\right)\,, \tag{3.70a}$$

$$\mathrm{D}^{gt}_{xy} = \mathrm{D}^{gt}_{xz} = \mathrm{D}^{gt}_{yz} = 0\,, \tag{3.70b}$$

which reduces Eq. (3.62) to the result obtained in [45].

Special Case 2

Finally, in the case of isotropic scattering, $P^*(\mathbf{\Omega}\cdot\mathbf{\Omega}') = 1/4\pi$ and

$$\hat{\boldsymbol{S}}(\mathbf{\Omega}) = -\frac{1}{4\pi}\int_{4\pi}\mathbf{\Omega}'\,\overline{s_{\mathbf{\Omega}}}(\mathbf{\Omega}')d\Omega' = 0\,, \tag{3.71}$$

since $\overline{s_{\mathbf{\Omega}}}(\mathbf{\Omega})$ is an even function of $\mathbf{\Omega}$ (as noted in Section 3.2). Introducing this result into Eqs. (3.56), we obtain $\boldsymbol{\tau}_n(\mathbf{\Omega}) = 0\ \forall\ n \geq 0$. Hence, by Eq. (3.55), $\boldsymbol{\tau}(\mathbf{\Omega}) = 0$, and Eqs. (3.63) can be writen as

$$\mathrm{D}_{xx}^{gt} = \frac{1}{2\overline{s}}\left(\frac{1}{4\pi}\int_{4\pi}\overline{s^2_{\mathbf{\Omega}}}(\mathbf{\Omega})\Omega_x^2 d\Omega\right), \tag{3.72a}$$

$$\mathrm{D}_{yy}^{gt} = \frac{1}{2\overline{s}}\left(\frac{1}{4\pi}\int_{4\pi}\overline{s^2_{\mathbf{\Omega}}}(\mathbf{\Omega})\Omega_y^2 d\Omega\right), \tag{3.72b}$$

$$\mathrm{D}_{zz}^{gt} = \frac{1}{2\overline{s}}\left(\frac{1}{4\pi}\int_{4\pi}\overline{s^2_{\mathbf{\Omega}}}(\mathbf{\Omega})\Omega_z^2 d\Omega\right), \tag{3.72c}$$

$$\mathrm{D}_{xy}^{gt} = \frac{1}{\overline{s}}\left(\frac{1}{4\pi}\int_{4\pi}\overline{s^2_{\mathbf{\Omega}}}(\mathbf{\Omega})\Omega_x\Omega_y d\Omega\right), \tag{3.72d}$$

$$\mathrm{D}_{xz}^{gt} = \frac{1}{\overline{s}}\left(\frac{1}{4\pi}\int_{4\pi}\overline{s^2_{\mathbf{\Omega}}}(\mathbf{\Omega})\Omega_x\Omega_z d\Omega\right), \tag{3.72e}$$

$$\mathrm{D}_{yz}^{gt} = \frac{1}{\overline{s}}\left(\frac{1}{4\pi}\int_{4\pi}\overline{s^2_{\mathbf{\Omega}}}(\mathbf{\Omega})\Omega_y\Omega_z d\Omega\right). \tag{3.72f}$$

A general diffusion equation with no off-diagonal terms (that is, without diffusion coefficients that depend on more than one direction) can be obtained in systems with azimuthal symmetry (such as in PBR problems). In this case, the probability distribution function for distance-to-collision is independent of the azimuthal angle φ; specifically, $\overline{s^m_{\mathbf{\Omega}}}(\mathbf{\Omega}) = \overline{s^m_{\mathbf{\Omega}}}(\mu)$ depends only upon the polar angle μ. Then, $\mathrm{D}_{xy}^{gt} = \mathrm{D}_{xz}^{gt} = \mathrm{D}_{yz}^{gt} = 0$, $\mathrm{D}_{xx}^{gt} = \mathrm{D}_{yy}^{gt}$, and we obtain the following anisotropic diffusion equation for $\Phi^{(0)}(\boldsymbol{x})$:

$$-\mathrm{D}_{xx}^{gt}\frac{\partial^2}{\partial x^2}\Phi^{(0)}(\boldsymbol{x}) - \mathrm{D}_{yy}^{gt}\frac{\partial^2}{\partial y^2}\Phi^{(0)}(\boldsymbol{x}) - \mathrm{D}_{zz}^{gt}\frac{\partial^2}{\partial z^2}\Phi^{(0)}(\boldsymbol{x}) + \frac{1-c}{\overline{s}}\Phi^{(0)}(\boldsymbol{x}) = Q(\boldsymbol{x}). \tag{3.73}$$

Thus, for problems with isotropic scattering and probability distribution function for distance-to-collision independent of the azimuthal angle φ, we obtain a standard anisotropic

diffusion equation (without off-diagonal terms) with $\mathrm{D}_{xx}^{gt} = \mathrm{D}_{yy}^{gt}$. We believe that this will also hold for problems with anisotropic scattering, but have not yet been able to prove it. (Hereafter, for simplicity, we will use the notation $\mathrm{D}_{uu}^{gt} = \mathrm{D}_{u}^{gt}$, for $u = \{x, y, z\}$).

Note: if $p_{s|\mathbf{\Omega}}(s|\mathbf{\Omega})$ were to decay algebraically as $s \longrightarrow \infty$ as:

$$p_{s|\mathbf{\Omega}}(s|\mathbf{\Omega}) \geq \frac{constant}{s^3} \quad \text{for} \quad s \geq 1\,, \tag{3.74}$$

then the asymptotic diffusion approximation developed here would be invalid, since this would imply

$$\overline{s^2_{\mathbf{\Omega}}}(\mathbf{\Omega}) = \int_0^\infty s^2 p_{s|\mathbf{\Omega}}(s|\mathbf{\Omega}) ds = \infty\,. \tag{3.75}$$

However, for physical reasons, such a situation will not occur in the problem we want to consider.

3.5 Reduction to the Classic Theory

We will now show that, with the classic assumption that the locations of the scattering centers are uncorrelated and do not depend upon direction, the results obtained by the generalized theory presented in this section reduce to the results of the classic theory.

In other words, we will now assume that

$$\Sigma_t(\mathbf{\Omega}, s) = \Sigma_t \equiv \text{constant}. \tag{3.76}$$

In this case, Eq. (3.5) can be rewritten as

$$\begin{aligned} &\frac{\partial \hat{\psi}}{\partial s}(\boldsymbol{x}, \mathbf{\Omega}, s) + \mathbf{\Omega} \cdot \boldsymbol{\nabla} \hat{\psi}(\boldsymbol{x}, \mathbf{\Omega}, s) + \Sigma_t \hat{\psi}(\boldsymbol{x}, \mathbf{\Omega}, s) \\ &\qquad = \delta(s)\, \Sigma_s \int_{4\pi} \int_0^\infty P(\mathbf{\Omega}' \cdot \mathbf{\Omega}) \hat{\psi}(\boldsymbol{x}, \mathbf{\Omega}', s')\, ds' d\Omega' + \delta(s) \frac{Q(\boldsymbol{x})}{4\pi}\,, \end{aligned} \tag{3.77}$$

where $\Sigma_s = c\Sigma_t$. Operating on this equation by $\int_{-\varepsilon}^{\infty}(\cdot)ds$ and using Eq. (3.9), we obtain

$$\begin{aligned} &\hat{\psi}(\boldsymbol{x}, \mathbf{\Omega}, \infty) - \hat{\psi}(\boldsymbol{x}, \mathbf{\Omega}, -\varepsilon) + \mathbf{\Omega} \cdot \boldsymbol{\nabla} \psi(\boldsymbol{x}, \mathbf{\Omega}) + \Sigma_t \psi(\boldsymbol{x}, \mathbf{\Omega}) \\ &\qquad = \Sigma_s \int_{4\pi} P(\mathbf{\Omega}' \cdot \mathbf{\Omega}) \psi(\boldsymbol{x}, \mathbf{\Omega}')\, d\Omega' + \frac{Q(\boldsymbol{x})}{4\pi}\,. \end{aligned} \tag{3.78}$$

Using the fact that $\hat{\psi}(\boldsymbol{x}, \boldsymbol{\Omega}, \infty) = \hat{\psi}(\boldsymbol{x}, \boldsymbol{\Omega}, -\varepsilon) = 0$, we have

$$\boldsymbol{\Omega} \cdot \boldsymbol{\nabla}\psi(\boldsymbol{x}, \boldsymbol{\Omega}) + \Sigma_t \psi(\boldsymbol{x}, \boldsymbol{\Omega}) = \Sigma_s \int_{4\pi} P(\boldsymbol{\Omega}' \cdot \boldsymbol{\Omega}) \psi(\boldsymbol{x}, \boldsymbol{\Omega}')\, d\Omega' + \frac{Q(\boldsymbol{x})}{4\pi}\,, \tag{3.79}$$

which is, of course, the classic linear Boltzmann equation as described in Eq. (2.31) [since $\Sigma_s P(\boldsymbol{\Omega}' \cdot \boldsymbol{\Omega}) = \Sigma_s(\boldsymbol{\Omega}' \cdot \boldsymbol{\Omega})$].

Moreover, if Eq. (3.76) holds, then Eq. (3.16) yields

$$p_{s|\boldsymbol{\Omega}}(s|\boldsymbol{\Omega}) = \Sigma_t e^{-\Sigma_t s} = p(s)\,; \tag{3.80}$$

that is, the probability distribution function for distance-to-collision is given by an exponential, which is the classic result in Eq. (2.12). Introducing Eq. (3.80) into Eq. (3.25), we can use Eq. (3.27) to obtain

$$\overline{s} = \overline{s_{\boldsymbol{\Omega}}}(\boldsymbol{\Omega}) = \frac{1}{\Sigma_t}\,, \tag{3.81a}$$

which is the classic mean free path given by Eq. (2.13). Also, the mean square free path is given by:

$$\overline{s^2} = \overline{s^2_{\boldsymbol{\Omega}}}(\boldsymbol{\Omega}) = \int_0^\infty s^2 p(s) ds = \frac{2}{\Sigma_t^2}\,. \tag{3.81b}$$

For the integral formulation, Eqs. (3.37) can now be easily reduced to their classic form in Eqs. (2.36), since Eq. (3.76) allows us to write

$$\tilde{p}(|\boldsymbol{x} - \boldsymbol{x}'|) = p(|\boldsymbol{x} - \boldsymbol{x}'|) = \Sigma_t e^{-\Sigma_t |\boldsymbol{x} - \boldsymbol{x}'|} \tag{3.82}$$

in Eq. (3.37a). Furthermore, Eq. (3.28) yields

$$\hat{f}(\boldsymbol{x}, \boldsymbol{\Omega}) = \Sigma_t \int_0^\infty \hat{\psi}(\boldsymbol{x}, \boldsymbol{\Omega}, s)\, ds = \Sigma_t \psi(\boldsymbol{x}, \boldsymbol{\Omega})\,, \tag{3.83}$$

and thus by Eq. (3.38b),

$$\hat{F}(\boldsymbol{x}) = \Sigma_t \int_{4\pi} \psi(\boldsymbol{x}, \boldsymbol{\Omega}')\, d\Omega' = \Sigma_t \Phi(\boldsymbol{x})\,. \tag{3.84}$$

Using Eq. (3.82) and the previous result in Eqs. (3.39b) and (3.39c), we obtain:

$$\psi(\boldsymbol{x},\boldsymbol{\Omega}) = \frac{1}{4\pi}\int_0^\infty \left[\Sigma_s\Phi(\boldsymbol{x}-s\boldsymbol{\Omega}) + Q(\boldsymbol{x}-s\boldsymbol{\Omega})\right] e^{-\Sigma_t s} ds\,, \tag{3.85a}$$

and

$$\Phi(\boldsymbol{x}) = \iiint \left[\Sigma_s\Phi(\boldsymbol{x}') + Q(\boldsymbol{x}')\right] \frac{e^{-\Sigma_t|\boldsymbol{x}-\boldsymbol{x}'|}}{4\pi|\boldsymbol{x}-\boldsymbol{x}'|^2}\, dV'\,. \tag{3.85b}$$

Equation (3.85b) is the classic integral transport equation for the scalar flux $\Phi(\boldsymbol{x})$, and Eq. (3.85a) is the classic expression for the angular flux $\psi(\boldsymbol{x},\boldsymbol{\Omega})$ in terms of $\Phi(\boldsymbol{x})$, for the case of isotropic scattering.

For the theory involving the asymptotic diffusion limit, if Eq. (3.76) holds, then we can use Eqs. (3.70) and (3.81) to reduce Eq. (3.62) to the classic diffusion expression in Eq. (2.37):

$$-\frac{1}{3\Sigma_t(1-c\overline{\mu}_0)}\nabla^2\Phi^{(0)}(\boldsymbol{x}) + \Sigma_t(1-c)\Phi^{(0)}(\boldsymbol{x}) = Q(\boldsymbol{x})\,. \tag{3.86}$$

In short, we have shown that when Eq. (3.76) holds, the generalized transport theory reduces to the classic transport theory, as it must.

3.6 A Discussion on $\Sigma_t(\boldsymbol{\Omega}, s)$

In order to use the generalized Boltzmann equation developed in this chapter, we need to know the function $\Sigma_t(\boldsymbol{\Omega}, s)$ [as given by Eq. (3.21)]. This means that we need to know $p_{s|\boldsymbol{\Omega}}(s|\boldsymbol{\Omega})$, the conditional distribution function for the distance-to-collision in a given direction $\boldsymbol{\Omega}$. Unfortunately, due to the statistical nature of the heterogeneous medium and its effect on the transport of particles, there is generally no analytical expression that can be used to obtain this value. Nevertheless, there is a logical and straightforward set of steps that can be followed in order to numerically estimate this quantity.

As an example, let us examine a 3-D pebble-bed reactor type of problem. We assume a system composed of solid fuel spheres immersed in a void background. If we consider a

particle P that is born (or scatters) at a random point (x, y, z) inside the sphere S_0, the total distance $\hat{s}$ that this particle will travel *inside the spheres* before experiencing a collision can be sampled from the exponential distribution given in Eq. (3.80), where Σ_t is the total cross section of the spheres.

Let ℓ be the line path starting at point (x, y, z) along which P travels, and let δ_{S_n} be the length of ℓ inside the sphere S_n. If $\delta_{S_0} < \hat{s}$, P will leak out of the sphere S_0 before experiencing a collision. It will then travel a distance δ_{V_1} along ℓ in the vaccum before entering a new sphere S_1. If $\delta_{S_1} < \hat{s} - \delta_{S_0}$, the particle will leak out of S_1 without experiencing a collision and will travel some distance δ_{V_2} along ℓ in the vacuum before entering another sphere (S_2). Eventually, if the particle does not leak out of the system, there will be a sphere S_N in which $\delta_{S_N} \geq \hat{s} - \sum_{n=0}^{N} \delta_{S_n}$, meaning that P will experience a collision within S_N (Figure 3.1). The distance travelled by this particle between birth and collision will hence be given by

$$s = \hat{s} + \sum_{n=1}^{N} \delta_{V_n}. \tag{3.87}$$

In a given realization of this system, we can find a homogenized estimate of $p_{s|\mathbf{\Omega}}(s|\mathbf{\Omega})$ for fixed $\mathbf{\Omega}$ by using the following procedure:

- Randomly choose a sphere in the system
- Randomly choose a point inside this sphere
- Using Eq. (3.87), calculate and store the distance s this particle will travel in the direction $\mathbf{\Omega}$ before experiencing a collision
- Repeat this process for a large number of particles

By tallying the results obtained with this process for different values of s, one can construct an approximation for $p_{s|\mathbf{\Omega}}(s|\mathbf{\Omega})$ in the fixed direction $\mathbf{\Omega}$. This process can be

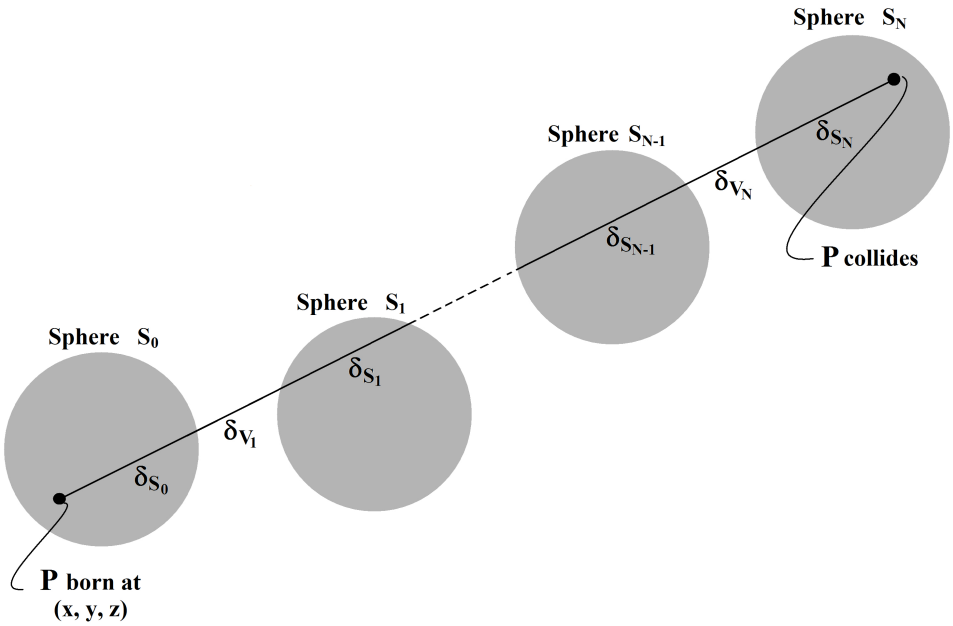

Figure 3.1: Linepath of a Particle Between Collisions

repeated for as many different directions $\mathbf{\Omega}$ as needed; for example, to solve the discrete ordinates S_N equations [25, 47] for this problem, this process has to be performed for N different directions $\mathbf{\Omega}$. Moreover, for systems in which the locations of the scattering centers do not depend on $\mathbf{\Omega}$, $p_{s|\mathbf{\Omega}}(s|\mathbf{\Omega}) = p_s(s)$ is also independent of angle; in this case, we have to estimate only one probability distribution function.

At this point, we must remark on a very important feature. Although the generalized Boltzmann equation requires the estimates of different probability distribution functions, which may become very time consuming, the generalized diffusion theory needs only estimates for the mean and mean square values of the distance-to-collision. In the diffusion problem, a simplified process is described below:

- Randomly choose a sphere in the system
- Randomly choose a point inside this sphere
- Using Eq. (3.87), calculate s and s^2

- Repeat this process for a large number of particles

Dividing $\sum s$ and $\sum s^2$ by the number of particles generated, we obtain $\overline{s_{\mathbf{\Omega}}}(\mathbf{\Omega})$ and $\overline{s^2_{\mathbf{\Omega}}}(\mathbf{\Omega})$, the mean and mean square distance-to-collision in the fixed direction $\mathbf{\Omega}$. This process can be repeated for as many different directions $\mathbf{\Omega}$ as needed. Once more, for systems in which the locations of the scattering centers do not depend on $\mathbf{\Omega}$, we have to estimate only $\overline{s}$ and $\overline{s^2}$, independent of direction.

CHAPTER IV

A Model 2-D Pebble-Bed Reactor Core

This chapter contains some preliminary work, where we consider a 2-D "flatland" (neutron transport occurs only in the (x, y)-plane) model of a pebble-bed reactor core. In this case, $\boldsymbol{x} = (x, y)$ and $\boldsymbol{\Omega} = (\cos\varphi, \sin\varphi)$, where $0 \leq \varphi < 2\pi$. The core consists of "fuel discs" of radius r piled up inside a square box with side L; vacuum boundary conditions are used. Hereafter, we use the term 2-D to describe this model. We have developed a Monte Carlo computer code capable of deriving random realizations of the 2-D core; and a second Monte Carlo code that performs 2-D neutron transport inside the heterogeneous core. We apply this second Monte Carlo code to both stochastic and crystal-like pilings of the discs. By comparing neutron transport Monte Carlo simulations in the heterogeneous cores, we can determine (i) the accuracy of the atomic mix approximation, and (ii) whether anisotropic effects occur.

4.1 2-D Packings

In this section we introduce the different approaches that we used to pack discs in the 2-D model of the reactor core. Section 4.1.1 describes the piling of crystal structures, while Section 4.1.2 discusses the case of a random piling of discs.

4.1.1 2-D Crystal Structures

Let $\underline{d} = 2r$ be the diameter of a fuel disc, and ε be the fixed distance between two discs in the same horizontal layer. With these quantities in mind, we place J_1 discs in the first layer of the system (at the bottom of the box), such that the distance between the left wall and the leftmost disc and the distance between the right wall and the rightmost disc are the same. The second layer contains $J_2 = J_1 - 1$ discs, each one placed on top of two discs of the first layer. The third and fourth layers will be identical to the first and second layers shifted vertically, so that the third layer lays on top of the second layer. This process is repeated until the box is filled. Notice that, starting with the third layer, we allow the leftmost and rightmost discs of the odd layers to be unstable under gravity if they do not touch a wall (they only rest upon one disc). Even though this is not physically correct, it is a valid approximation of the infinite system when L is large. An example of this type of piling is shown in Figure 4.1.

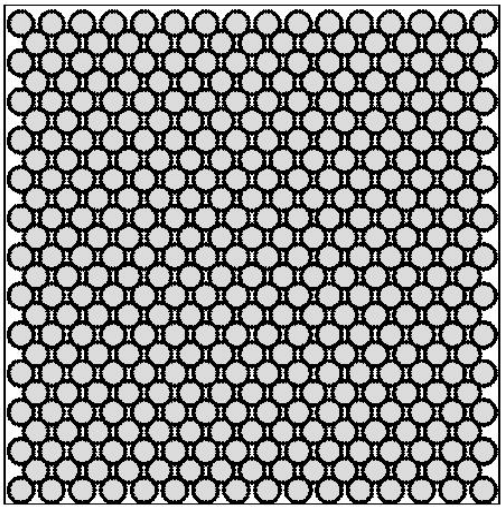

Figure 4.1: Example of a 2-D Crystal Structure (with $\varepsilon = 0.25\underline{d}$) in a System with Side $L = 20\underline{d}$

The height h_i of the i^{th} layer can be defined directly from the previous layers by

$$h_i = h_{i-1} + \sqrt{\underline{d}^2 - \left(\frac{\underline{d}+\varepsilon}{2}\right)^2} = h_1 + (i-1)\sqrt{\underline{d}^2 - \left(\frac{\underline{d}+\varepsilon}{2}\right)^2}\,,\ \forall\ i \geq 1\,. \tag{4.1}$$

We do not allow any disc to overlap another disc or the limits of the box. This implies that, in order to maintain the crystal symmetry of the structure, ε must have a maximum:

$$\varepsilon_{max} = \underline{d}(\sqrt{3} - 1)\,. \tag{4.2}$$

For $\varepsilon = 0$ and $\varepsilon = \varepsilon_{max}$, the centers of adjacent discs form a hexagonal lattice (each disc touches 6 neighbouring discs). In fact, the packing structure obtained for $\varepsilon = \varepsilon_{max}$ is equivalent to the 90 degrees rotation of the one obtained with $\varepsilon = 0$. This is the classic "honeycomb" lattice, proved to have the highest packing fraction of all possible circle

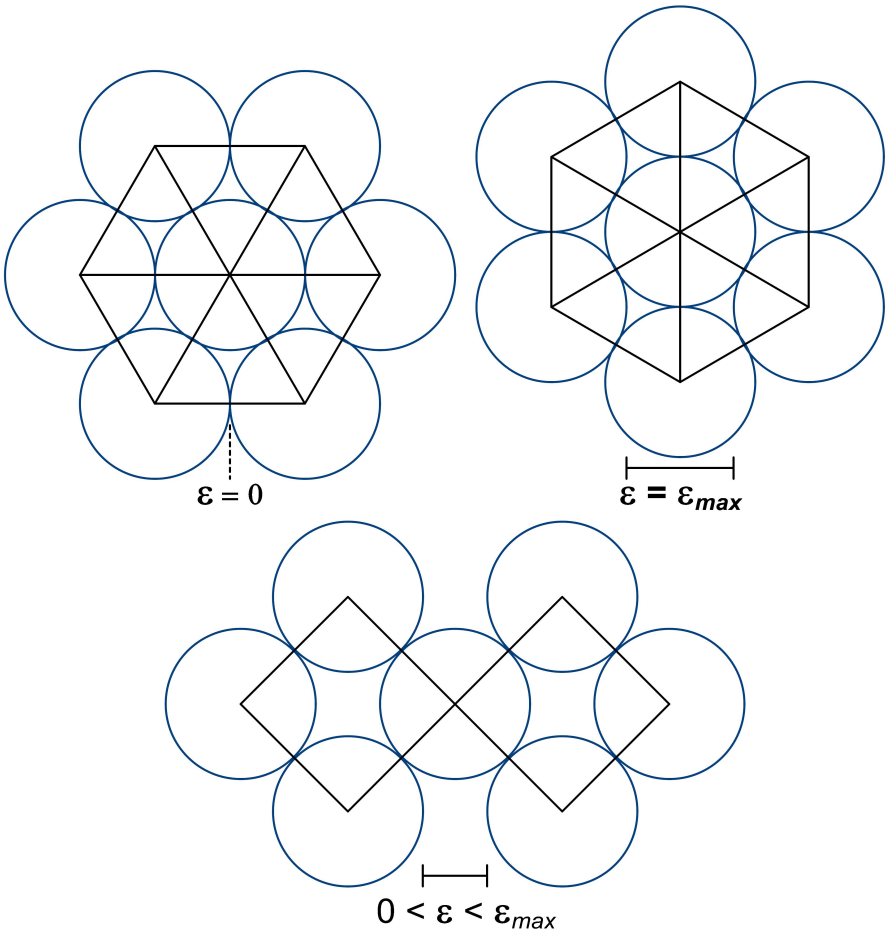

Figure 4.2: Diamond and Hexagonal Lattices in 2-D Crystal Structures with Different Values of ε

packings [19]. For the cases in which $0 < \varepsilon < \varepsilon_{max}$, each disc touches 4 neighbouring discs, with their centers forming a diamond lattice (Figure 4.2). If $\varepsilon > \varepsilon_{max}$, the piling

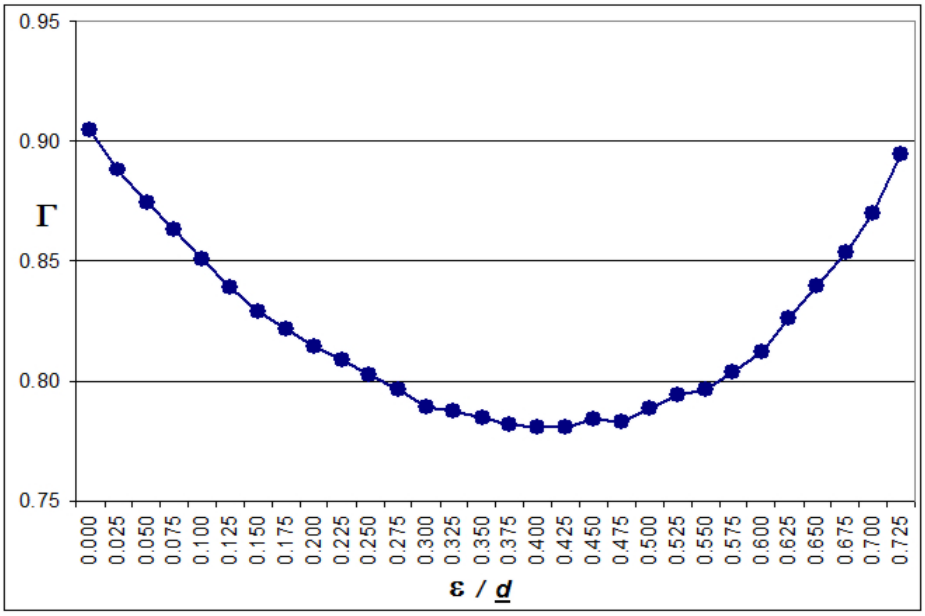

Figure 4.3: Packing Fractions in 2-D Crystal Structures with Different Values of ε

will either lose its crystal diamond structure or allow overlapping discs.

For the 2-D model, we define the packing fraction Γ as the ratio between the total area of the fuel discs and the area of the box. The graph in Figure 4.3 shows the packing fraction Γ as a function of $\varepsilon/\underline{d}$ (in increments of 0.025).

4.1.2 2-D Random Structures

The random piling is built by a sequential release of discs of diameter $\underline{d}$; the packing is carried on using an adaptation of the ballistic deposition model presented in [54]. In this

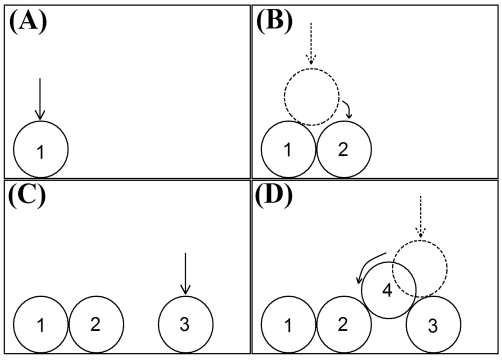

Figure 4.4: Steps of a Random 2-D Packing Process

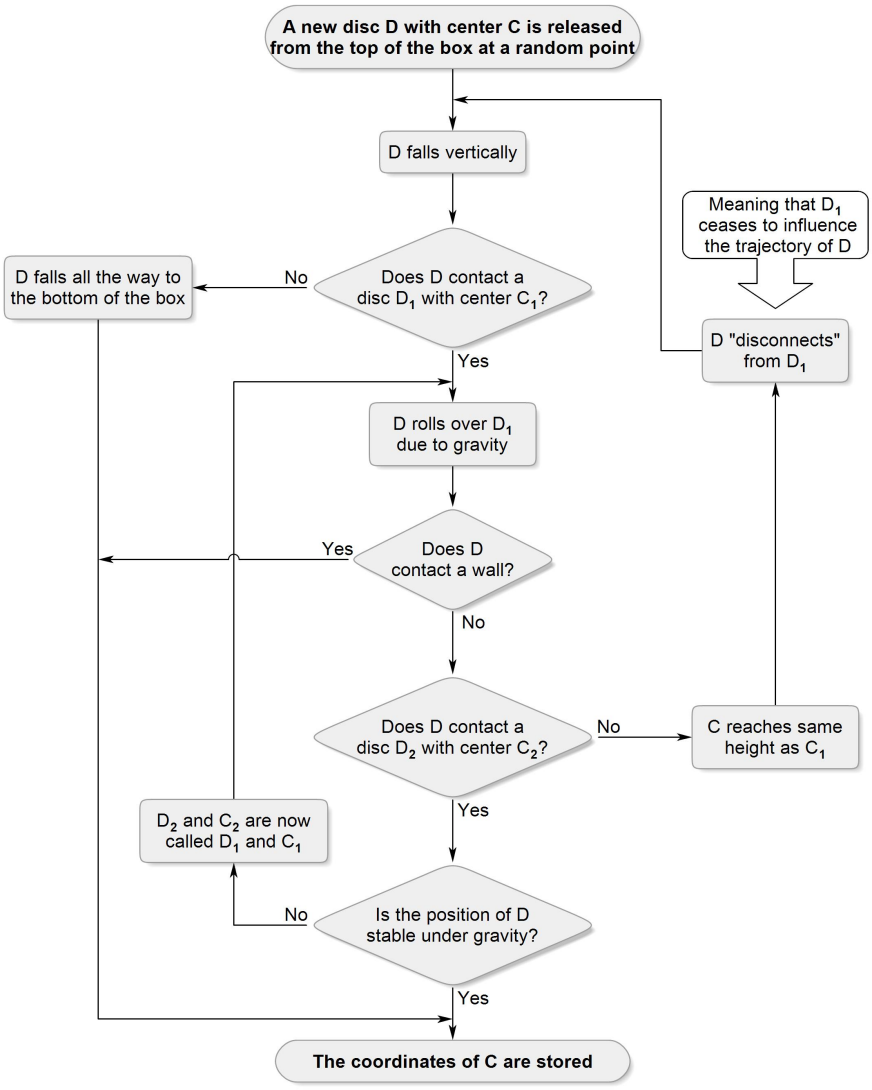

Figure 4.5: Flow Diagram for the Dropping of a Disc in the 2-D System

model, each disc is released at a random point above the box. It then follows a steepest descent trajectory until it reaches a position that is stable under gravity, in which case it is frozen in place - once the position of the disc is locked, it can no longer move. Figure 4.4 contains snapshots of a packing performed with this process: **(A)** disc 1 descends vertically to the bottom of the box, where it becomes locked in place; **(B)** disc 2 descends until it touches the frozen disc 1; then it rolls down disc 1 until it touches the bottom of the box, where it is locked in place; **(C)** disc 3 descends vertically to the bottom of the

box; **(D)** disc 4 descends until it touches the frozen disc 3; then it rolls down disc 3 until it touches disc 2; since discs 2 and 3 cannot move, disc 4 is stable and is locked in place. Figure 4.5 contains a flux diagram for the addition of a new disc into the box.

Since frozen discs cannot move, the inclusion of a new disc will not cause the system to rearrange; that is, cascading events (such as avalanches) will not happen. Moreover, no velocity or friction coefficients are taken into account; the only restriction is that a disc can never, at any point of its trajectory, overlap the limits of the box or another disc. Once a disc has reached its final stable position, a new disc is released; this process is repeated until the box is filled. An example of random piling is shown in Figure 4.6.

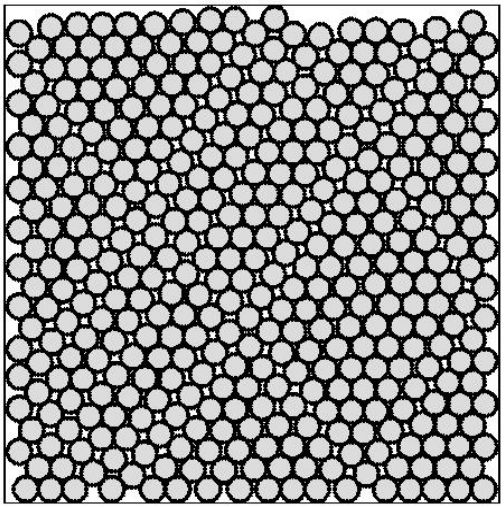

Figure 4.6: Example of a 2-D Random Structure in a System with Side $L = 20\underline{d}$

For this work, we developed 100 different random packings in a 2-D system with $L = 300\underline{d}$. With Γ being the packing fraction of a single realization (as defined in the previous section), we found the average packing fraction to be $\overline{\Gamma} = 0.817$, with 0.00134 as the standard deviation.

4.2 2-D Monte Carlo Results

For all 2-D problems in this work, the packing of discs of diameter $\underline{d}$ took place in a square box with side $L = 300\underline{d}$. We assumed the background material in which the discs were piled to be vacuum; the parameters used for the material of the discs are given in Table 4.1.

Table 4.1: 2-D parameters for discs with diameter $\underline{d}$.

$\underline{d}\Sigma_t$	$\underline{d}\Sigma_s$	$\underline{d}\Sigma_a$	$c = \Sigma_s/\Sigma_t$	$P(\mathbf{\Omega} \cdot \mathbf{\Omega}')$
1.0	0.99	0.01	0.99	$1/2\pi$

Given a realization of the model core, we choose the disc closest to the center of the system to be the one where particles will be born. In this approach we focus on the transport of particles generated by this single fuel disc, since the particles generated by different discs will have (on average) the same behavior. The particles' histories within the system are determined by a Monte Carlo transport code. The history of a single particle is summarized in the flow diagram shown in Figure 4.7; the distance s traveled by a particle between collisions is calculated using Eq. (3.87).

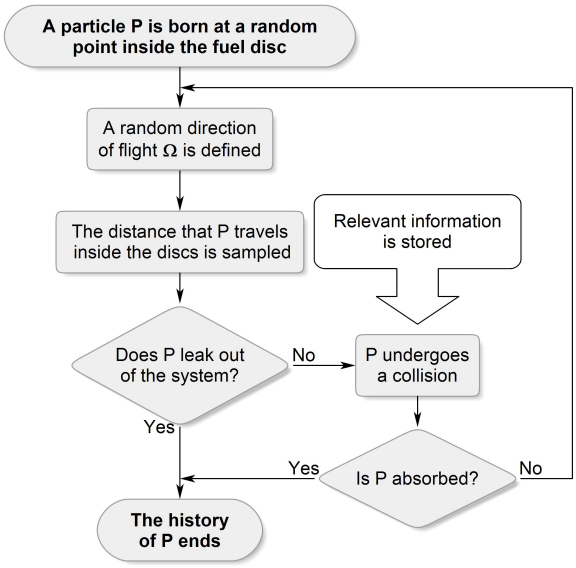

Figure 4.7: Flow Diagram for the History of a Particle

4.2.1 Monte Carlo in 2-D Crystal Structures

Monte Carlo (MC) numerical transport results for 2-D crystal systems are depicted in Table 4.2. Using the Central Limit theorem [55], we found the statistical error to be (with 95% confidence) less than 0.038% for all values of $\overline{s}$, $\overline{x}$, and $\overline{y}$, and less than 0.085% for all values of $\overline{s^2}$, $\overline{x^2}$, and $\overline{y^2}$.

We notice the existence of an anisotropic effect in these systems. The different crystal structures generated by different values of ε have a clear, albeit small, influence on the

Table 4.2: MC results for 2-D crystal structures with different values of ε in a system with side $L = 300\underline{d}$. The histories of 300,000 particles were simulated in each structure.

$\varepsilon/\underline{d}$	$\overline{s}/\underline{d}$	$\overline{s^2}/\underline{d}^2$	$\overline{x}/\underline{d}$	$\overline{x^2}/\underline{d}^2$	$\overline{y}/\underline{d}$	$\overline{y^2}/\underline{d}^2$
0.000	1.10244	2.44410	7.79482	122.29243	7.79344	121.22575
0.025	1.12047	2.52776	7.92930	126.54002	7.91526	125.82595
0.050	1.13765	2.60955	8.04732	130.31563	8.04243	129.74593
0.075	1.15394	2.68889	8.16239	133.93388	8.16276	133.70556
0.100	1.16936	2.76587	8.27385	137.70277	8.28182	137.60788
0.125	1.18403	2.84029	8.38382	141.39732	8.39830	141.53241
0.150	1.19772	2.91117	8.48645	144.88046	8.50279	145.16813
0.175	1.21039	2.97788	8.57762	148.05934	8.60259	148.49665
0.200	1.22195	3.03960	8.66731	151.13043	8.68654	151.43461
0.225	1.23259	3.09780	8.74645	153.96186	8.77103	154.36769
0.250	1.24219	3.15069	8.82424	156.66775	8.84127	156.86334
0.275	1.25043	3.19685	8.89391	159.13655	8.90388	159.11226
0.300	1.25751	3.23740	8.95186	161.18709	8.96459	161.30808
0.325	1.26336	3.27091	8.99615	162.86061	9.00843	162.99574
0.350	1.26788	3.29743	9.03573	164.30590	9.03042	163.62808
0.375	1.27116	3.31524	9.05269	164.95272	9.04941	164.62668
0.400	1.27260	3.32532	9.08103	166.06989	9.06589	164.81296
0.425	1.27276	3.32627	9.08721	166.13262	9.06497	164.86495
0.450	1.27127	3.31716	9.07764	165.84179	9.04821	164.44010
0.475	1.26794	3.29768	9.05287	165.09427	9.01132	163.05926
0.500	1.26291	3.26842	9.01663	163.72652	8.97285	161.64332
0.525	1.25593	3.22831	8.96543	161.80768	8.91994	159.77961
0.550	1.24683	3.17666	8.89755	159.27108	8.84508	157.06033
0.575	1.23560	3.11401	8.81852	156.52926	8.75221	153.76830
0.600	1.22197	3.03946	8.71229	152.63346	8.64451	150.02422
0.625	1.20592	2.95443	8.58650	148.52579	8.52299	145.71070
0.650	1.18693	2.85529	8.44626	143.67400	8.38250	141.00162
0.675	1.16510	2.74442	8.27471	137.75901	8.22431	135.72128
0.700	1.14000	2.62119	8.07621	131.25257	8.04472	129.89065
0.725	1.11125	2.48469	7.86459	124.43457	7.83701	123.25003

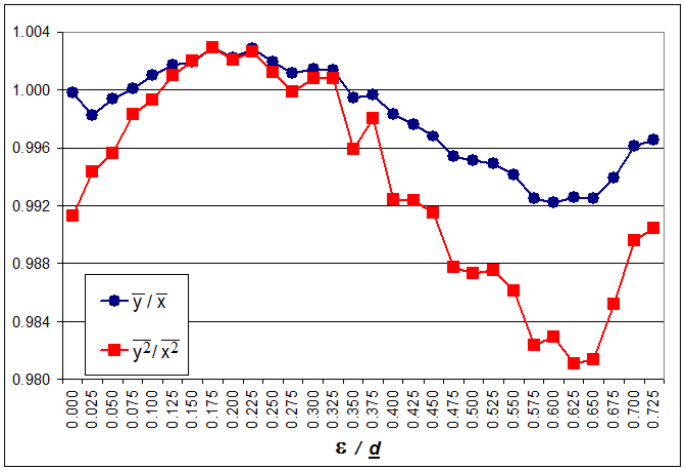

Figure 4.8: Ratios Between Vertical and Horizontal Mean and Mean Square Distances of a Particle to its Point of Birth in 2-D Crystal Structures with Different Values of ε

transport of particles (Figure 4.8). Further confirmation of this anisotropy is seen when comparing the relative differences from the vertical direction, given by:

(4.3a) $$S_1(\mathbf{\Omega}) = \frac{\overline{s_{\mathbf{\Omega}}}(\mathbf{\Omega}) - \overline{s_{\mathbf{\Omega}}}(\vec{\boldsymbol{j}})}{\overline{s_{\mathbf{\Omega}}}(\vec{\boldsymbol{j}})},$$

(4.3b) $$S_2(\mathbf{\Omega}) = \frac{\overline{s^2_{\mathbf{\Omega}}}(\mathbf{\Omega}) - \overline{s^2_{\mathbf{\Omega}}}(\vec{\boldsymbol{j}})}{\overline{s^2_{\mathbf{\Omega}}}(\vec{\boldsymbol{j}})};$$

and:

(4.4a) $$U_1(\mathbf{\Omega}) = \frac{\overline{\rho}(\mathbf{\Omega}) - \overline{\rho}(\vec{\boldsymbol{j}})}{\overline{\rho}(\vec{\boldsymbol{j}})},$$

(4.4b) $$U_2(\mathbf{\Omega}) = \frac{\overline{\rho^2}(\mathbf{\Omega}) - \overline{\rho^2}(\vec{\boldsymbol{j}})}{\overline{\rho^2}(\vec{\boldsymbol{j}})};$$

where $\overline{\rho}(\mathbf{\Omega})$ and $\overline{\rho^2}(\mathbf{\Omega})$ represent the mean and mean square distances of a particle to its point of birth in the direction $\mathbf{\Omega}$, and $\vec{\boldsymbol{j}} = (0, 1)$ is the unit vector in the y-direction. These quantities are depicted as percent functions of $|\Omega_y| = |\cos\varphi|$ in Figure 4.9, for two different crystal structures.

The first thing to notice is that S_2, U_1, and U_2 clearly show that the behavior of the particles depend upon direction. While $\overline{s_{\mathbf{\Omega}}}$ remains close to a constant troughout the system, $\overline{s^2_{\mathbf{\Omega}}}$ varies by more than 3.5% in both systems - this is a clear indication that the diffusion

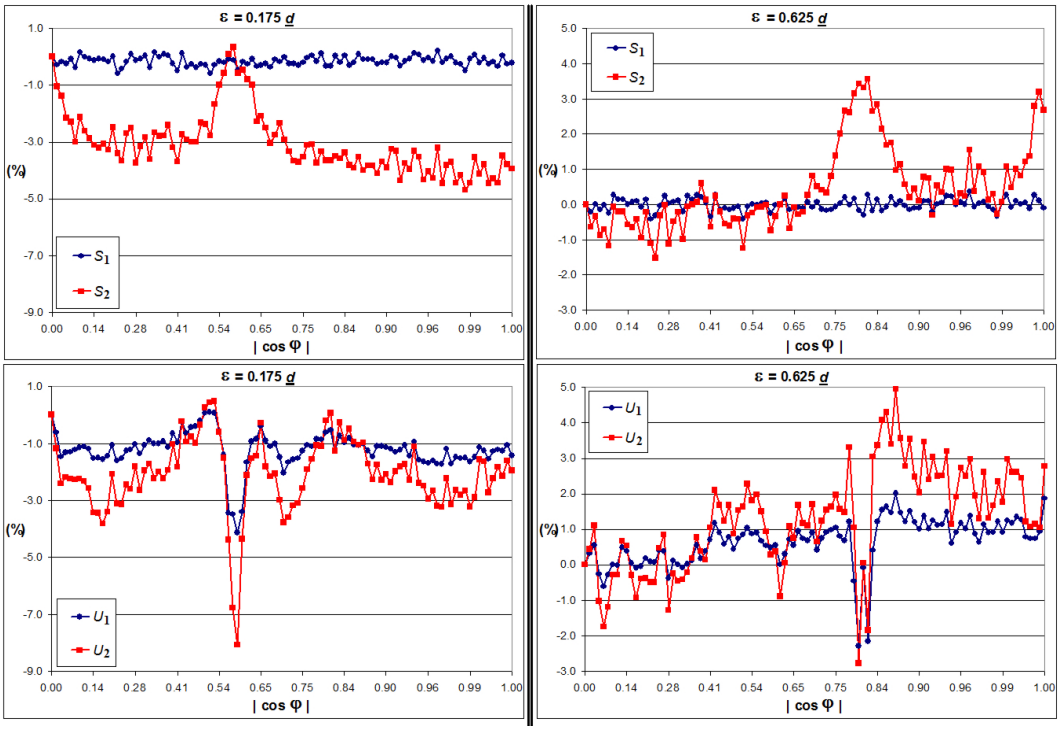

Figure 4.9: Percent Relative Differences from the Vertical Direction [as defined in Eqs. (4.3) and (4.4)] as Functions of $|\Omega_y| = |\cos\varphi|$ in Two Distinct 2-D Crystal Structures

coefficients must be different for the x and y directions, since $\overline{s^2_{\Omega}}$ plays an important role in their derivation [see Eq. (3.72)].

The valleys in the graphs of U_1 and U_2 are not unexpected; they appear near the angles formed between the centers of a disc and the centers of the adjacent discs. These angles satisfy $|\cos\varphi| = 0.5875$ and $|\cos\varphi| = 0.8125$ for $\varepsilon = 0.175\underline{d}$ and $\varepsilon = 0.625\underline{d}$, respectively.

4.2.2 Monte Carlo in 2-D Random Structures

For each realization of the random system, we have calculated the histories of 20,000 particles; the statistical error in each given realization was found to be (with 97.5% confidence) less than 0.052% for all values of $\overline{s}$, $\overline{x}$, and $\overline{y}$, and less than 0.116% for all values of $\overline{s^2}$, $\overline{x^2}$, and $\overline{y^2}$. We have developed 100 different realizations (adding to a total of 2,000,000 particles); the average Monte Carlo results and the statistical error bounds (with 95% con-

Table 4.3: Ensemble-averaged MC results for 2-D random structures in a system with side $L = 300\underline{d}$. A total of 100 different random realizations were generated; the histories of 20,000 particles were simulated in each realization.

	$\overline{s}/\underline{d}$	$\overline{s^2}/\underline{d}^2$	$\overline{x}/\underline{d}$	$\overline{x^2}/\underline{d}^2$	$\overline{y}/\underline{d}$	$\overline{y^2}/\underline{d}^2$
Ensemble Average	1.21941	3.03092	8.65893	150.58600	8.69107	151.78946
Statistical Error	0.145%	0.308%	0.181%	0.373%	0.158%	0.339%

fidence) are given in Table 4.3.

Once more, we observe a small - but consistent - anisotropic effect. We found $\overline{y} > \overline{x}$ and $\overline{y^2} > \overline{x^2}$ for *every* realization of the system; in particular, the ensemble-averaged values yield $\overline{y}/\overline{x} = 1.00371$ and $\overline{y^2}/\overline{x^2} = 1.00799$. Further confirmation of this anisotropy can again be seen with the expressions given by Eqs. (4.3) and (4.4), this time using the ensemble-averaged values of $\overline{s_{\mathbf{\Omega}}}(\mathbf{\Omega})$, $\overline{s^2_{\mathbf{\Omega}}}(\mathbf{\Omega})$, $\overline{\rho}(\mathbf{\Omega})$, and $\overline{\rho^2}(\mathbf{\Omega})$. The percent relative differences are shown in Figure 4.10 as functions of $|\Omega_y| = |\cos\varphi|$.

4.3 Theoretical and Monte Carlo Estimates

In this section, we compare the values of the diffusion coefficients (and k_D) obtained numerically through Monte Carlo with those estimated by atomic mix and the proposed generalized theory.

4.3.1 Results in 2-D Crystal Structures

Introducing the numerically obtained results for $\overline{s}$ (as shown in Table 4.2) into Eq. (2.50), we obtain a Monte Carlo estimate for the absorption cross section, denoted Σ_a^{mc}. Using this estimate and the numerical results $\overline{x^2}$ and $\overline{y^2}$ shown in Table 4.2, Eqs. (2.53a)

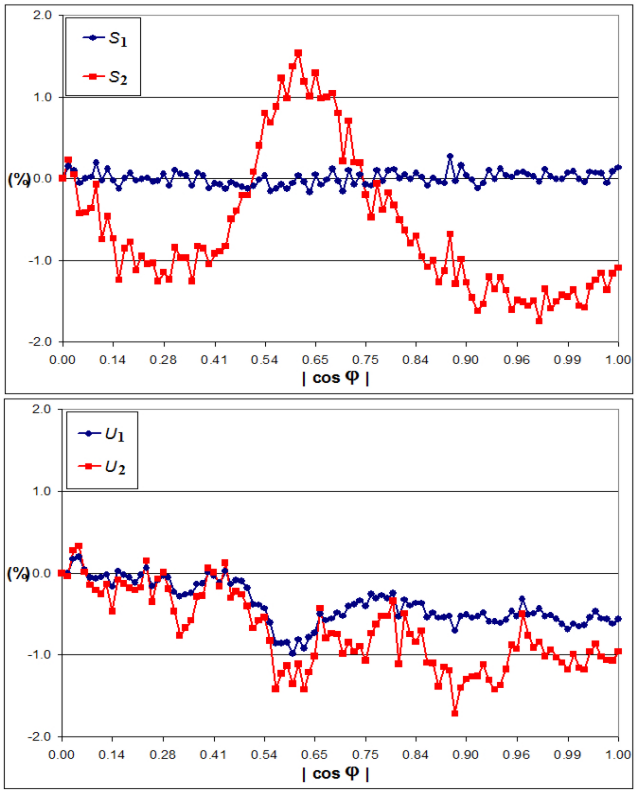

Figure 4.10: Percent Relative Differences from the Vertical Direction [as defined in Eqs. (4.3) and (4.4)] as Functions of $|\Omega_y| = |\cos\varphi|$ in the 2-D Random System

and (2.53b) yield the 2-D numerical diffusion coefficients

(4.5a) $$\mathrm{D}_x^{mc} = \overline{x^2}\frac{\Sigma_a^{mc}}{2} ,$$

(4.5b) $$\mathrm{D}_y^{mc} = \overline{y^2}\frac{\Sigma_a^{mc}}{2} ,$$

for 2-D crystal structures.

The 2-D atomic mix diffusion coefficient [see Eq. (2.64)] for crystal structures is given by:

(4.6) $$\mathrm{D}^{am} = \frac{1}{2}\left(\frac{1}{\Gamma\Sigma_t}\right) ,$$

where Γ is the packing fraction of the system and Σ_t is given by Table 4.1.

Assuming the locations of the scattering centers to be independent of direction, the 2-D isotropic diffusion coefficient obtained by the generalized theory [see Eq. (3.70)] is given

Table 4.4: Numerical (MC) and theoretical estimates for the diffusion coefficients in 2-D crystal structures with different values of ε.

$\varepsilon/\underline{d}$	$\mathrm{D}_x^{mc}/\underline{d}$	$\mathrm{D}_y^{mc}/\underline{d}$	$\mathrm{D}^{am}/\underline{d}$	$\mathrm{D}^{iso}/\underline{d}$	$\mathrm{D}_x^{gt}/\underline{d}$	$\mathrm{D}_y^{gt}/\underline{d}$
0.000	0.55465	0.54981	0.55290	0.55425	0.55436	0.55414
0.025	0.56467	0.56149	0.56319	0.56400	0.56465	0.56334
0.050	0.57274	0.57024	0.57213	0.57345	0.57472	0.57218
0.075	0.58033	0.57934	0.57952	0.58254	0.58426	0.58083
0.100	0.58879	0.58839	0.58784	0.59132	0.59349	0.58915
0.125	0.59710	0.59767	0.59614	0.59971	0.59713	0.60228
0.150	0.60482	0.60602	0.60326	0.60765	0.60476	0.61053
0.175	0.61162	0.61343	0.60846	0.61507	0.61198	0.61815
0.200	0.61840	0.61964	0.61402	0.62187	0.61869	0.62506
0.225	0.62455	0.62619	0.61830	0.62831	0.62510	0.63152
0.250	0.63061	0.63140	0.62300	0.63410	0.63095	0.63725
0.275	0.63633	0.63623	0.62810	0.63915	0.63629	0.64201
0.300	0.64090	0.64138	0.63364	0.64361	0.64109	0.64613
0.325	0.64455	0.64509	0.63521	0.64726	0.64511	0.64942
0.350	0.64796	0.64528	0.63712	0.65019	0.65190	0.64847
0.375	0.64883	0.64754	0.63939	0.65201	0.65316	0.65086
0.400	0.65248	0.64754	0.64048	0.65325	0.65380	0.65270
0.425	0.65265	0.64767	0.64048	0.65336	0.65348	0.65324
0.450	0.65227	0.64675	0.63784	0.65233	0.65308	0.65158
0.475	0.65103	0.64301	0.63869	0.65020	0.65152	0.64889
0.500	0.64821	0.63996	0.63399	0.64700	0.64888	0.64512
0.525	0.64417	0.63610	0.62976	0.64261	0.64492	0.64031
0.550	0.63870	0.62984	0.62793	0.63694	0.63959	0.63430
0.575	0.63341	0.62224	0.62212	0.63006	0.63295	0.62717
0.600	0.62454	0.61386	0.61566	0.62183	0.62465	0.61902
0.625	0.61582	0.60415	0.60535	0.61249	0.61524	0.60973
0.650	0.60523	0.59398	0.59562	0.60140	0.60375	0.59906
0.675	0.59119	0.58244	0.58574	0.58888	0.59065	0.58710
0.700	0.57567	0.56969	0.57477	0.57482	0.57582	0.57382
0.725	0.55988	0.55455	0.55877	0.55898	0.55912	0.55885

by the following expression:

$$\mathrm{D}^{iso} = \frac{1}{2}\left(\frac{\overline{s^2}}{2\overline{s}}\right), \tag{4.7}$$

where $\overline{s}$ and $\overline{s^2}$ are the numerical values shown in Table 4.2.

We note that, since diffusion occurs only in a plane, the diffusion coefficients in Eqs. (4.6) and (4.7) contain a factor of $1/2$ instead of the classic 3-D factor $1/3$. This comes from $\frac{1}{2\pi}\int_0^{2\pi}\cos^2(\varphi)\,d\varphi = \frac{1}{2\pi}\int_0^{2\pi}\sin^2(\varphi)\,d\varphi = 1/2$.

Finally, since scattering is isotropic, the 2-D (anisotropic) diffusion coefficients ob-

tained by the generalized theory are given by [see Eqs. (3.72)]:

$$\mathrm{D}_x^{gt} = \frac{1}{2\overline{s}} \left(\frac{1}{2\pi} \int_0^{2\pi} \overline{s^2_{\mathbf{\Omega}}}(\mathbf{\Omega}) \cos^2(\varphi)\, d\varphi \right) , \tag{4.8a}$$

$$\mathrm{D}_y^{gt} = \frac{1}{2\overline{s}} \left(\frac{1}{2\pi} \int_0^{2\pi} \overline{s^2_{\mathbf{\Omega}}}(\mathbf{\Omega}) \sin^2(\varphi)\, d\varphi \right) , \tag{4.8b}$$

where $\mathbf{\Omega} = (\cos\varphi, \sin\varphi)$, $\overline{s}$ is given by the numerical values shown in Table 4.2, and $\overline{s^2_{\mathbf{\Omega}}}(\mathbf{\Omega})$ is also numerically calculated for each system. All values of the diffusion coefficients are shown in Table 4.4.

We define the percent differences between the theoretical and the Monte Carlo esti-

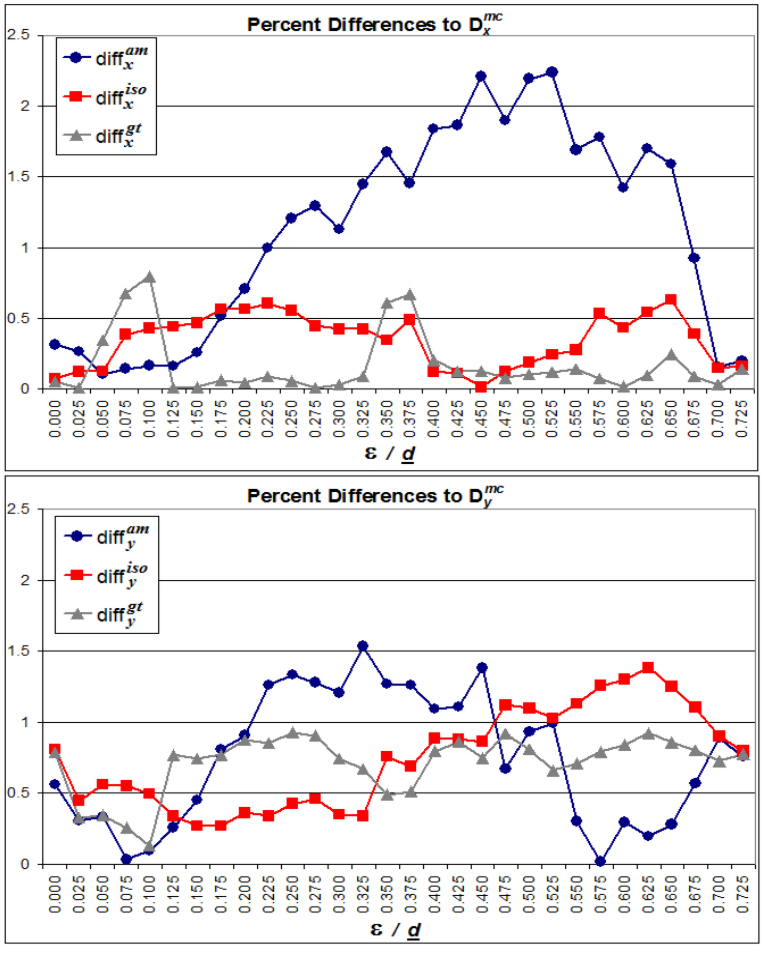

Figure 4.11: Percent Differences Between Theoretical and Monte Carlo Estimates for the Diffusion Coefficients in 2-D Crystal Structures with Different Values of ε

mates for the diffusion coefficients as:

$$\text{diff}_x^{am} = 100\frac{|\mathrm{D}^{am} - \mathrm{D}_x^{mc}|}{\mathrm{D}_x^{mc}}, \quad \text{diff}_y^{am} = 100\frac{|\mathrm{D}^{am} - \mathrm{D}_y^{mc}|}{\mathrm{D}_y^{mc}}, \tag{4.9a}$$

$$\text{diff}_x^{iso} = 100\frac{|\mathrm{D}^{iso} - \mathrm{D}_x^{mc}|}{\mathrm{D}_x^{mc}}, \quad \text{diff}_y^{iso} = 100\frac{|\mathrm{D}^{iso} - \mathrm{D}_y^{mc}|}{\mathrm{D}_y^{mc}}, \tag{4.9b}$$

$$\text{diff}_x^{gt} = 100\frac{|\mathrm{D}_x^{gt} - \mathrm{D}_x^{mc}|}{\mathrm{D}_x^{mc}}, \quad \text{diff}_y^{gt} = 100\frac{|\mathrm{D}_y^{gt} - \mathrm{D}_y^{mc}|}{\mathrm{D}_y^{mc}}; \tag{4.9c}$$

these differences are depicted in Figure 4.11 as functions of $\varepsilon/\underline{d}$.

As expected, the atomic mix model presents small errors when the packing fraction is high. For $\varepsilon \leq 0.075\underline{d}$ and $\varepsilon \geq 0.6\underline{d}$, the estimate D^{am} is accurate enough to fall in between the Monte Carlo results D_x^{mc} and D_y^{mc}. However, as the packing fraction decreases (and $\overline{s}$ increases), atomic mix consistently underestimates the diffusion coefficients, differing by as much as 2.23% and 1.53% from D_x^{mc} and D_y^{mc}, respectively.

The generalized theory has maximum errors differences of 0.8% and 1.38% for D_x and D_y. However, apart from systems with very high packing fractions, it seems to have a better performance than atomic mix. Since the anisotropic effect in these systems is very small, the anisotropic estimates D^{gt} and the isotropic estimate D^{iso} are very close. Nevertheless, at least for the prediction of D_x, we can argue that D_x^{gt} is generally a better choice than D^{iso}. Moreover, with one single exception ($\varepsilon = 0.275\underline{d}$), D^{gt} correctly predicted the general anisotropic behavior of all the systems; that is, $\mathrm{D}_x^{gt} > \mathrm{D}_y^{gt}$ when $\mathrm{D}_x^{mc} > \mathrm{D}_y^{mc}$ and $\mathrm{D}_x^{gt} < \mathrm{D}_y^{gt}$ when $\mathrm{D}_x^{mc} < \mathrm{D}_y^{mc}$ for all but one of the systems simulated.

Table 4.5: Parameters applied in Eq. (2.43) to calculate the different estimates of k_D in 2-D systems.

	Monte Carlo	Atomic Mix	Isotropic Generalized Theory	Anisotropic Generalized Theory
D_x	Eq. (4.5a)	Eq. (4.6)	Eq. (4.7)	Eq. (4.8a)
D_y	Eq. (4.5b)	Eq. (4.6)	Eq. (4.7)	Eq. (4.8b)
Σ_a	$\frac{1-c}{\overline{s}}$	$\langle\Sigma_a\rangle = \Gamma\Sigma_a$	$\frac{1-c}{\overline{s}}$	$\frac{1-c}{\overline{s}}$

To discuss the magnitude of the differences between predictions made by the atomic mix model and the generalized theory, we consider estimates for k_D. Assuming dimensions for the 2-D model reactor core that are comparable to those of the MPBR design [35] (width $X = 58.33\underline{d}$ and height $Y = 166.67\underline{d}$), we adapt Eq. (2.43) for the different methods presented (as summarized in Table 4.5). The resulting values of k_D are shown in Table 4.6, as calculated by:

$$\frac{k_D^{mc}}{\nu\Sigma_f} = \left[\Sigma_a^{mc} + \pi^2\left(\frac{\mathrm{D}_x^{mc}}{X^2} + \frac{\mathrm{D}_y^{mc}}{Y^2}\right)\right]^{-1}, \tag{4.10a}$$

$$\frac{k_D^{am}}{\nu\Sigma_f} = \left[\Gamma\Sigma_a + \pi^2\left(\frac{1}{X^2} + \frac{1}{Y^2}\right)\mathrm{D}^{am}\right]^{-1}, \tag{4.10b}$$

$$\frac{k_D^{iso}}{\nu\Sigma_f} = \left[\Sigma_a^{mc} + \pi^2\left(\frac{1}{X^2} + \frac{1}{Y^2}\right)\mathrm{D}^{iso}\right]^{-1}, \tag{4.10c}$$

$$\frac{k_D^{gt}}{\nu\Sigma_f} = \left[\Sigma_a^{mc} + \pi^2\left(\frac{\mathrm{D}_x^{gt}}{X^2} + \frac{\mathrm{D}_y^{gt}}{Y^2}\right)\right]^{-1}; \tag{4.10d}$$

where Γ is the packing fraction and $\overline{s}$ is shown in Table 4.2.

We define the percent differences between the theoretical and Monte Carlo estimates for k_D as:

$$\mathrm{diff}_k^{am} = 100\frac{|k_D^{am} - k_D^{mc}|}{k_D^{mc}}, \tag{4.11a}$$

$$\mathrm{diff}_k^{iso} = 100\frac{|k_D^{iso} - k_D^{mc}|}{k_D^{mc}}, \tag{4.11b}$$

$$\mathrm{diff}_k^{gt} = 100\frac{|k_D^{gt} - k_D^{mc}|}{k_D^{mc}}; \tag{4.11c}$$

these differences are depicted in Figure 4.12 as functions of $\varepsilon/\underline{d}$.

We emphasize again that k_D is the eigenvalue of the problem described by Eqs. (2.41), not the eigenvalue of the problem described by Eqs. (2.34). The problem (2.41) is simpler than the problem (2.34) in two ways: (i) it is a *diffusion* problem, not a transport problem; and (ii) it has been homogenized (its coefficients are spatially constant). We expect that for the problem considered, $k_D \approx k$, but we cannot be sure of the difference between

Table 4.6: Numerical (MC) and theoretical estimates for k_D (assuming MPBR-like 2-D core dimensions: $X = 58.33\underline{d}$ and $Y = 166.67\underline{d}$) in 2-D crystal structures with different values of ε.

$\varepsilon/\underline{d}$	$k_D^{mc}/(\nu\Sigma_f)$	$k_D^{am}/(\nu\Sigma_f)$	$k_D^{iso}/(\nu\Sigma_f)$	$k_D^{gt}/(\nu\Sigma_f)$
0.000	91.95481	92.22298	91.95118	91.94879
0.025	92.91822	93.35687	92.92751	92.91309
0.050	93.86249	94.32233	93.83424	93.80579
0.075	94.74185	95.10556	94.67407	94.63504
0.100	95.52472	95.97272	95.44844	95.39819
0.125	96.24715	96.82265	96.17045	96.23118
0.150	96.91120	97.53837	96.82870	96.89759
0.175	97.52523	98.05410	97.42465	97.49921
0.200	98.06378	98.59805	97.95934	98.03728
0.225	98.55189	99.01299	98.43866	98.51787
0.250	98.97360	99.46240	98.86520	98.94356
0.275	99.31516	99.94530	99.22426	99.29593
0.300	99.61180	100.46333	99.52585	99.58952
0.325	99.85916	100.60847	99.77316	99.82786
0.350	100.04165	100.78508	99.95952	99.91586
0.375	100.21257	100.99327	100.10404	100.07463
0.400	100.19536	101.09323	100.15259	100.13854
0.425	100.19988	101.09323	100.15889	100.15577
0.450	100.12210	100.85096	100.10036	100.08121
0.475	99.96474	100.92927	99.96323	99.92980
0.500	99.74379	100.49520	99.75385	99.70617
0.525	99.43713	100.10152	99.45904	99.40106
0.550	99.04304	99.92976	99.06826	99.00214
0.575	98.50751	99.37920	98.57502	98.50369
0.600	97.91397	98.75755	97.96199	97.89327
0.625	97.15093	97.74637	97.21431	97.14817
0.650	96.23153	96.76985	96.31008	96.25480
0.675	95.19647	95.75558	95.23648	95.19552
0.700	93.94949	94.60383	93.95512	93.93276
0.725	92.42304	92.87259	92.43192	92.42903

these two eigenvalues. Our purpose in presenting various estimates of k_D is to illustrate the magnitude of the expected changes in quantities that are important to potential users of pebble-bed reactors, due to the changes in the definitions of the homogenized cross sections and diffusion coefficients.

The first thing to notice from Figure 4.12 is the significant difference between the estimates of the atomic mix and the generalized theory (we emphasize that differences on the order of 0.1% in k_D are significant). As we expected, the accuracy of the atomic mix

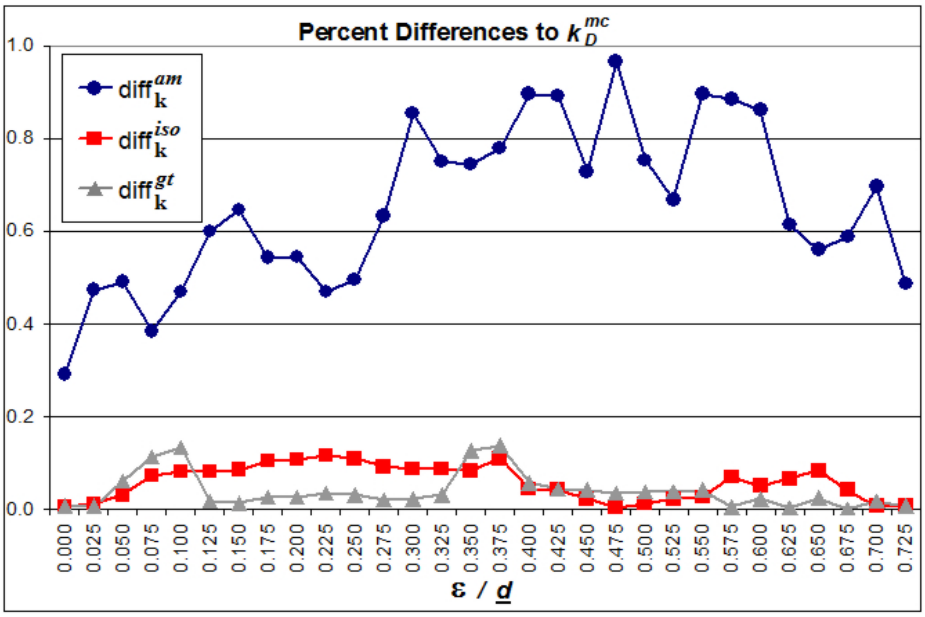

Figure 4.12: Percent Differences Between Theoretical and Monte Carlo Estimates for k_D (assuming MPBR-like 2-D core dimensions) in 2-D Crystal Structures with Different Values of ε

model deteriorates as the packing fraction decreases. The generalized theory is clearly an improvement over atomic mix in all cases: the *maximum* difference obtained with the generalized theory was 0.138%, while the *minimum* difference obtained with the atomic mix model was 0.292%. Both the anisotropic and the isotropic estimates present better accuracy (up to 0.93%) than the atomic mix estimates, being at least 0.27% more accurate in all simulated systems.

4.3.2 Results in 2-D Random Structures

To obtain estimates for the diffusion coefficients in a 2-D random system we use the same procedure presented for the crystal structures, together with the ensemble-averaged results in Table 4.2 and the ensemble-averaged packing fraction $\overline{\Gamma} = 0.817$. The estimates and the percent differences between theoretical and Monte Carlo estimates are shown in Tables 4.7 and 4.8.

We can see that, while the atomic mix model yields small errors in its estimate of the diffusion coefficient, the results obtained with the generalized theory are much more

Table 4.7: Numerical (MC) and theoretical estimates for the diffusion coefficients in the 2-D random system.

$D_x^{mc}/\underline{d}$	$D_y^{mc}/\underline{d}$	$D^{am}/\underline{d}$	$D^{iso}/\underline{d}$	$D_x^{gt}/\underline{d}$	$D_y^{gt}/\underline{d}$
0.61745	0.62239	0.61199	0.62139	0.61991	0.62287

Table 4.8: Percent differences between theoretical and Monte Carlo estimates for the diffusion coefficients in the 2-D random system.

diff_x^{am}	diff_y^{am}	diff_x^{iso}	diff_y^{iso}	diff_x^{gt}	diff_y^{gt}
0.88428	1.67011	0.63759	0.16031	0.39843	0.07775

accurate. Once more, the atomic mix results underestimate the diffusion coefficients, while the isotropic estimate D^{iso} falls in betwen the values of D_x^{mc} and D_y^{mc}. Moreover, the anisotropic estimates D^{gt} correctly predict the diffusion behavior (larger in the y-direction).

We can also obtain estimates for k_D, with a similar procedure to the one applied to the crystal structures; the results are shown in Tables 4.9 and 4.10. As expected, the

Table 4.9: Numerical (MC) and theoretical estimates for k_D in the 2-D random system (assuming MPBR-like 2-D core dimensions: $X = 58.33\underline{d}$ and $Y = 166.67\underline{d}$).

$k_D^{mc}/(\nu\Sigma_f)$	$k_D^{am}/(\nu\Sigma_f)$	$k_D^{iso}/(\nu\Sigma_f)$	$k_D^{gt}/(\nu\Sigma_f)$
97.91738	98.40062	97.81141	97.84737

Table 4.10: Percent differences between theoretical and Monte Carlo estimates for k_D in the 2-D random system (assuming MPBR-like 2-D core dimensions).

diff_k^{am}	diff_k^{iso}	diff_k^{gt}
0.49352	0.10822	0.07150

generalized theory is significantly more accurate than the atomic mix model. The estimates k_D^{iso} and k_D^{gt} are more than 0.38% and 0.42% more accurate than the atomic mix estimate k_D^{am} (a performance more than four times better in both cases).

In this chapter we have calculated (using Monte Carlo) the "true" values of the diffu-

sion coefficients for different 2-D models of pebble-bed reactor cores. We have shown that, when compared to these values, the generalized theory is (in general) significantly more accurate than the atomic mix model. Moreover, the generalized theory successfully predicts even very small anisotropic effects in the estimates of the diffusion coefficients.

Estimates of the diffusion eigenvalue k_D show that the generalized theory is more accurate than atomic mix (by up to 0.93%). However, we have not directly shown that the estimate of k [the mean eigenvalue of the heterogeneous-medium transport problem described by Eqs. (2.34)] obtained with the generalized theory is more accurate than the atomic mix estimate. Nevertheless, because the generalized theory is consistently more accurate than atomic mix for quantities that have been estimated by Monte Carlo, it is reasonable to expect that the difference between the accuracy of these methods in estimating k_D will translate to the estimation of k. In other words, the estimates of k obtained with the generalized theory should be more accurate than the atomic mix estimates of k by approximately the same amount observed in the diffusion case.

CHAPTER V

A Model 3-D Pebble-Bed Reactor Core

This chapter presents the applications of the proposed generalized diffusion theory to 3-D pebble-bed reactor cores. For simplicity, we do not simulate the actual cylindrical geometry of a pebble-bed core, but rather the simpler geometry of hard spheres of radius r packed inside a cubic box with side L. Once more, we have developed a Monte Carlo computer code capable of deriving random realizations of the 3-D system; and a second Monte Carlo code that performs 3-D neutron transport inside the heterogeneous core. We apply this second Monte Carlo code to both stochastic and crystal-like pilings of the spheres. Comparisons between the numerical Monte Carlo results and the results obtained with the proposed generalized theory are presented, as well as comparisons with the atomic mix theory and its corrections. We close the chapter with a discussion regarding the behavior of particles generated by spheres located close to the edges of the system, where packing fractions are rather different than in the middle of the system.

5.1 3-D Packings

In this section we introduce the different approaches we used to pack hard spheres in the 3-D system. Section 5.1.1 describes the piling of crystal structures, while Section 5.1.2 discusses the case of a random piling of spheres.

5.1.1 3-D Crystal Structures

There are several possible ways of piling identical hard spheres in a crystal-like structure. For the study of the pebble-bed problem, structures that are worth mentioning are the simple cubic (with packing fraction $\Gamma \approx 0.52$), the BCC: body-centered cubic ($\Gamma \approx 0.68$), the HCP: hexagonal close-packed ($\Gamma \approx 0.74$), and the FCC: face-centered cubic ($\Gamma \approx 0.74$). In fact, the problem of determining the packing fraction of identical spheres in a container has been under study for a long time. The maximum packing fraction of $\pi/\sqrt{18} \approx 0.74048$ was first conjectured by Kepler in 1611 [80] in his work *Strena*

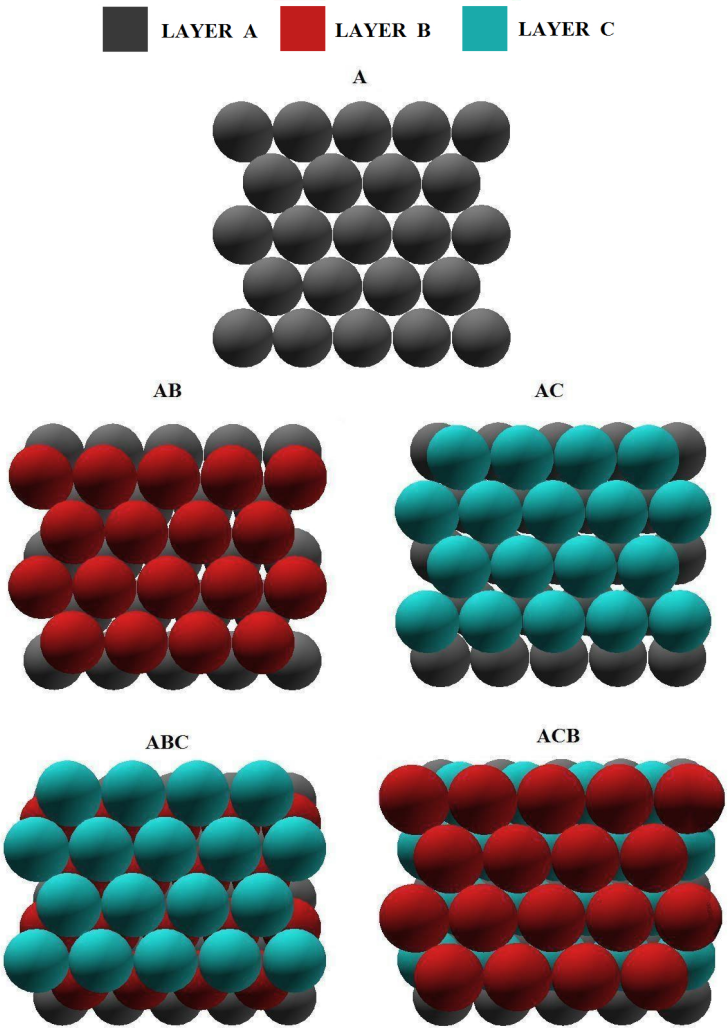

Figure 5.1: Sequential Construction of FCC Structures

seu de nive sexangula (On the Six-Cornered Snowflake), and only recently it was shown to be correct [32].

To achieve this maxium packing fraction, we have to start with a first layer (A) of spheres with centers arranged in a hexagonal lattice (similar to the cases $\varepsilon = 0$ and $\varepsilon = \varepsilon_{max}$ shown in Figure 4.2). A second layer (also arranged in a hexagonal lattice) is then positioned on top of the first, with each sphere centered above the gaps between spheres on the first layer. Notice that there are two possible positionings (B and C) for this second layer. Every sequence of A, B, and C without immediate repetition of the same one is possible and yields the same packing fraction. In particular, the sequence where every other layer is the same (ABABAB... or ACACAC...) is the HCP structure; and the sequence where every third layer is the same (ABCABC... or ACBACB...) is the FCC structure (Figure 5.1).

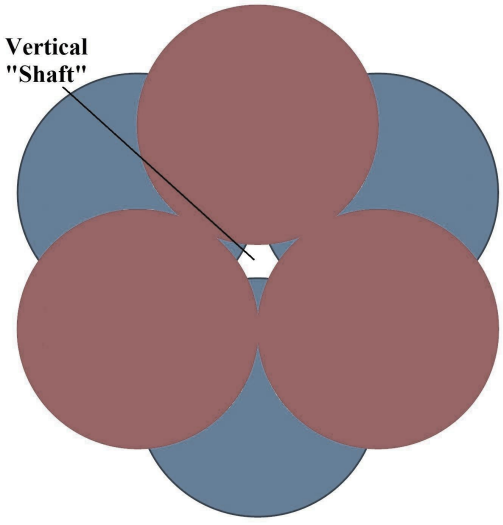

Figure 5.2: Example of Vertical “Shaft” in a HCP Structure

In this work we have opted for face-centered systems, since they are capable of yielding the highest packing fractions. Although HCP structures yield the same packing fractions as the FCC, they generate vertical “shafts” in the system (Figure 5.2) that would allow

very long streaming paths and bias the transport in that direction. Hence, we discarded the option of simulating systems with HCP-like layers. We describe the packing of the simulated structures next.

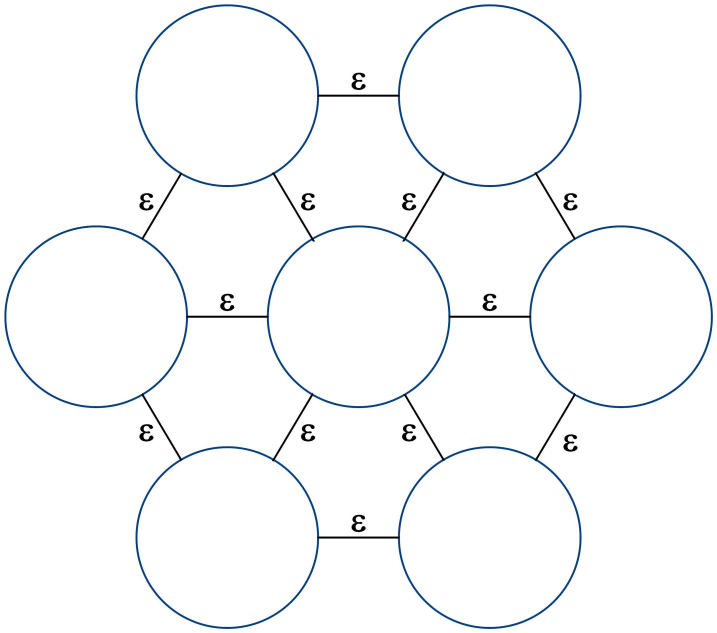

Figure 5.3: Arrangement of Spheres in a Layer with a Given Distance ε

Let $\underline{d} = 2r$ be the diameter of a fuel sphere, and ε be the fixed distance between spheres in the same layer, as shown in Figure 5.3. Bearing in mind that we do not allow spheres to overlap the limits of the cubic box in which they are packed, we place the first layer (A) of spheres in the system, at the bottom of the box - and then lock them in place. We then proceed to fill the system in a face-centered fashion; that is, positioning the second (B) and third (C) layers and sequentially repeating this structure. The height h_i of the i^{th} layer can be defined directly from the previous layers by

$$h_i = h_{i-1} + \sqrt{\underline{d}^2 - \frac{1}{3}(\underline{d}+\varepsilon)^2} = h_1 + (i-1)\sqrt{\underline{d}^2 - \frac{1}{3}(\underline{d}+\varepsilon)^2}\,,\ \forall\ i \geq 1\,. \tag{5.1}$$

Notice that these structures allow spheres at the edges of the packing to be unstable under gravity if they do not touch a wall (they only rest upon two other spheres). As in the 2-D

case, this is a valid approximation of the infinite system when L is large. An example of this type of piling is shown in Figure 5.4.

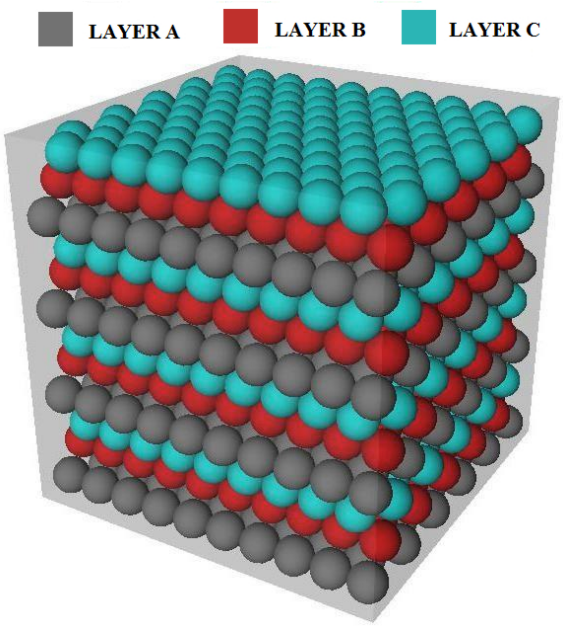

Figure 5.4: Example of a 3-D Crystal Structure (FCC: $\varepsilon = 0$) in a System with Side $L = 10\underline{d}$

For $\varepsilon = 0$, this packing method yields the classic FCC structure, with coordination number (number of spheres contacted by a given sphere) 12; that is, each sphere inside the system touches 12 other spheres. For instance, a typical sphere in layer i touches 3 spheres in layer $i - 1$, 3 spheres in layer $i + 1$, and 6 spheres in layer i itself (Figure 5.5).

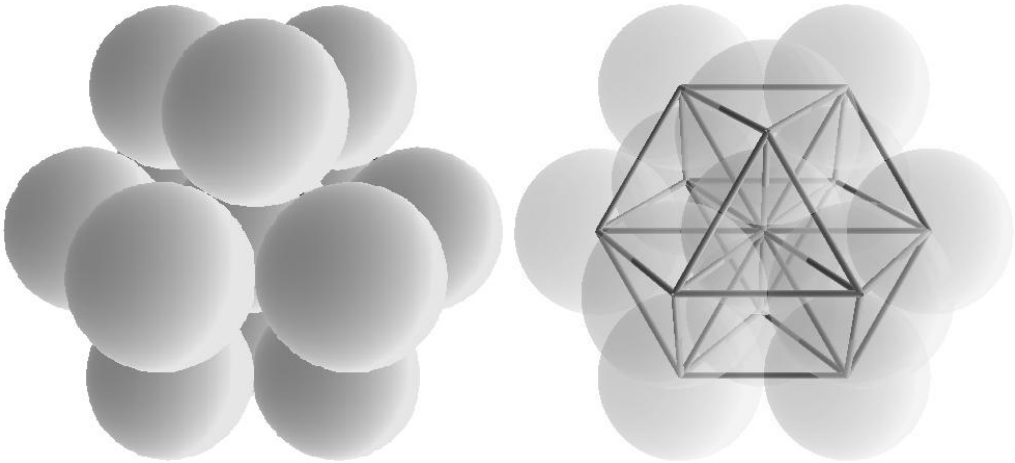

Figure 5.5: Arrangement of Spheres in a 3-D Crystal Structure with $\varepsilon = 0$

For the cases with $\varepsilon > 0$, however, the "cubic" feature of these face-centered systems is lost; the structure resembles that of a face-centered orthorhombic. Moreover, since we do not allow spheres to overlap each other, ε must not exceed a maximum value, in order to maintain the crystal-like structure of the packing:

$$\varepsilon_{max} = \underline{d}\left(\frac{2}{3}\sqrt{6} - 1\right) . \tag{5.2}$$

The packing structures generated with $0 < \varepsilon < \varepsilon_{max}$ have coordination number 6; a typical sphere in layer i touches 3 spheres in layer $i - 1$ and 3 spheres in layer $i + 1$, as depicted in Figure 5.6.

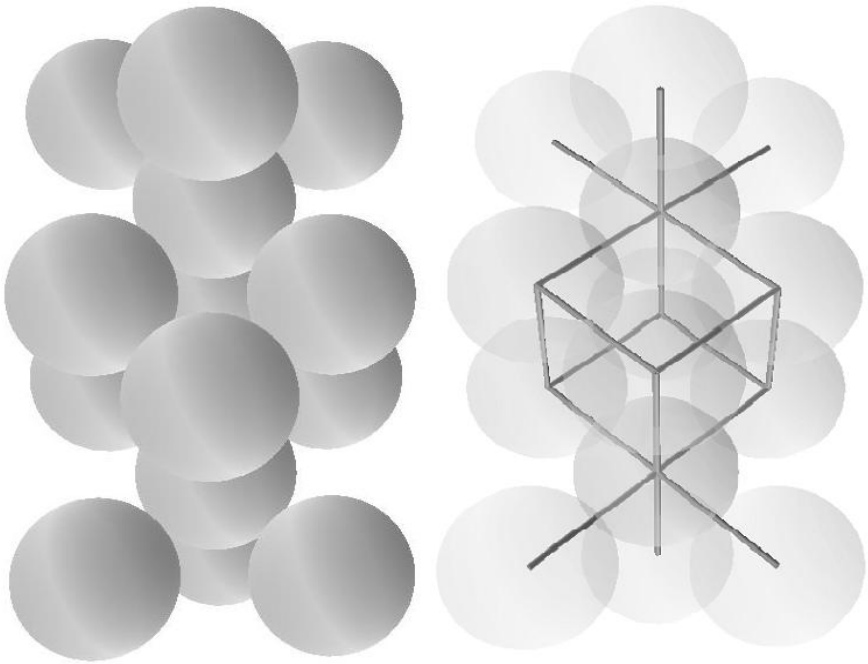

Figure 5.6: Arrangement of Spheres in a 3-D Crystal Structure with $0 < \varepsilon < \varepsilon_{max}$

Contrary to what happens in the case of the 2-D crystal structures presented in the previous chapter, the 3-D packing generated with $\varepsilon = \varepsilon_{max}$ is *not* a rotation of the one generated with $\varepsilon = 0$. It is rather a geometrically different structure, with coordination number 8; a typical sphere in layer i touches three spheres in layer $i - 1$, three spheres in layer $i + 1$, one sphere in layer $i - 3$, and one sphere in layer $i + 3$ (Figure 5.7).

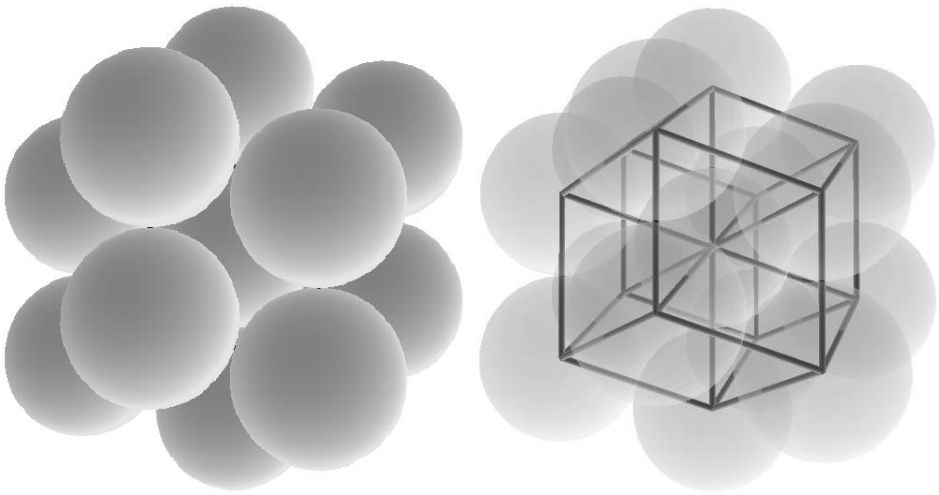

Figure 5.7: Arrangement of Spheres in a 3-D Crystal Structure with $\varepsilon = \varepsilon_{max}$

We define the packing fraction Γ as the ratio between the total volume of the fuel spheres and the volume of the box. The graph in Figure 5.8 shows the packing fraction Γ as a function of $\varepsilon/\underline{d}$ (in increments of 0.025).

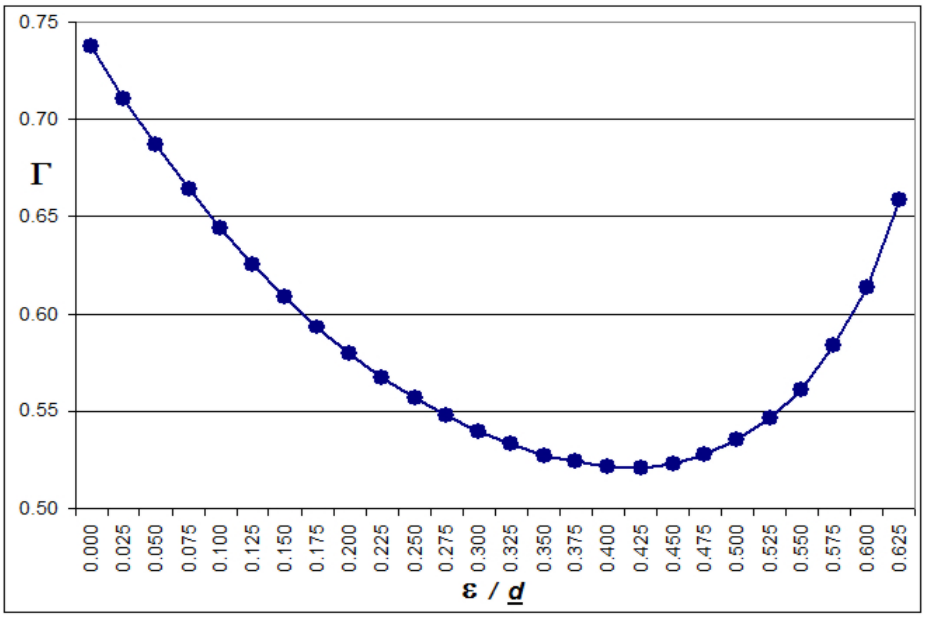

Figure 5.8: Packing Fractions in 3-D Crystal Structures with Different Values of ε

5.1.2 3-D Random Structures

Random close packing, and in particular random close packing of hard spheres, has been the subject of several studies, due to its many applications. As summarized in [95], exhaustive experimental work has lead to believe that randomly packed spheres of the same diameter cannot have a packing fraction larger than ≈ 0.64; in fact, recent analytical work yields the same results [74]. It has also been argued, however, that the definition of random packing itself is not well-defined [82, 83].

For the problem of pebble-bed cores, the most accepted average packing fraction ranges from 0.60 to 0.62, values that were experimentally validated by El Wakil [28]. However, the probability of occurrence of any single packing structure is not quantified, and as pointed out by Ougouag & Terry [59], there exists neither experimental evidence nor theoretical proof to support the assertion that other packing arrangements within the core are impossible. In fact, it has been shown [18] that changes in the friction coefficients have a significant influence on the structuring of the pebbles; under certain loading circumstances, packing fractions of 0.59 are possible.

A large variety of methods have been used to model pebble-bed cores. High-fidelity methods, modeling the dynamic behavior of spheres, have been the subject of recent research [18, 60, 61, 70, 71]. These methods must be used when keeping track of pebble position history is necessary; for the problem we are to approach, however, the path history of pebbles is not relevant. Since we are only interested in the final resting positions of the spheres, a low-fidelity method (which does not model the dynamic behavior of the spheres) was used.

Low-fidelity methods based on sequential models were summarized in [34]. In that work, every model starts with a first layer in which the horizontal projections of the centers of spheres form a square lattice, with lattice spacing equal to the sphere diameter.

Then, this first layer is randomly disordered from a purely horizontal plane by adding random vertical displacements to the coordinates of all the spheres. The ballistic deposition method [33, 53] was found to have the second highest packing fraction amongst the methods analyzed; a variation of the Bennett procedure [6] was found to reach the highest packing fraction. However, this procedure is entirely deterministic; that is, the randomness of the packings comes only from the randomness originally put in the first layer. We find that this is an undesirable feature for our packing structures, since one of our interests is to find how much the effect of gravity in the randomness of the system affects the transport of particles. Thus, in this work, we chose to develop a variation of the ballistic deposition method.

In our ballistic algorithm, each sphere is released at a random point above the box. It then follows a steepest descent trajectory until it reaches a position that is stable under gravity, in which case it has its coordinates stored. This method is the exact 3-D analogy of the 2-D algorithm described in Chapter IV. Figure 5.10 contains a flux diagram for the dropping of a new sphere into the box. Given a (incomplete) realization of the system, we randomly drop and store the coordinates of 20 different *tentative* spheres; we then choose the one with the lowest z-coordinate to be added to the system, and discard the 19 remaining ones. Once a sphere is added to the system, its position is locked; that is, the sphere is frozen in place.

As in the 2-D case, rearrangement of spheres and/or cascading events cannot happen. No velocity or friction coefficients are taken into account; the only restriction is that a sphere can never, at any point of its trajectory, overlap the limits of the box or another sphere. Once the tentative sphere with the lowest z-coordinate is added to the system, the process is repeated; spheres continue to be added until the box is filled. An example of a random piling obtained with this procedure is shown in Figure 5.9.

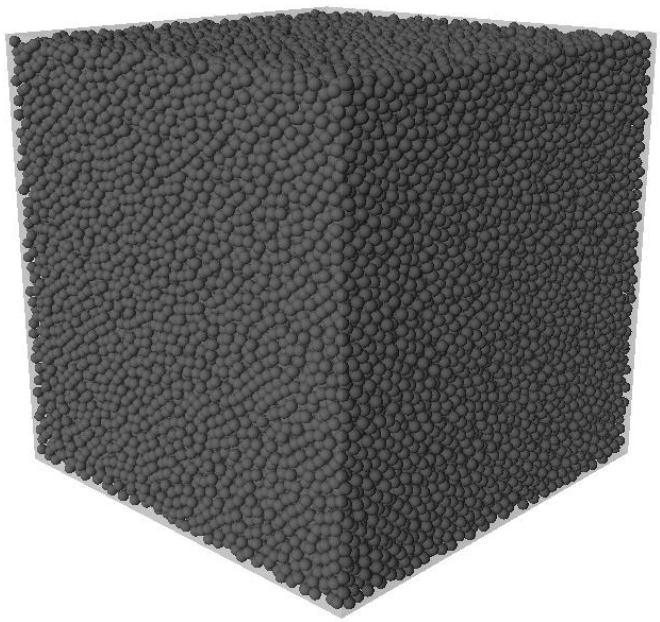

Figure 5.9: Example of a 3-D Random Structure in a System with Side $L = 40\underline{d}$

We have developed 25 different random packings in a 3-D system with $L = 40\underline{d}$. With Γ being the packing fraction of a single realization (as defined in the previous section), we found the average packing fraction to be $\overline{\Gamma} = 0.58083$, with a standard deviation of 0.00096. In other words, the average number of spheres in these 3-D random systems is $\approx 70,995$.

5.2 3-D Monte Carlo Results in the Interior of the System

For all 3-D problems in this work, we assumed the background material in which the spheres were piled to be vacuum; the parameters used for the material of the spheres are given in Table 5.1.

Table 5.1: 3-D parametes for spheres with diameter $\underline{d}$.

$\underline{d}\Sigma_t$	$\underline{d}\Sigma_s$	$\underline{d}\Sigma_a$	$c = \Sigma_s/\Sigma_t$	$P(\mathbf{\Omega} \cdot \mathbf{\Omega}')$
1.0	0.99	0.01	0.99	$1/4\pi$

The particle histories within the system are determined by 3-D generalizations of the Monte Carlo transport code used in Section 4.2; however, the algorithm developed for

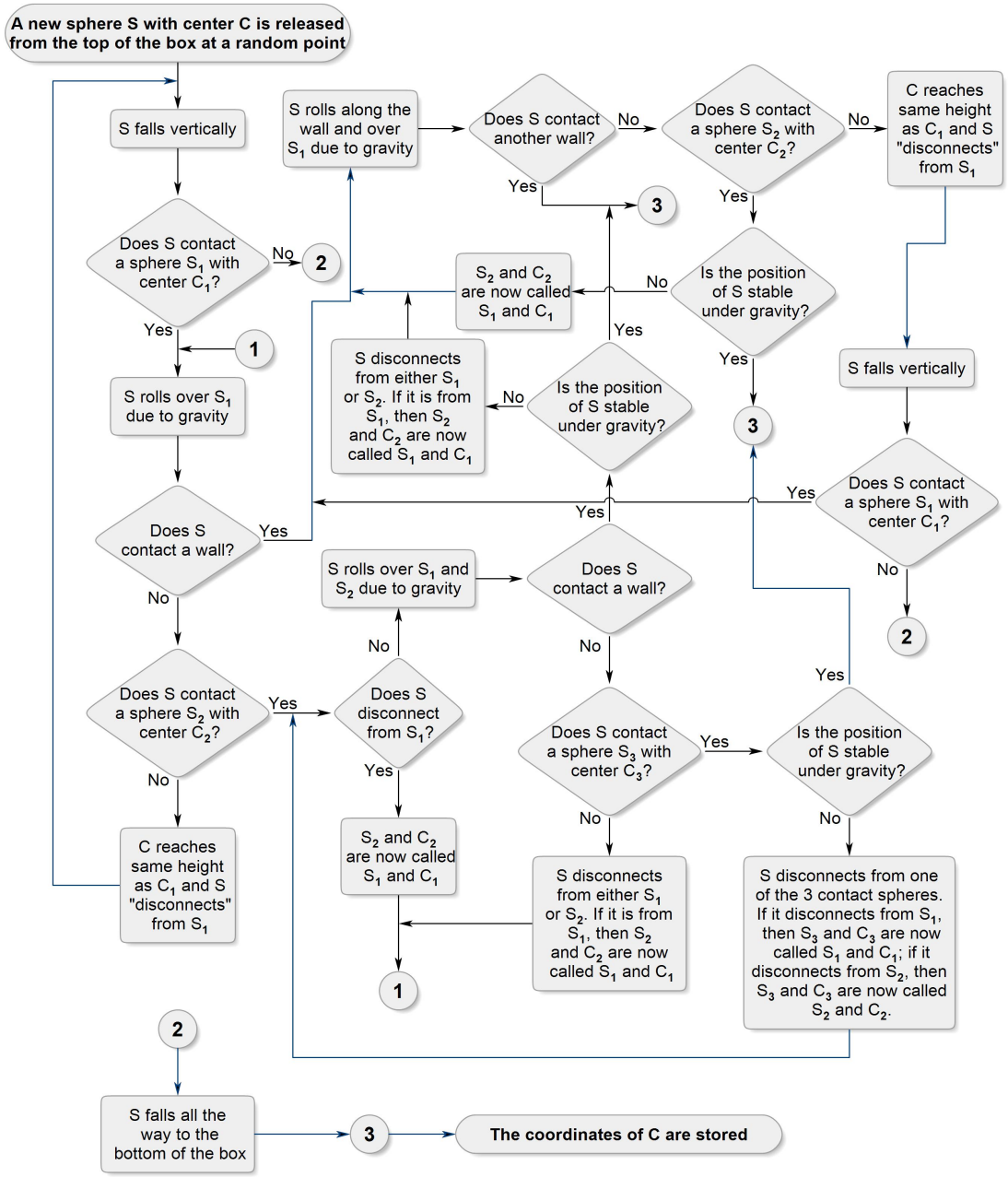

Figure 5.10: Flow diagram for the Dropping of a Sphere in the 3-D System

the 3-D crystal structures is slightly different from the one developed for the 3-D random system.

We remark that, for any given 3-D system (crystal or random), a realization containing N spheres with coordinates (x_n, y_n, z_n) and a realization containing N spheres with coordinates (y_n, x_n, z_n), where $1 \leq n \leq N$, have the same probability of occurring. Therefore, when investigating the behavior of particles born in a fuel sphere in the middle of the system, we can assume without loss of generality that:

$$\overline{hor} = \overline{x} = \overline{y}\,, \tag{5.3a}$$

$$\overline{hor^2} = \overline{x^2} = \overline{y^2}\,. \tag{5.3b}$$

5.2.1 Monte Carlo in 3-D Crystal Structures

For all 3-D crystal problems in this work, the packing of spheres of diameter $\underline{d}$ took place in a cubic box with side $L = 290\underline{d}$; vacuum boundary conditions were used. Similarly to the 2-d case, we choose the sphere closest to the center of the system to be the one in which particles are born. The history of a single particle follows the same flow diagram shown in Figure 4.7, only adapted to 3-D transport (with spheres instead of discs). The

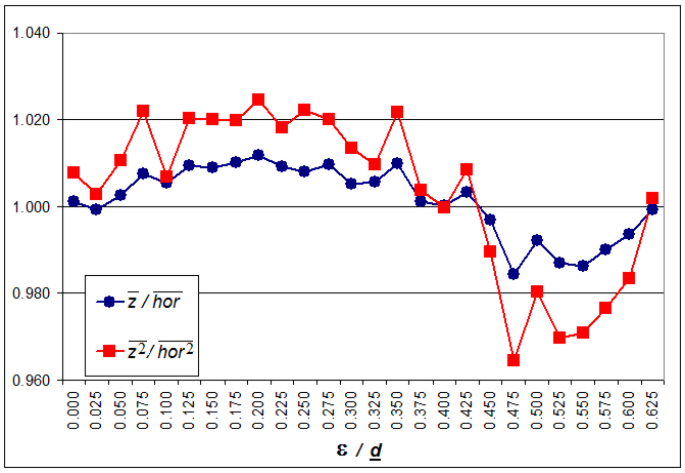

Figure 5.11: Ratios Between Vertical and Horizontal Mean and Mean Square Distances of a Particle to its Point of Birth in 3-D Crystal Structures with Different Values of ε

Table 5.2: MC results for 3-D crystal structures with different values of ε in a system with side $L = 290\underline{d}$. The histories of 300,000 particles were simulated in each structure.

$\varepsilon/\underline{d}$	$\overline{s}/\underline{d}$	$\overline{s^2}/\underline{d}^2$	$\overline{hor}/\underline{d}$	$\overline{hor^2}/\underline{d}^2$	$\overline{z}/\underline{d}$	$\overline{z^2}/\underline{d}^2$
0.000	1.34966	3.76028	7.86774	124.40169	7.87782	125.37097
0.025	1.40024	4.06739	8.20709	135.29977	8.20095	135.68256
0.050	1.44980	4.38396	8.49519	145.23597	8.51642	146.78897
0.075	1.49796	4.70532	8.78978	155.60595	8.85481	159.00754
0.100	1.54468	5.03165	9.08917	167.19589	9.13705	168.31550
0.125	1.59095	5.36910	9.38276	177.53969	9.47071	181.15697
0.150	1.63490	5.70310	9.66450	188.17203	9.75241	191.97140
0.175	1.67669	6.03321	9.94300	199.51534	10.04338	203.48092
0.200	1.71637	6.35806	10.17061	208.77255	10.28980	213.91024
0.225	1.75333	6.67078	10.43792	220.07136	10.53453	224.10086
0.250	1.78767	6.97721	10.67728	229.26777	10.76313	234.35732
0.275	1.81922	7.26247	10.89470	239.98549	11.00032	244.80900
0.300	1.84612	7.51579	11.09692	248.90336	11.15294	252.24146
0.325	1.86840	7.72747	11.24028	256.31604	11.30485	258.80532
0.350	1.88661	7.91195	11.35309	260.50649	11.46512	266.16833
0.375	1.90147	8.04712	11.45959	266.35971	11.47376	267.35975
0.400	1.90747	8.11751	11.53704	269.08663	11.53866	269.06003
0.425	1.90740	8.12093	11.50078	267.91521	11.54000	270.20440
0.450	1.90172	8.05849	11.54538	269.95565	11.51047	267.14227
0.475	1.88544	7.89289	11.44029	264.99021	11.26061	255.59326
0.500	1.86102	7.65323	11.24693	256.23253	11.15866	251.19675
0.525	1.82224	7.28018	11.01100	245.47882	10.86749	238.06746
0.550	1.77235	6.82467	10.64469	228.85540	10.49701	222.15935
0.575	1.70621	6.25848	10.18627	209.76425	10.08509	204.88036
0.600	1.62085	5.57871	9.60916	186.40456	9.54723	183.30478
0.625	1.51135	4.78760	8.88388	158.85279	8.87763	159.14278

maximum number of particles that leaked out of any given system is 129 out of 300,000 (for the system with $\varepsilon = 0.425\underline{d}$); the average number of leaking particles is ≈ 49.

Monte Carlo (MC) transport numerical results for 3-D crystal systems are depicted in Table 5.2. The statistical error (with 95% confidence) is less than 0.043% for all values of $\overline{s}$, $\overline{hor}$, and $\overline{z}$, and less than 0.094% for all values of $\overline{s^2}$, $\overline{hor^2}$, and $\overline{z^2}$.

As expected, we detect an anisotropic effect in these systems that is even larger than the one found in the 2-D crystal structure (Figure 5.11). Further confirmation is easily seen

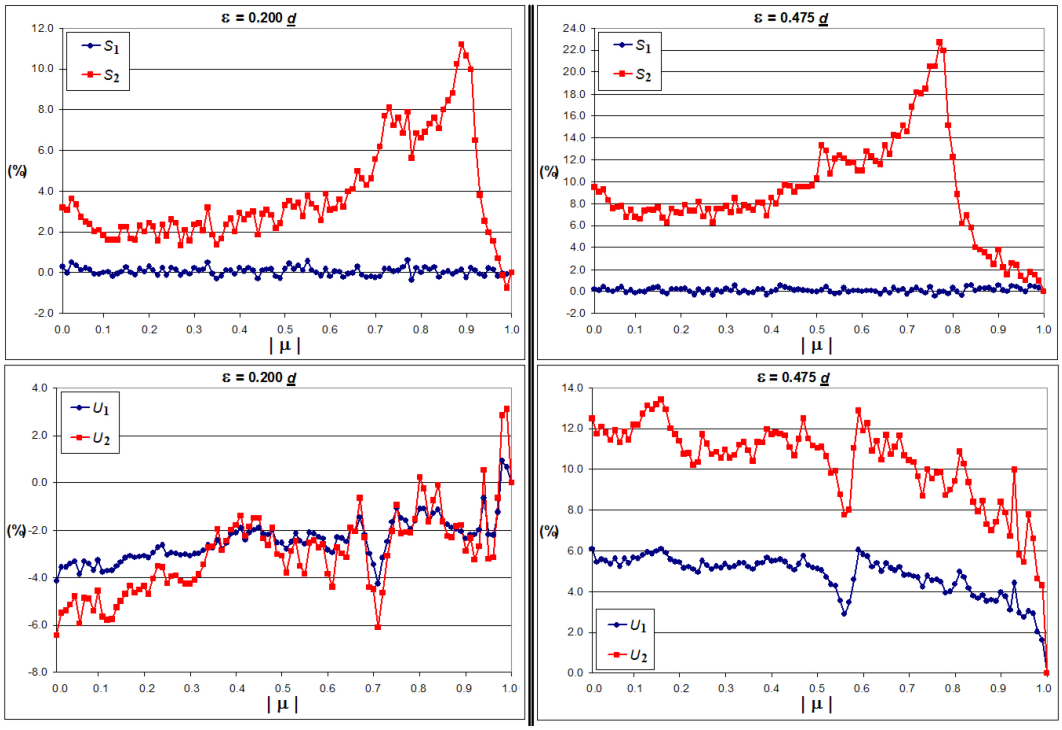

Figure 5.12: Percent Relative Differences from the Vertical Direction [as defined in Eqs. (5.4) and (5.5)] as Functions of $|\Omega_z| = |\mu|$ in Two Distinct 3-D Crystal Structures

when comparing the relative differences from the vertical direction given by:

(5.4a) $$S_1(\mathbf{\Omega}) = \frac{\overline{s_{\mathbf{\Omega}}}(\mathbf{\Omega}) - \overline{s_{\mathbf{\Omega}}}(\vec{\boldsymbol{k}})}{\overline{s_{\mathbf{\Omega}}}(\vec{\boldsymbol{k}})},$$

(5.4b) $$S_2(\mathbf{\Omega}) = \frac{\overline{s^2_{\mathbf{\Omega}}}(\mathbf{\Omega}) - \overline{s^2_{\mathbf{\Omega}}}(\vec{\boldsymbol{k}})}{\overline{s^2_{\mathbf{\Omega}}}(\vec{\boldsymbol{k}})};$$

and:

(5.5a) $$U_1(\mathbf{\Omega}) = \frac{\overline{\rho}(\mathbf{\Omega}) - \overline{\rho}(\vec{\boldsymbol{k}})}{\overline{\rho}(\vec{\boldsymbol{k}})},$$

(5.5b) $$U_2(\mathbf{\Omega}) = \frac{\overline{\rho^2}(\mathbf{\Omega}) - \overline{\rho^2}(\vec{\boldsymbol{k}})}{\overline{\rho^2}(\vec{\boldsymbol{k}})}.$$

Here, $\overline{\rho}(\mathbf{\Omega})$ and $\overline{\rho^2}(\mathbf{\Omega})$ again represent the mean and mean square distances of a particle to its point of birth in the direction $\mathbf{\Omega}$, and $\vec{\boldsymbol{k}} = (0, 0, 1)$ is the unit vector in the z-direction. These quantities are depicted as percent functions of $|\Omega_z| = |\cos\theta| = |\mu|$ in Figure 5.12, for two different crystal structures.

Once again, S_2, U_1, and U_2 clearly show a direction-dependent behavior of the particles. While $\overline{s_{\mathbf{\Omega}}}$ remains close to a constant troughout the system, $\overline{s^2_{\mathbf{\Omega}}}$ varies by more than 11.0% in one system and twice that in another, indicating that the diffusion coefficients must be different for the vertical and horizontal directions.

As in the 2-D case, there are valleys in the graphs of U_1 and U_2 near the angles formed between the centers of a sphere and the centers of the adjacent spheres. These angles satisfy $|\mu| = 0.7211$ and $|\mu| = 0.5242$ for $\varepsilon = 0.200\underline{d}$ and $\varepsilon = 0.475\underline{d}$, respectively.

5.2.2 Monte Carlo in 3-D Random Structures

For all 3-D random systems in this work, the packing of spheres of diameter $\underline{d}$ took place in a cubic box with side $L = 40\underline{d}$. For the case described in this section, in which we choose the sphere closest to the center of the packing structure to be the one where particles are born, vacuum boundary conditions were used.

However, the system in which particles travel is not composed by all the spheres in the packing. Since at this point we are interested in the behavior of particles in the interior of the system, we want to minimize the effect of the boundaries of the box (walls, top, bottom). According to the work in [4], we need to consider spheres that are three to five diameters off-walls in order to have a packing structure that is not influenced by the walls and by the bottom.

Let us draw an imaginary box with side $L^*(\omega) = L - 2\omega\underline{d}$ inside the system, such that its walls are a distance $\omega\underline{d}$ away from the walls of the box. We define the packing fraction $\Gamma^*(\omega)$ as the ratio between the total volume of spheres inside this imaginary box (including partial spheres) and the volume of the imaginary box. For each of the simulated systems, we found that the fluctuations in $\Gamma^*(\omega)$ ceased being significant around $\omega = 2\underline{d}$, as was the case in the experiment performed in [48]. Nevertheless, for the sake of accuracy, we allow particles to travel only inside the imaginary box with side $L^*(3)$ (Figure 5.13). For the

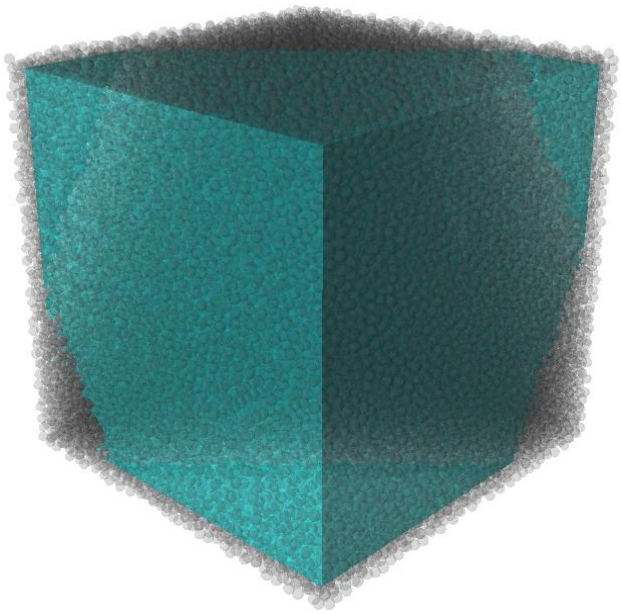

Figure 5.13: Imaginary Box with Side $L^*(3) = 34\underline{d}$ Positioned Inside a 3-D Random Realization of a System with Side $L = 40\underline{d}$

25 simulated random packings, we found $\overline{\Gamma^*} = \overline{\Gamma^*}(3) = 0.59524$ as the average packing fraction, with a standard deviation of 0.00126. In other words, the average total volume of spheres inside the imaginary box is approximately the volume of 44,682 spheres.

The difference in the algorithm is in dealing with particles that leak out of this imaginary box. Let the center of the box be at the origin, and let us assume that a particle P that had its last collision at point (x_0, y_0, z_0) inside a sphere S_a leaks out of the imaginary box through the plane $x = -(L - 3\underline{d})/2$. First, defining the coordinates of the center of S_a as (x_a, y_a, z_a), we locate the sphere S_b with the closest center to the point $(-x_a - \underline{d}, y_a, z_a)$. Then, we *reinsert* P into the system at the point $(x_b + x_0 - x_a, y_b + y_0 - y_a, z_b + z_0 - z_a)$, where (x_b, y_b, z_b) are the coordinates of the center of S_b (Figure 5.14). Finally, we shift the whole system so that now the coordinates of the center of the box are $(x_0, 0, 0)$, and proceed with the history of the particle. A similar process is used if the particle leaks through any of the other walls; we repeat this reinsertion and shifting procedure as many times as necessary. In other words, particles are traveling in an infinite "quasi-periodic"

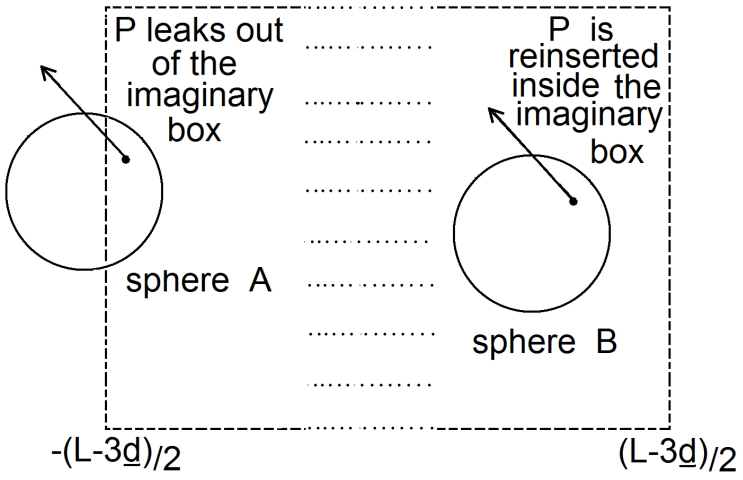

Figure 5.14: Reinsertion of a Particle in the Imaginary Box

structure; here, we use the term "quasi-periodic" because the system is not always shifted by the same values in a given direction.

For each realization of the random system, we have calculated the histories of 100,000 particles; the statistical error in each given realization was found to be (with 97.5% confidence) less than 0.078% for all values of $\overline{s}$, $\overline{hor}$, and $\overline{z}$, and less than 0.177% for all values of $\overline{s^2}$, $\overline{hor^2}$, and $\overline{z^2}$. As we mentioned, we have developed 25 different realizations (adding to a total of 2,500,000 particles); the average Monte Carlo results and the statistical errors bounds (with 95% confidence) are given in Table 5.3.

Although each single realization presents a small (generally less than 1%) anisotropic effect (Figure 5.15), we observe that they are not consistent; in fact, the ensemble-averaged

Table 5.3: Ensemble-averaged MC results for 3-D random structures in a "quasi-periodic" infinite system. A total of 25 different random realizations were generated; the histories of 100,000 particles were simulated in each realization.

	$\overline{s}/\underline{d}$	$\overline{s^2}/\underline{d}^2$	$\overline{hor}/\underline{d}$	$\overline{hor^2}/\underline{d}^2$	$\overline{z}/\underline{d}$	$\overline{z^2}/\underline{d}^2$
Ensemble Average	1.76450	6.77858	10.52172	226.01146	10.52960	226.59695
Statistical Error	0.206%	0.452%	0.269%	0.543%	0.296%	0.607%

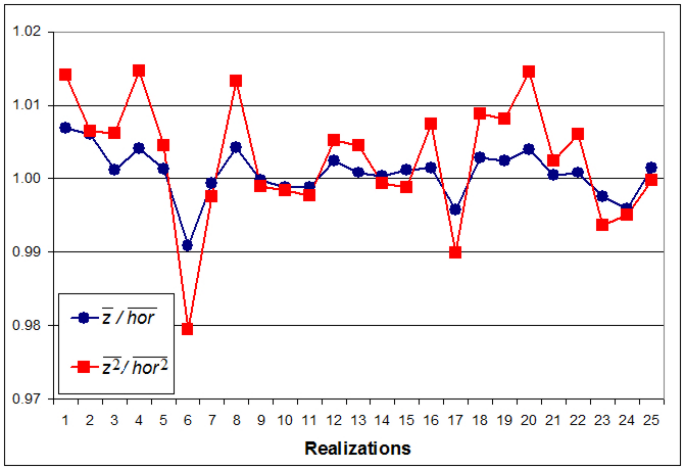

Figure 5.15: Ratios Between Vertical and Horizontal Mean and Mean Square Distances of a Particle to its Point of Birth in 3-D Random Realizations of the System

values yield $\overline{z}/\overline{hor} = 1.00075$ and $\overline{z^2}/\overline{hor^2} = 1.00259$, which represent an average anisotropy that is smaller than the small one observed in the 2-D case. Using the ensemble-averaged values of $\overline{s_{\mathbf{\Omega}}}(\mathbf{\Omega})$, $\overline{s^2_{\mathbf{\Omega}}}(\mathbf{\Omega})$, $\overline{\rho}(\mathbf{\Omega})$, and $\overline{\rho^2}(\mathbf{\Omega})$ with the expressions given by Eqs. (5.4) and (5.5), we see no indication that particles should travel further in any one direction (Figure 5.16).

We remark that we are working with a packing fraction of 59.5%, which is about 2% smaller than the generally assumed average packing fraction in a pebble-bed core (60%-62%). Nevertheless, there is no reason to believe that higher packing fractions in physical random structures of pebble-beds will introduce diffusion anisotropy in the system; if anything, the small anisotropic effects in each realization should be even smaller, since the void fraction of the system decreases.

We believe that, if enough realizations of the system are simulated, one should find that $\overline{z}/\overline{hor}$ and $\overline{z^2}/\overline{hor^2}$ approach a value of $\approx$1. This indicates that, at least for fuel spheres in the interior of the system, it should not be necessary to worry about anisotropic diffusion. However, the diffusion of particles that are born in spheres positioned close to the walls *will* be anisotropic; we discuss this case in Section 5.4.

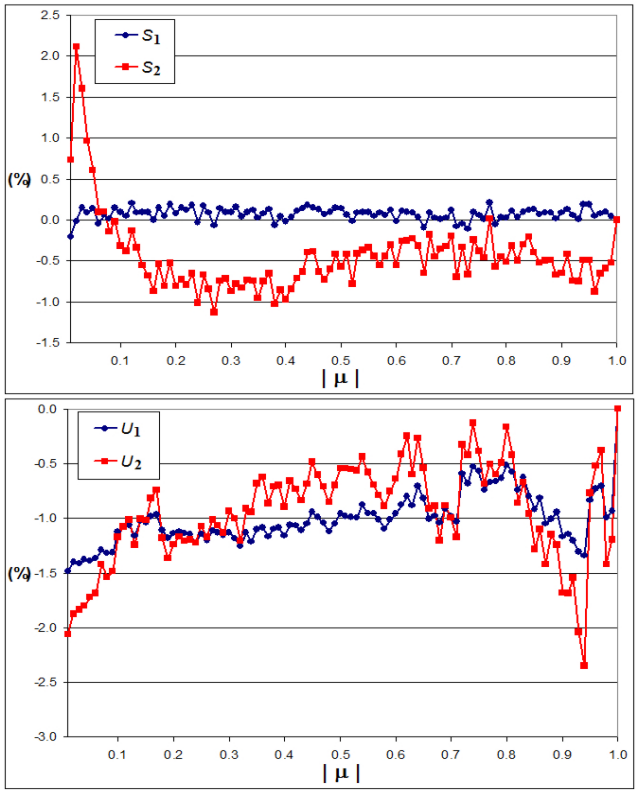

Figure 5.16: Percent Relative Differences from the Vertical Direction [as defined in Eqs. (5.4) and (5.5)] as Functions of $|\Omega_z| = |\mu|$ in the 3-D Random System

5.3 Theoretical and Monte Carlo Estimates in the Interior of a 3-D System

5.3.1 Results in 3-D Crystal Structures

Introducing the numerically obtained results for $\overline{s}$ (as shown in Table 5.2) into Eq. (2.50), we obtain (as in the 2-D case) a Monte Carlo estimate for the absorption cross section, denoted Σ_a^{mc}. Using this estimate and the numerical results $\overline{hor^2}$ and $\overline{z^2}$ shown in Table 5.2, Eqs. (2.53) yield the 3-D numerical diffusion coefficients

$$\mathrm{D}_{hor}^{mc} = \overline{hor^2}\frac{\Sigma_a^{mc}}{2}\,, \tag{5.6a}$$

$$\mathrm{D}_{z}^{mc} = \overline{z^2}\frac{\Sigma_a^{mc}}{2}\,, \tag{5.6b}$$

for 3-D crystal structures.

The atomic mix diffusion coefficient for crystal structures is given by [see Eq. (2.64)]:

$$\mathrm{D}^{am} = \frac{1}{3}\left(\frac{1}{\Gamma\Sigma_t}\right) , \tag{5.7}$$

where Γ is the packing fraction of the system and Σ_t is shown in Table 5.1. Using this result, we calculate the diffusion corrections proposed by Behrens [see Eq. (2.67)] and Lieberoth [see Eq. (2.69)]:

$$\mathrm{D}^{B} = \left[1 + \frac{\phi^2}{(1+\phi)^2}\left(\frac{2}{3}r\Sigma_t \mathrm{Q}_B + \frac{\frac{4}{3}r\Sigma_t}{\exp\left[\frac{4}{3}r\Sigma_t\right] - 1} - 1\right)\right]\mathrm{D}^{am} ; \tag{5.8}$$

$$\begin{aligned}\mathrm{D}^{L} = \Bigg\{1 + \frac{\phi^2}{(1+\phi)^2}\Bigg[&\frac{2}{3}r\Sigma_t \mathrm{Q}_L \\ &+ \frac{4}{3}r\Sigma_t\left(\frac{2r^2\Sigma_t^2}{2r^2\Sigma_t^2 - 1 + (1+2r\Sigma_t)e^{-2r\Sigma_t}} - 1\right) - 1\Bigg]\Bigg\}\mathrm{D}^{am} ,\end{aligned} \tag{5.9}$$

where Σ_t is shown in Table 5.1, $r = \underline{d}/2$ is the radius of the spheres, Q_B and Q_L are given by Eqs. (2.66) and (2.68), and for each packing fraction Γ:

$$\phi = \frac{1-\Gamma}{\Gamma} . \tag{5.10}$$

Using the numerical values for $\overline{s}$ and $\overline{s^2}$ shown in Table 5.2, the isotropic diffusion coefficient obtained by the generalized theory (assuming the locations of the scattering centers to be independent of direction) is given by [see Eq. (3.70)]:

$$\mathrm{D}^{iso} = \frac{1}{3}\left(\frac{\overline{s^2}}{2\overline{s}}\right) . \tag{5.11}$$

Finally, since scattering is isotropic, the anisotropic diffusion coefficients obtained by the generalized theory are given by [see Eqs. (3.72)]:

$$\mathrm{D}^{gt}_{hor} = \frac{1}{2\overline{s}}\left(\frac{1}{4\pi}\int_{4\pi}\overline{s^2_{\mathbf{\Omega}}}(\mathbf{\Omega})\Omega_x^2\, d\Omega\right) = \frac{1}{2\overline{s}}\left(\frac{1}{4\pi}\int_{4\pi}\overline{s^2_{\mathbf{\Omega}}}(\mathbf{\Omega})\Omega_y^2\, d\Omega\right) , \tag{5.12a}$$

$$\mathrm{D}^{gt}_{z} = \frac{1}{2\overline{s}}\left(\frac{1}{4\pi}\int_{4\pi}\overline{s^2_{\mathbf{\Omega}}}(\mathbf{\Omega})\Omega_z^2\, d\Omega\right) , \tag{5.12b}$$

where $\mathbf{\Omega} = (\sqrt{1-\mu^2}\cos\varphi, \sqrt{1-\mu^2}\sin\varphi, \mu)$, $\overline{s}$ is given by the numerical values shown in Table 5.2, and $\overline{s^2_{\mathbf{\Omega}}}(\mathbf{\Omega})$ is also numerically calculated for each system. All estimates

Table 5.4: Numerical (MC) and theoretical estimates for the diffusion coefficients in 3-D crystal structures with different values of ε.

$\varepsilon/\underline{d}$	$\mathrm{D}_{hor}^{mc}/\underline{d}$	$\mathrm{D}_{z}^{mc}/\underline{d}$	$\mathrm{D}^{am}/\underline{d}$	$\mathrm{D}^{B}/\underline{d}$	$\mathrm{D}^{L}/\underline{d}$	$\mathrm{D}^{iso}/\underline{d}$	$\mathrm{D}_{hor}^{gt}/\underline{d}$	$\mathrm{D}_{z}^{gt}/\underline{d}$
0.000	0.46086	0.46445	0.45191	0.46330	0.46465	0.46435	0.46433	0.46439
0.025	0.48313	0.48450	0.46917	0.48048	0.48517	0.48413	0.48358	0.48524
0.050	0.50088	0.50624	0.48521	0.49650	0.50448	0.50397	0.50272	0.50648
0.075	0.51939	0.53075	0.50193	0.51324	0.52482	0.52353	0.52173	0.52712
0.100	0.54120	0.54482	0.51777	0.52913	0.54427	0.54290	0.54100	0.54671
0.125	0.55797	0.56933	0.53304	0.54447	0.56317	0.56246	0.55977	0.56784
0.150	0.57548	0.58710	0.54777	0.55930	0.58154	0.58139	0.57812	0.58793
0.175	0.59497	0.60679	0.56183	0.57349	0.59918	0.59971	0.59656	0.60601
0.200	0.60818	0.62315	0.57514	0.58693	0.61597	0.61739	0.61390	0.62438
0.225	0.62758	0.63907	0.58758	0.59950	0.63174	0.63410	0.63061	0.64110
0.250	0.64125	0.65548	0.59830	0.61035	0.64538	0.65049	0.64696	0.65756
0.275	0.65958	0.67284	0.60862	0.62081	0.65856	0.66534	0.66239	0.67125
0.300	0.67412	0.68316	0.61770	0.63001	0.67020	0.67852	0.67567	0.68422
0.325	0.68593	0.69259	0.62538	0.63780	0.68006	0.68931	0.68673	0.69448
0.350	0.69041	0.70541	0.63235	0.64487	0.68903	0.69896	0.69675	0.70336
0.375	0.70040	0.70303	0.63586	0.64843	0.69354	0.70534	0.70385	0.70832
0.400	0.70535	0.70528	0.63912	0.65174	0.69775	0.70927	0.70929	0.70923
0.425	0.70230	0.70830	0.63927	0.65190	0.69794	0.70960	0.70959	0.70961
0.450	0.70977	0.70237	0.63689	0.64948	0.69487	0.70625	0.70769	0.70336
0.475	0.70279	0.67781	0.63163	0.64414	0.68810	0.69771	0.69954	0.69403
0.500	0.68842	0.67489	0.62307	0.63546	0.67709	0.68540	0.68841	0.67937
0.525	0.67356	0.65323	0.60977	0.62197	0.66003	0.66587	0.66954	0.65851
0.550	0.64563	0.62674	0.59386	0.605853	0.63972	0.64177	0.64567	0.63397
0.575	0.61471	0.60040	0.57079	0.58254	0.61048	0.61134	0.61463	0.60477
0.600	0.57502	0.56546	0.54306	0.55456	0.57566	0.57364	0.57596	0.56901
0.625	0.52553	0.52649	0.50628	0.51760	0.53015	0.52796	0.52864	0.52660

for the diffusion coefficients are shown in Table 5.4. We define the percent differences between the theoretical and Monte Carlo estimates for the diffusion coefficients as:

$$\text{diff}_{hor}^{am} = 100\frac{|\mathrm{D}^{am} - \mathrm{D}_{hor}^{mc}|}{\mathrm{D}_{hor}^{mc}}, \quad \text{diff}_{z}^{am} = 100\frac{|\mathrm{D}^{am} - \mathrm{D}_{z}^{mc}|}{\mathrm{D}_{z}^{mc}}, \tag{5.13a}$$

$$\text{diff}_{hor}^{B} = 100\frac{|\mathrm{D}^{B} - \mathrm{D}_{hor}^{mc}|}{\mathrm{D}_{hor}^{mc}}, \quad \text{diff}_{z}^{B} = 100\frac{|\mathrm{D}^{B} - \mathrm{D}_{z}^{mc}|}{\mathrm{D}_{z}^{mc}}, \tag{5.13b}$$

$$\text{diff}_{hor}^{L} = 100\frac{|\mathrm{D}^{L} - \mathrm{D}_{hor}^{mc}|}{\mathrm{D}_{hor}^{mc}}, \quad \text{diff}_{z}^{L} = 100\frac{|\mathrm{D}^{L} - \mathrm{D}_{z}^{mc}|}{\mathrm{D}_{z}^{mc}}, \tag{5.13c}$$

$$\text{diff}_{hor}^{iso} = 100\frac{|\mathrm{D}^{iso} - \mathrm{D}_{hor}^{mc}|}{\mathrm{D}_{hor}^{mc}}, \quad \text{diff}_{z}^{iso} = 100\frac{|\mathrm{D}^{iso} - \mathrm{D}_{z}^{mc}|}{\mathrm{D}_{z}^{mc}}, \tag{5.13d}$$

$$\text{diff}_{hor}^{gt} = 100\frac{|\mathrm{D}_{hor}^{gt} - \mathrm{D}_{hor}^{mc}|}{\mathrm{D}_{hor}^{mc}}, \quad \text{diff}_{z}^{gt} = 100\frac{|\mathrm{D}_{z}^{gt} - \mathrm{D}_{z}^{mc}|}{\mathrm{D}_{z}^{mc}}; \tag{5.13e}$$

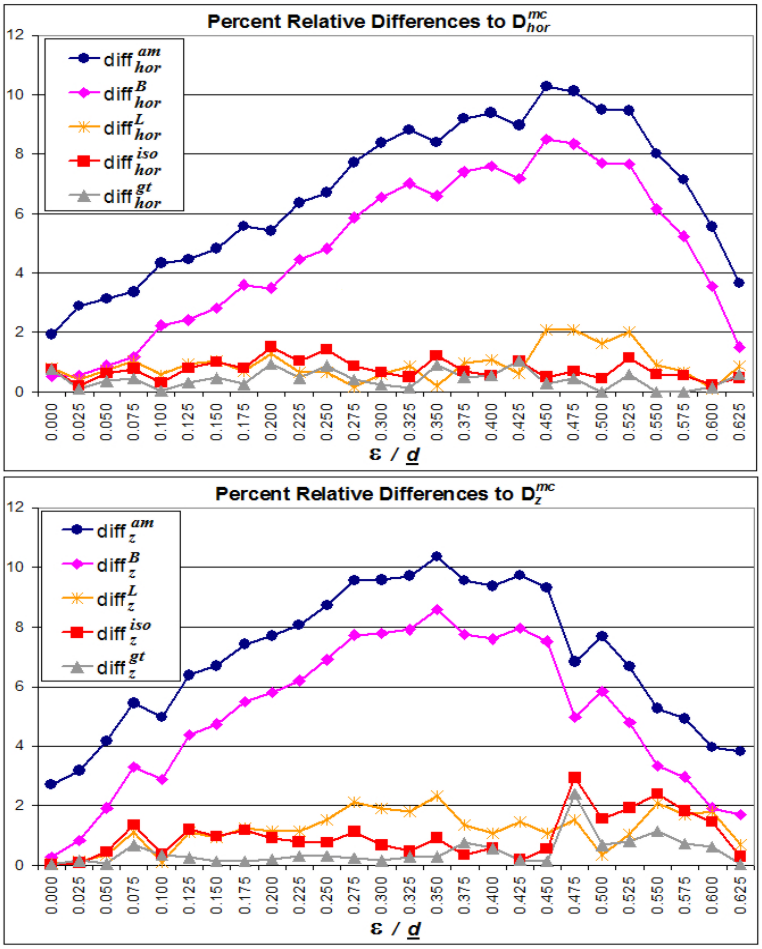

Figure 5.17: Percent Differences Between Theoretical and Monte Carlo Estimates for the Diffusion Coefficients in 3-D Crystal Structures with Different Values of ε

these differences are depicted in Figure 5.17 as functions of $\varepsilon/\underline{d}$.

In general, the results obtained with classic atomic mix and the correction proposed by Behrens differ from the numerical results by large amounts; they consistently underestimate the diffusion coefficients in both directions. The correction presented by Lieberoth yields much smaller differences, even though it also tends to underestimate the diffusion coefficients.

The isotropic version of the generalized theory has maximum differences in its estimates of the diffusion coefficients (compared to Monte Carlo) of 1.52% and 2.94% in the horizontal and vertical directions, respectively; its average differences, however, are about

0.75% in the horizontal direction and about 0.97% in the vertical direction. These are smaller than the average differences obtained with the Lieberoth correction, namely about 0.91% in the horizontal direction and about 1.20% in the vertical direction. In general, the isotropic version of the generalized theory seems to be an improvement over the Lieberoth correction, albeit a small one.

On the other hand, it is clear from the graphs that the anisotropic estimates D^{gt} are an improvement over both D^{iso} and D^{L}, with average differences (compared to Monte Carlo) of about 0.42% in the horizontal direction and about 0.44% in the vertical direction. Moreover, with one single exception ($\varepsilon = 0.625\underline{d}$), D^{gt} correctly predicted the general anisotropic behavior of all the systems; that is, $\mathrm{D}^{gt}_{hor} > \mathrm{D}^{gt}_{z}$ when $\mathrm{D}^{mc}_{hor} > \mathrm{D}^{mc}_{z}$ and $\mathrm{D}^{gt}_{hor} < \mathrm{D}^{gt}_{z}$ when $\mathrm{D}^{mc}_{hor} < \mathrm{D}^{mc}_{z}$ for all but one of the systems simulated.

To further examine the general improvement introduced by the proposed generalized theory, we shall once more consider the estimates for k_D. Assuming dimensions for the 3-D model reactor core that are comparable to those of the MPBR design [35] (width and length $X = Y = 58.33\underline{d}$ and height $Z = 166.67\underline{d}$), we adapt Eq. (2.43) for the different methods presented (as summarized in Table 5.5). The resulting estimates for k_D are shown

Table 5.5: Parameters applied in Eq. (2.43) to calculate the different estimates of k_D in 3-D systems.

	Monte Carlo	Atomic Mix	Behrens Correction	Lieberoth Correction	Isotropic Generalized Theory	Anisotropic Generalized Theory
D_{hor}	Eq. (5.6a)	Eq. (5.7)	Eq. (5.8)	Eq. (5.9)	Eq. (5.11)	Eq. (5.12a)
D_{z}	Eq. (5.6b)	Eq. (5.7)	Eq. (5.8)	Eq. (5.9)	Eq. (5.11)	Eq. (5.12b)
Σ_a	$\dfrac{1-c}{\overline{s}}$	$\langle\Sigma_a\rangle = \Gamma\Sigma_a$	$\langle\Sigma_a\rangle = \Gamma\Sigma_a$	$\langle\Sigma_a\rangle = \Gamma\Sigma_a$	$\dfrac{1-c}{\overline{s}}$	$\dfrac{1-c}{\overline{s}}$

in Table 5.6, as calculated by:

$$\frac{k_D^{mc}}{\nu\Sigma_f} = \left[\Sigma_a^{mc} + \pi^2\left(\frac{\mathrm{D}_{hor}^{mc}}{X^2} + \frac{\mathrm{D}_{hor}^{mc}}{Y^2} + \frac{\mathrm{D}_z^{mc}}{Z^2}\right)\right]^{-1}, \tag{5.14a}$$

$$\frac{k_D^{am}}{\nu\Sigma_f} = \left[\Gamma\Sigma_a + \pi^2\left(\frac{1}{X^2} + \frac{1}{Y^2} + \frac{1}{Z^2}\right)\mathrm{D}^{am}\right]^{-1}, \tag{5.14b}$$

$$\frac{k_D^{B}}{\nu\Sigma_f} = \left[\Gamma\Sigma_a + \pi^2\left(\frac{1}{X^2} + \frac{1}{Y^2} + \frac{1}{Z^2}\right)\mathrm{D}^{B}\right]^{-1}, \tag{5.14c}$$

$$\frac{k_D^{L}}{\nu\Sigma_f} = \left[\Gamma\Sigma_a + \pi^2\left(\frac{1}{X^2} + \frac{1}{Y^2} + \frac{1}{Z^2}\right)\mathrm{D}^{L}\right]^{-1}, \tag{5.14d}$$

$$\frac{k_D^{iso}}{\nu\Sigma_f} = \left[\Sigma_a^{mc} + \pi^2\left(\frac{1}{X^2} + \frac{1}{Y^2} + \frac{1}{Z^2}\right)\mathrm{D}^{iso}\right]^{-1}, \tag{5.14e}$$

$$\frac{k_D^{gt}}{\nu\Sigma_f} = \left[\Sigma_a^{mc} + \pi^2\left(\frac{\mathrm{D}_{hor}^{gt}}{X^2} + \frac{\mathrm{D}_{hor}^{gt}}{Y^2} + \frac{\mathrm{D}_z^{gt}}{Z^2}\right)\right]^{-1}; \tag{5.14f}$$

where Γ is the packing fraction and $\overline{s}$ is shown in Table 5.2.

We define the percent differences between the theoretical and Monte Carlo estimates for k_D as:

$$\mathrm{diff}_k^{am} = 100\frac{|k_D^{am} - k_D^{mc}|}{k_D^{mc}}, \tag{5.15a}$$

$$\mathrm{diff}_k^{B} = 100\frac{|k_D^{B} - k_D^{mc}|}{k_D^{mc}}, \tag{5.15b}$$

$$\mathrm{diff}_k^{L} = 100\frac{|k_D^{L} - k_D^{mc}|}{k_D^{mc}}, \tag{5.15c}$$

$$\mathrm{diff}_k^{iso} = 100\frac{|k_D^{iso} - k_D^{mc}|}{k_D^{mc}}, \tag{5.15d}$$

$$\mathrm{diff}_k^{gt} = 100\frac{|k_D^{gt} - k_D^{mc}|}{k_D^{mc}}; \tag{5.15e}$$

these differences are depicted in Figure 5.18 as functions of $\varepsilon/\underline{d}$.

As expected, the estimates obtained with classic atomic mix and the correction proposed by Behrens present large differences from the numerical results. The correction presented by Lieberoth yields very good results for about half of the simulated systems, with a tendency to overestimate k_D. Its average difference is about 0.41%, with a maximum difference of 1.2%.

Table 5.6: Numerical (MC) and theoretical estimates for k_D (assuming MPBR-like core dimensions: $X = Y = 58.33\underline{d}$ and $Z = 166.67\underline{d}$) in 3-D crystal structures with different values of ε.

$\varepsilon/\underline{d}$	$k_D^{mc}/(\nu\Sigma_f)$	$k_D^{am}/(\nu\Sigma_f)$	$k_D^{B}/(\nu\Sigma_f)$	$k_D^{L}/(\nu\Sigma_f)$	$k_D^{iso}/(\nu\Sigma_f)$	$k_D^{gt}/(\nu\Sigma_f)$
0.000	97.58288	98.44325	97.76846	97.68922	97.39104	97.39204
0.025	98.84931	100.06906	99.37643	99.09216	98.79396	98.82156
0.050	100.17096	101.45132	100.74101	100.24476	99.99948	100.06342
0.075	101.24252	102.76434	102.03454	101.29732	101.02358	101.11708
0.100	101.96950	103.89202	103.14283	102.16037	101.87404	101.97479
0.125	102.83270	104.87715	104.10844	102.87550	102.58342	102.72761
0.150	103.48212	105.73625	104.94804	103.46190	103.13813	103.31560
0.175	103.83053	106.47656	105.66914	103.93190	103.56153	103.73373
0.200	104.43167	107.10790	106.28184	104.29975	103.87406	104.06619
0.225	104.48197	107.63967	106.79584	104.57936	104.08955	104.28288
0.250	104.74960	108.05413	107.19474	104.77277	104.18357	104.37921
0.275	104.57970	108.41679	107.54220	104.91949	104.24430	104.40789
0.300	104.49298	108.70694	107.81885	105.01771	104.23325	104.39115
0.325	104.41399	108.93180	108.03221	105.07908	104.21271	104.35572
0.350	104.64459	109.12010	108.21001	105.11817	104.12932	104.25107
0.375	104.47299	109.20910	108.29372	105.13200	104.15245	104.23472
0.400	104.33200	109.28884	108.36851	105.14148	104.06941	104.06832
0.425	104.51070	109.29248	108.37191	105.14184	104.04565	104.04594
0.450	103.89318	109.23469	108.31774	105.13536	104.09922	104.01967
0.475	103.93815	109.10130	108.19230	105.11485	104.17707	104.07569
0.500	104.09478	108.86604	107.96992	105.06265	104.24449	104.07818
0.525	103.87292	108.45490	107.57862	104.93346	104.30821	104.10498
0.550	104.05663	107.88718	107.03426	104.69781	104.24121	104.02590
0.575	103.73273	106.90901	106.08909	104.18764	103.90122	103.72091
0.600	103.02719	105.47138	104.68946	103.28534	103.08139	102.95631
0.625	101.49969	103.08484	102.34981	101.54685	101.34941	101.31383

The isotropic version of the generalized theory yields a small improvement over the Lieberoth correction, as predicted before. In comparison to the numerical estimates, k_D^{iso} is more accurate than k_D^L in 15 out of the 26 cases analyzed; its average difference is about 0.26%, with maximum difference of 0.54%.

Finally, we can see a systematic improvement introduced by the anisotropic generalized theory; its average difference is about 0.16%, with maximum difference of 0.44%. In comparison to the numerical estimates, k_D^{gt} is more accurate than k_D^L in 17 out of the 26 cases analyzed, being at least twice as accurate in 14 of these cases, and at least 10 times as accurate in 6 of these cases.

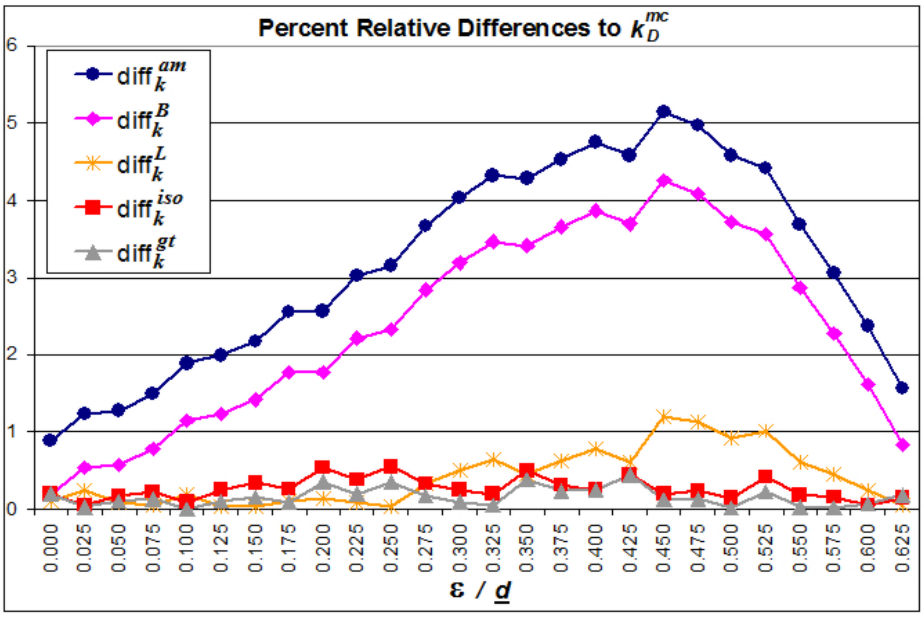

Figure 5.18: Percent Differences Between Theoretical and Monte Carlo Estimates for k_D (assuming MPBR-like core dimensions) in 3-D Crystal Structures with Different Values of ε

5.3.2 Results in 3-D Random Structures

To obtain estimates for the diffusion coefficients in the 3-D random system we use the same procedure presented for the crystal structures, together with the ensemble-averaged results in Table 5.2 and the ensemble-averaged packing fraction $\overline{\Gamma^*} = 0.59524$. The estimates and the percent relative differences are shown in Tables 5.7 and 5.8.

Table 5.7: Numerical (MC) and theoretical estimates for the diffusion coefficients in the 3-D random system.

$D_{hor}^{mc}/\underline{d}$	$D_{z}^{mc}/\underline{d}$	$D^{am}/\underline{d}$	$D^{B}/\underline{d}$	$D^{L}/\underline{d}$	$D^{iso}/\underline{d}$	$D_{hor}^{gt}/\underline{d}$	$D_{z}^{gt}/\underline{d}$
0.64044	0.64210	0.56000	0.57164	0.59688	0.64027	0.63954	0.64173

Table 5.8: Percent differences between theoretical and Monte Carlo estimates for the diffusion coefficients in the 3-D random system.

diff_{hor}^{am}	diff_{hor}^{B}	diff_{hor}^{L}	diff_{hor}^{iso}	diff_{hor}^{gt}
12.56027	10.74273	6.80179	0.02595	0.13971
diff_{z}^{am}	diff_{z}^{B}	diff_{z}^{L}	diff_{z}^{iso}	diff_{z}^{gt}
12.78620	10.97335	7.04259	0.28427	0.05735

We should remark that the ratios $\mathrm{D}^B/\mathrm{D}^{am} = 1.02079$ and $\mathrm{D}^L/\mathrm{D}^{am} = 1.06586$ obtained here are similar to the ratios presented by Lieberoth [48] in a similar situation: for pebbles with total cross section $\underline{d}\Sigma_t \approx 1.05182$ piled in an experimental random structure with packing fraction 0.6308, he obtained $\mathrm{D}^B/\mathrm{D}^{am} = 1.023$ and $\mathrm{D}^L/\mathrm{D}^{am} = 1.058$.

The results in Tables 5.7 and 5.8 are a clear indication of the superiority of the generalized theory over the classic atomic mix and its corrections; the estimates for the diffusion coefficients in both the isotropic and anisotropic versions of the new theory are more than 20 times more accurate than the classic methods when compared to the numerical estimates. Moreover, the results of D^{gt} correctly recognize even the small anisotropic behavior of the diffusion, yielding a larger coefficient in the vertical direction.

We can also obtain estimates for k_D, with a similar procedure to the one applied to the crystal structures; the results are shown in Tables 5.9 and 5.10.

Table 5.9: Numerical (MC) and theoretical estimates for k_D in the 3-D random system (assuming MPBR-like core dimensions: $X = Y = 58.33\underline{d}$ and $Z = 166.67\underline{d}$).

$k_D^{mc}/(\nu\Sigma_f)$	$k_D^{am}/(\nu\Sigma_f)$	$k_D^{B}/(\nu\Sigma_f)$	$k_D^{L}/(\nu\Sigma_f)$	$k_D^{iso}/(\nu\Sigma_f)$	$k_D^{gt}/(\nu\Sigma_f)$
104.05192	106.38445	105.57956	103.87550	104.06939	104.10957

Table 5.10: Percent differences between theoretical and Monte Carlo estimates for k_D in the 3-D random system (assuming MPBR-like core dimensions).

diff_k^{am}	diff_k^{B}	diff_k^{L}	diff_k^{iso}	diff_k^{gt}
2.24169	1.46815	0.16955	0.01678	0.05540

The differences for the classic atomic mix and the Behrens correction are large, as expected. The generalized theory yields very accurate results; also, k_D^{iso} and k_D^{gt} are very similar, which is not surprising since the anisotropic effect is very small. However, given its poor performance in predicting the diffusion coefficients, the accuracy of the Lieberoth correction in predicting k_D is unexpected, even though it is still more than 0.1% less

accurate than the results obtained with the generalized theory. It turns out that this apparent accuracy comes from a lucky choice of parameters X, Y, and Z in the estimate of k_D.

Table 5.11: Numerical (MC) and theoretical estimates for k_D in the 3-D random system (assuming PBMR-like core dimensions: $X = Y = 61.67\underline{d}$ and $Z = 150\underline{d}$).

$k_D^{mc}/(\nu\Sigma_f)$	$k_D^{am}/(\nu\Sigma_f)$	$k_D^{B}/(\nu\Sigma_f)$	$k_D^{L}/(\nu\Sigma_f)$	$k_D^{iso}/(\nu\Sigma_f)$	$k_D^{gt}/(\nu\Sigma_f)$
107.83624	109.83164	109.04683	107.38308	107.85559	107.8921566

Table 5.12: Percent differences between theoretical and Monte Carlo estimates for k_D in the 3-D random system (assuming PBMR-like core dimensions).

diff_k^{am}	diff_k^{B}	diff_k^{L}	diff_k^{iso}	diff_k^{gt}
1.85040	1.12262	0.42023	0.01794	0.05185

For instance, by slightly changing the core dimensions so that now they resemble those of the PBMR design of a reactor core [36] ($X = Y = 61.67\underline{d}$ and $Z = 150\underline{d}$), diff_k^L increases by about 148.0%, while diff_k^{iso} and diff_k^{gt} change by less than 7.0%. For this choice of parameters, the generalized theory estimates for k_D yield results that are more than 0.4% (and about one order of magnitude) more accurate than the ones obtained with the atomic mix and its corrections (Tables 5.11 and 5.12). In fact, due to their lack of accuracy on estimating the coefficients D, the term $\left(\frac{1}{X^2} + \frac{1}{Y^2} + \frac{1}{Z^2}\right)$ D in the expressions of k_D^{am}, k_D^B, and k_D^L will make them very sensitive to changes in the parameters X, Y, and Z. Another example of this fact can be seen when we use core dimensions resembling those of the HTR-PM design of a reactor core [92] ($X = Y = 66.67\underline{d}$ and $Z = 183.33\underline{d}$); the results of this choice of dimensions are shown in Tables 5.13 and 5.14. Once more, the generalized theory maintains the same excellent level of accuracy, while the accuracy of the atomic mix model and of both the Behrens and the Lieberoth corrections present a large variation.

In this section we have shown that, for 3-D models of pebble-bed reactor cores, the

Table 5.13: Numerical (MC) and theoretical estimates for k_D in the 3-D random system (assuming HTR-PM-like core dimensions: $X = Y = 66.67\underline{d}$ and $Z = 183.33\underline{d}$).

$k_D^{mc}/(\nu\Sigma_f)$	$k_D^{am}/(\nu\Sigma_f)$	$k_D^{B}/(\nu\Sigma_f)$	$k_D^{L}/(\nu\Sigma_f)$	$k_D^{iso}/(\nu\Sigma_f)$	$k_D^{gt}/(\nu\Sigma_f)$
114.93912	116.22541	115.48561	113.91345	114.95596	114.99307

Table 5.14: Percent differences between theoretical and Monte Carlo estimates for k_D in the 3-D random system (assuming HTR-PM-like core dimensions).

diff_k^{am}	diff_k^{B}	diff_k^{L}	diff_k^{iso}	diff_k^{gt}
1.11910	0.47546	0.89236	0.01465	0.04694

atomic mix model and the Behrens correction yield very inaccurate results. The correction proposed by Lieberoth performs a good improvement in the estimates of the diffusion coefficients for the crystal structures, but it fails to do the same in the case of random packings. We have also shown that the proposed generalized theory: (i) is generally more accurate than the atomic mix model and its corrections in crystal structures, and significantly more accurate in random structures; and (ii) successfully reproduces even very small anisotropic effects in the estimates of the diffusion coefficients.

We have also concluded that, in the case of diffusion in the interior of the 3-D system, one should not have to worry about anisotropic diffusion. The anisotropic effect was found to be very small (and inconsistent) for the tested packing fraction, and it is likely to be even smaller for higher packing fractions, as is the accepted case in pebble-beds. Nevertheless, diffusion will be anisotropic for particles that are born in pebbles close to the walls; we discuss this in the next section.

5.4 Boundary Layers of the 3-D Model Core

This section presents an investigation of the anisotropic behavior of particles generated by pebbles that are located close to the boundary walls of a random system, where the packing fraction is (in general) significantly smaller than in the middle of the system.

Due to the effect of the walls on the packing structure, it is only natural to expect that the transport of particles will be affected. We use the Monte Carlo code described in Section 5.1.2 to pack spheres of radius r in a cubic box with side L. An adaptation of the Monte Carlo code presented in Section 5.2.2 is presented in Section 5.4.1, to perform 3-D neutron transport in this heterogeneous structure. We close the section by showing that, to some extent, this anisotropic behavior can be approximated with the generalized theory presented in Chapter III, while atomic mix and its corrections fail to do the same.

5.4.1 Monte Carlo Results in a Boundary of the 3-D System

Once again, the packing of spheres of diameter $\underline{d}$ takes place in a cubic box with side $L = 40\underline{d}$. Here, however, particles are born in a pebble positioned close to a wall, instead of at the center of the system; reflective boundary conditions were used. In this case, the system in which particles travel differs slightly from the one described in Section 5.2.2.

Let us assume that the system with side L in which the pebbles are packed has its center at the origin; in other words, the coordinates of the system satisfy $-L/2 \leq x \leq L/2$, $-L/2 \leq y \leq L/2$, and $-L/2 \leq z \leq L/2$. We focus on the histories of particles that are born in pebbles whose centers have coordinates C_ξ that are a (small) distance ξ away from the wall positioned at the plane $x = -L/2$.

If a particle P traveling with direction $\mathbf{\Omega} = (\Omega_x, \Omega_y, \Omega_z)$ collides against the wall at $x = -L/2$, it will be reflected into the system with direction $\mathbf{\Omega}' = (-\Omega_x, \Omega_y, \Omega_z)$. Apart from this case, however, particles are not allowed to travel within a distance $\omega = 3\underline{d}$ to the other walls; the "reinsertion and shifting" procedure described in Section 5.2.2 is applied. In other words, particles are now travelling in a semi-infinite "quasi-periodic" structure, with a (left) boundary at the plane $x = -L/2$.

Since the packing fraction close to the boundary walls is smaller than in the interior of the system, we predict that particles will travel smaller distances in the direction normal to

Table 5.15: MC results for particles born in pebbles centered at a distance ξ from the boundary wall.

$\xi/\underline{d}$	$\overline{s}/\underline{d}$	$\overline{s^2}/\underline{d}^2$	$\overline{\rho}/\underline{d}$	$\overline{\rho^2}/\underline{d}^2$	$\overline{y^2}/\overline{x^2}$	$\overline{z^2}/\overline{x^2}$
Results for the 3-D Random Packing Structure P-I						
0.5	1.78545	6.97070	21.36191	690.71789	1.02877	1.02343
≈1.5	1.78253	6.94344	21.33145	689.81624	1.02088	1.01877
≈2.5	1.78028	6.92283	21.31240	690.38114	1.02586	1.02151
≈3.5	1.77874	6.91236	21.32874	689.59039	1.03422	1.02169
≈4.5	1.77776	6.90049	21.29395	691.20843	1.01422	1.00291
≈5.5	1.77645	6.88687	21.29016	691.97071	1.00838	1.00172
Results for the 3-D Random Packing Structure P-II						
0.5	1.78124	6.93019	21.36768	690.31560	1.03969	1.03792
≈1.5	1.77973	6.91639	21.34016	691.97697	1.04399	1.03692
≈2.5	1.77562	6.88624	21.24827	687.14057	1.01676	1.02763
≈3.5	1.77191	6.85770	21.20520	684.18691	1.01017	0.99079
≈4.5	1.77265	6.86074	21.19400	684.01374	1.00388	1.00752
≈5.5	1.77107	6.84641	21.18157	684.65500	0.99773	0.99802
Results for the 3-D Random Packing Structure P-III						
0.5	1.78863	6.99390	21.49490	701.01234	1.00103	1.02955
≈1.5	1.78437	6.96283	21.35406	690.49666	1.01902	1.02471
≈2.5	1.78205	6.93889	21.29538	687.13363	0.99899	1.00639
≈3.5	1.78063	6.92687	21.25170	685.45438	0.99803	1.00607
≈4.5	1.77847	6.90744	21.26572	690.03643	0.99468	1.00722
≈5.5	1.77722	6.89719	21.28677	691.51940	0.98344	1.00643

the wall. That is, for the semi-infinite system we are simulating, we expect that $\overline{x^2}$ will be consistently smaller than both $\overline{y^2}$ and $\overline{z^2}$ (similarly, we expect $\overline{x}$ to be smaller than $\overline{y}$ and $\overline{z}$).

We have investigated a total of 18 cases: for six different choices of ξ, we examined the behavior of particles being born in pebbles with centers C_ξ in three different random packing structures (P-I, P-II, and P-III). The histories of 100,000 particles were simulated in each of these cases; Table 5.15 presents the Monte Carlo results for $\overline{s}$ and $\overline{s^2}$.

We must bear in mind that we are now working with a problem in which the diffusion coefficients depend on space; therefore, the derivation of the expressions in Eqs. (2.53) can no longer be performed. However, Eqs. (2.53) are exact expressions when diffusion is

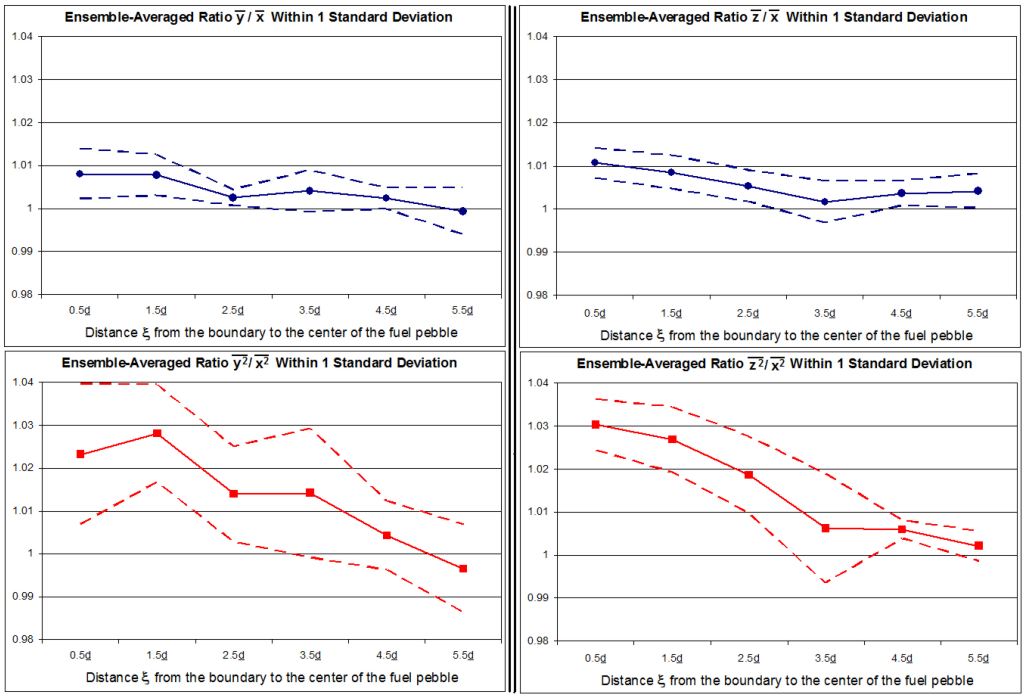

Figure 5.19: Ensemble-Averages (within 1 Standard Deviation) of the Ratios for Mean and Mean Square Distances to Point of Birth of Particles Born in a Pebble with Center C_ξ

independent of space; this indicates that the mean square distances of particles from their point of birth play an important role in the values of the diffusion coefficients. For this reason, Table 5.15 also shows the results for $\overline{\rho^2}$ and for the ratios $\overline{y^2}/\overline{x^2}$ and $\overline{z^2}/\overline{x^2}$, where we can clearly observe the predicted anisotropic effect. In each of the 18 cases simulated, the statistical error was found to be (with 95% confidence) less than 0.069% for all values of $\overline{s}$, $\overline{x}$, $\overline{y}$, and $\overline{z}$; and less than 0.159% for all values of $\overline{s^2}$, $\overline{x^2}$, $\overline{y^2}$, and $\overline{z^2}$.

The ensemble-averaged values for the ratios $\overline{y}/\overline{x}$, $\overline{z}/\overline{x}$, $\overline{y^2}/\overline{x^2}$, and $\overline{z^2}/\overline{x^2}$ are depicted in Figure 5.19. The most remarkable feature observed is that, as predicted, particles born in pebbles positioned close to the wall have mean square migration distances in the x-direction (normal to the wall) that are about 3% smaller than in the other directions.

5.4.2 Theoretical Estimates in a Boundary of the 3-D System

We can use the numerical values for $\overline{s}$, $\overline{s^2}$, $\overline{s_{\Omega}}$, and $\overline{s_{\Omega}^2}$ to obtain estimates for D^{iso}, D_x^{gt}, D_y^{gt}, and D_z^{gt}. As we mentioned, Eqs. (2.53) are not accurate anymore; nevertheless, we will use them to obtain the following approximations:

$$\overline{\rho_{gt}^2} \approx \frac{2}{\Sigma_a^{mc}}(\mathrm{D}_x^{gt} + \mathrm{D}_y^{gt} + \mathrm{D}_z^{gt}) = \frac{2}{\Sigma_a^{mc}}(3\mathrm{D}^{iso})\,, \tag{5.16a}$$

$$\frac{\overline{y_{gt}^2}}{\overline{x_{gt}^2}} \approx \frac{\mathrm{D}_y^{gt}}{\mathrm{D}_x^{gt}}\,, \tag{5.16b}$$

$$\frac{\overline{z_{gt}^2}}{\overline{x_{gt}^2}} \approx \frac{\mathrm{D}_z^{gt}}{\mathrm{D}_x^{gt}}\,. \tag{5.16c}$$

For the values of $\overline{\rho^2}$ shown in Table 5.15, we define the percent difference between the generalized theory and the Monte Carlo estimates as:

$$\mathrm{diff}_{\rho}^{gt} = 100\frac{|\overline{\rho_{gt}^2} - \overline{\rho^2}|}{\overline{\rho^2}}\,. \tag{5.17}$$

The results and comparisons can be seen in Table 5.16.

Table 5.16: Generalized theory approximations for the behavior of particles born in pebbles centered at a distance ξ from the boundary wall; comparisons with MC results are shown.

$\xi/\underline{d}$	$\frac{\overline{\rho_{gt}^2}}{\underline{d}^2}$	$\mathrm{diff}_{\rho}^{gt}$	$\frac{\overline{y_{gt}^2}}{\overline{x_{gt}^2}}$	$\frac{\overline{y_{gt}^2}}{\overline{x_{gt}^2}} - \frac{\overline{y^2}}{\overline{x^2}}$	$\frac{\overline{z_{gt}^2}}{\overline{x_{gt}^2}}$	$\frac{\overline{z_{gt}^2}}{\overline{x_{gt}^2}} - \frac{\overline{z^2}}{\overline{x^2}}$
0.5	696.49308	0.35702	1.02551	0.00234	1.02831	-0.00199
≈1.5	694.08863	0.48140	1.02674	-0.00122	1.02479	-0.00202
≈2.5	691.59869	0.49119	1.01143	-0.00244	1.01496	-0.00355
≈3.5	689.89783	0.50804	1.01311	-0.00103	1.00932	0.00314
≈4.5	688.95554	0.07786	1.00304	-0.00122	1.00325	-0.00264
≈5.5	687.68201	0.24655	0.99563	-0.00088	1.00272	0.00066

Even though we are making use of Eqs. (2.53) as an approximation, we can see that the generalized theory yields very accurate predictions of $\overline{\rho^2}$. Even more remarkable is the accuracy obtained in the prediction of the anisotropic behavior, as can be seen from the small differences it yields when compared with the Monte Carlo estimates of the ratios of the mean square migration distances of particles.

It is not clear if a similar procedure can be used with atomic mix; nevertheless, while such a procedure would not yield an anisotropic result, it might be able to approximate $\overline{\rho^2}$. The underlining question is: what value should be chosen for the average packing fraction? There is a sharp transition in the packing fraction as one moves away from the wall; within a distance of three diameters from the wall, the average packing fraction varies from 0.49626 near the wall to 0.59527 in the interior of the system (it remains very close to 0.59527 for distances larger than three diameters). This agrees with the results obtained in [71], in which the results of a high-fidelity method found that the packing fraction varies from 0.5 to 0.6 near the boundary regions of a cylindrical pebble-bed model core .

We calculate the estimate for the atomic mix diffusion coefficient D_i^{am} for three different packing fractions Γ_i, namely: the lowest found value $\Gamma_1 = 0.49626$, an intermediary value $\Gamma_2 = 0.54577$, and the average packing fraction $\Gamma_3 = 0.59527$, obtained away from the wall. We use the approximation

$$\overline{\rho^2}_i^{am} \approx \frac{2}{\Gamma_i \Sigma_a}(3\mathrm{D}_i^{am}) \tag{5.18}$$

and define the percent differences between this estimate and the Monte Carlo values as:

$$\mathrm{diff}_\rho^{am}(i) = 100\frac{|\overline{\rho^2}_i^{am} - \overline{\rho^2}|}{\overline{\rho^2}}\,. \tag{5.19}$$

The results obtained with these approximations are shown in Table 5.17. We can see that,

Table 5.17: Percent differences between MC results and atomic mix approximations for $\overline{\rho^2}$ (the mean square distance of a particle to its point of birth) of particles born in pebbles centered at a distance ξ from the boundary wall.

$\xi/\underline{d}$	0.5	≈1.5	≈2.5	≈3.5	≈4.5	≈5.5
$\mathrm{diff}_\rho^{am}(1)$	17.01374	17.56462	17.99933	18.31013	17.96487	17.80023
$\mathrm{diff}_\rho^{am}(2)$	3.25208	2.79661	2.43718	2.18021	2.46567	2.60180
$\mathrm{diff}_\rho^{am}(3)$	18.67333	18.29046	17.98832	17.77232	18.01228	18.12671

in this case, atomic mix seems to work best when we choose an intermediary packing

fraction, between the minimum value found near the wall and the average value found in the interior of the system. Nonetheless, even in this case its accuracy fails to match the accuracy demonstrated by the generalized theory for this problem. Moreover, the theory behind the corrections for the atomic mix model do not apply in this case; in fact, they yield meaningless results, even more inaccurate than the ones obtained with the classic atomic mix.

Obviously, a convenient choice for Γ will improve the accuracy obtained with this model. Given $\overline{\rho^2}$, we can even calculate the best choice by solving Eq. (5.18) for Γ - but this would ruin the purpose of the problem, which is to estimate $\overline{\rho^2}$. In actuality, for this type of problem, there is not an available procedure to make this choice in a nonartificial way; in practice, the value $\Gamma_3 = 0.59527$ would be chosen.

We have shown that, for 3-D models of pebble-bed reactor cores, there exists an anisotropic effect near the walls of the system; this effect will cause particles that are born close to a boundary wall to travel smaller distances in the direction normal to this wall. We have also shown that, although we cannot use the generalized theory to find an exact expression of the migration distances of particles, we can still get accurate predictions of the anisotropic effect. Moreover, both versions of the generalized theory (isotropic and anisotropic) yield very accurate predictions of $\overline{\rho^2}$, the mean square distance of particles to their points of birth. Finally, we have discussed that a similar (but inaccurate) process can be performed with the atomic mix model; however, it will require an artificial choice for the value of the packing fraction of the structure.

In this chapter, we have calculated (using Monte Carlo) the "true" values of the diffusion coefficients for different 3-D models of pebble-bed reactor cores. We have shown that, when compared to these values, the generalized theory is significantly more accurate than the atomic mix model and the results obtained with the Behrens correction. In crystal

structures, the generalized theory yields better accuracy than the correction proposed by Lieberoth (in general), but not by large amounts. However, for 3-D random structures, the estimates for the diffusion coefficients obtained by the generalized theory are more than 20 times more accurate than the estimates yielded by the Lieberoth correction. Once more, the generalized theory successfully reproduces even very small anisotropic effects in the estimates of the diffusion coefficients.

Estimates of the diffusion eigenvalue k_D show that the generalized theory is significantly more accurate than the atomic mix approach and its correction models. As we discussed in the last chapter, it is reasonable to expect that the difference between the accuracy of these methods in estimating k_D will translate to the estimation of k, the actual eigenvalue of the heterogeneous transport problem.

CHAPTER VI

Conclusions

Due to the rising costs of fossil fuels (and the environmental impact induced by them), a worldwide effort is underway to develop more economical, efficient, and clean ways of generating electricity. This effort has driven the current "nuclear renaissance", which has the High-Temperature Gas-Cooled Reactor concept as the forefront candidate to a new generation of nuclear plants. In particular, the Pebble-Bed Reactor (PBR) stands out as the most promising design to be pursued, due to its three main features: its several safety advantages over other reactor designs, its high thermal efficiency (45%-50%), and its capability of attaining high temperatures useful for hydrogen production. Unfortunately, due to the high complexity of its heterogeneous dynamic design, the understanding of neutron behavior inside its core is far from that of more conventional reactors.

The behavior of neutrons inside the PBR core is generally modeled by a diffusion approximation. In practice, this approximation uses spatially-homogenized cross sections, obtained by volume-averaging over the constituent materials, weighted by their respective volume fractions. Once this (atomic mix) procedure is completed, mathematical corrections can be applied to the diffusion coefficients to reduce the error produced by the "neutron streaming" effect; this effect is produced by the optically thin, helium-filled portions of the core. The main advantage of this method is in its simplicity: the only information

needed to apply it is the values of the cross sections and the volume fractions of each material in the core.

There are several difficulties with this approach. This method inherently assumes that the probability distribution function for distance-to-collision is exponential; we show that, due to the neutron streaming effect outside the pebbles, this assumption is not valid. Moreover, the accuracy of the atomic mix model is linked to the mean size of each "chunk" of the system's constituent materials; the smaller each chunk is compared to a mean free path, the more accurate is the atomic mix approximation. However, the pebbles are O(1) mean free paths thick; this is *not* considered small, and therefore the accuracy of this model must be called into question.

In this work, we present a new approach called *generalized theory*, in which we propose to replace the true nonexponential probability distribution function for the distance-to-collision by its ensemble average. This ensemble-averaged probability distribution function is then used at all points to determine how far particles travel between collisions. This causes the cross sections of the homogenized system to be functions of both angle ($\mathbf{\Omega}$) and distance-to-collision (s); the angular dependence can be dropped by assuming the locations of the scattering centers to be independent of direction.

With this method, we obtain a *generalized Boltzmann equation* that preserves all relevant asymptotic limits, reducing to the classic Boltzmann equation in the case of a homogeneous system. The disadvantage is that there is no simple way to obtain expressions for these s-dependent cross sections; they need to be numerically estimated. Nevertheless, we use this result to develop a *generalized diffusion equation* (GDE), which do not depend upon the variable s, but rather on its mean and mean square values $\overline{s}$ and $\overline{s^2}$. The GDE also preserves all relevant limits, reducing to classic diffusion in homogeneous systems. Moreover, it yields anisotropic diffusion coefficients when the locations of the scattering

centers depend upon direction. More work is required than in the atomic mix approach; to apply the GDE, one must obtain estimates for $\overline{s}$ and $\overline{s^2}$. This information is all microscopic in nature, and a simple Monte Carlo code can generate accurate estimates.

We initially developed a Monte Carlo code to simulate the transport of neutrons inside model 2-D PBR cores. Different versions of these model cores were created: crystal packings were sequentially built, and a version of the ballistic deposition algorithm was developed to generate random realizations. Overall, when compared to the Monte Carlo results, we have shown that the generalized theory yields more accurate results for the diffusion coefficients than the atomic mix approach, and even the small anisotropic effects detected in these simulations were successfully predicted. Furthermore, for the case of random structures, we showed that these small differences in the diffusion coefficients yield differences on the order of 0.4% in the estimates of the k_D eigenvalue (assuming core dimensions comparable to those of the MPBR design). As we have mentioned, k plays an important role in the nuclear chain reaction, and errors on the order of 0.1% in its estimate are significant.

With the promising 2-D results, we proceeded to work on the 3-D case, where packing fractions are smaller (which increases the neutron streaming effect). We adapted our Monte Carlo code to simulate transport in these 3-D systems, and we used both crystal (face-centered) and random structures. The random structures were generated using a more complex ballistic algorithm to build random packings of ≈71,000 spheres, which were then extended to an infinite system in a "quasi-periodic" fashion. When compared to the Monte Carlo results, we have shown that both atomic mix and the correction proposed by Behrens generally fail to estimate the diffusion coefficients in a reasonable way; nevertheless, for crystal structures, the correction proposed by Lieberoth yields results that are comparable in accuracy to those obtained with the generalized theory. However, for

3-D random structures, the diffusion coefficients obtained with the correction proposed by Lieberoth differ from those obtained with Monte Carlo by ≈7.0%, while the generalized theory yields results that are less than 0.3% apart from the Monte Carlo results.

This difference in the estimates of the diffusion coefficients has a significant impact in the estimates of the k_D eigenvalue. When compared to Monte Carlo, the generalized theory estimates of k_D are very accurate for any reasonable choice of the core dimensions, while the estimates obtained with the Lieberoth correction are very sensitive to changes in these dimensions. Assuming different core dimensions, the difference between the Monte Carlo and the generalized theory estimates of k_D remained below 0.056%. On the other hand, the difference between the Lieberoth correction and the Monte Carlo estimates jumped from 0.17% (for the MPBR-like dimensions) to 0.42% (for the PBMR-like dimensions) and to 0.89% (for the HTR-PM-like dimensions).

We finished the 3-D study with an investigation of the behavior of particles that are born close to the walls of the core; specifically, we focused on the mean square distances of a particle to its point of birth. We found that there is a clear anisotropic effect, which was expected due to the fundamental differences between the packing structures in the interior of the system and close to the walls. The generalized theory yields very good predictions for this anisotropic effect, even though we made use of a mathematically innacurate expression to obtain these approximations. On the other hand, we discussed that using the atomic mix model in a similar approach would only yield meaningful results under an artificial choice of packing fractions, which would be meaningless for practical purposes. In future work, we intend to develop accurate numerical space-dependent diffusion coefficients for particles born close to the wall, in order to (i) test the accuracy of the generalized theory in predicting space-dependent diffusion coefficients in these regions, and (ii) analyzing the global effect caused by this anisotropic effect.

It is important to remark that none of our assumptions restrain the generalized theory introduced in this work to applications in reactor cores. In fact, we know of at least one other important application: it has recently been shown that the locations of the scattering centers (water droplets) in clouds are correlated in ways that measurably affect radiative transfer within the cloud [11, 14, 22, 37, 38, 39, 62, 72]. In such cases, if one models the cloud by taking the water droplets to be randomly-positioned scattering centers, then the positions of the scattering centers are correlated, and the theory developed here would apply.

To summarize, we have proposed a new theory to model particle transport in stochastic heterogeneous media. This theory requires more information about a random system than the atomic mix method; if a random system is diffusive, then only $\overline{s}$ and $\overline{s^2}$ need to be estimated (for anisotropic diffusion, they will depend on $\mathbf{\Omega}$). This extra information is all microscopic in nature; it is not a closure relation, as in the Levermore-Pomraning method [63, 85]. The theory uses this microscopic data in a generalized Boltzmann equation or in a generalized diffusion equation to determine approximate mean macroscopic quantities. We have numerically shown that, at least for problems of the pebble-bed kind, this new approach is significantly more accurate than the classic approaches currently in use.

In the future, we intend to extend the present work for problems with anisotropic scattering, as well as for energy-dependent systems. Although it is computationally expensive, the algorithm to obtain $\Sigma_t(\mathbf{\Omega}, s)$ is straightforward; we intend to use it to generate results that can be applied to the generalized Boltzmann equation in order to estimate k. Monte Carlo benchmark results for k in this heterogeneous system will need to be developed; we also intend to do this. Finally, having developed a theory for the mean flux of particles, the next logical step from the theoretical point of view is to try to develop a similar theory that is capable of calculating variance; this is one of our goals.

BIBLIOGRAPHY

BIBLIOGRAPHY

[1] Adams, M.L., Larsen, E.W., and Pomraning, G.C. *Benchmark Results for Particle Transport in a Binary Markov Statistical Medium.* J. Quant. Spectrosc. Radiat. Transfer **42**, 253 (1989).

[2] Arfken, G. *Mathematical Methods for Physicists.* Academic Press, Orlando, 1985.

[3] Audic, S. and Frisch, H. *Monte Carlo Simulation of a Radiative Transfer Problem in a Random Medium - Application to a Binary Mixture.* J. Quant. Spectrosc. Radiat. Transfer **50**, 127 (1993).

[4] Bedenig, D. *Probleme des Kugelhaufens und Körniger Schüttungen.* Proc. THTR Symposium. Jülich, Germany (1968).

[5] Behrens, D.J. *The Effect of Holes in a Reacting Material on the Passage of Neutrons.* Proc. Phys. Soc. A **62**, 607 (1949).

[6] Bennett, C.H. *Serially Deposited Amorphous Aggregates of Hard Spheres.* J. Appl. Phys. **43**, 2727 (1972).

[7] Bernnat, W. and Feltes, W. *Models for Reactor Physics Calculations for HTR Pebble-Bed modular Reactors.* Nucl. Eng. Design **222**, 331 (2003).

[8] Billingsley, P. *Probability and Measure.* John Wiley & Sons, New York, 1995.

[9] Boisse, P. *Radiative Transfer Inside Clumpy Media - The Penetration of UV Photons Inside Molecular Clouds.* Astronomy & Astrophysics **228**, 483 (1990).

[10] Boltzmann, L. *Weitere Studien über Wärmegleichgewicht unter Gasmolekülen.* Wiener Berichte **66**, 275 (1872).

[11] Borovoi, A. *On the Extinction of Radiation by a Homogeneous but Spatially Correlated Random Medium: Comment.* J. Opt. Soc. Am. A **19**, 2517 (2002).

[12] Brantley, P.S. *A Comparison of Monte Carlo Particle Transport Algorithms for binary Stochastic Media.* International Conference on Advances in Mathematics, Computational Methods, and Reactor Physics. Saratoga, United States of America (2009).

[13] Brantley, P.S. and Palmer, T.S. *Levermore-Pomraning Model Results for an Interior Source Binary Stochastic Medium Benchmark Problem.* International Conference on Advances in Mathematics, Computational Methods, and Reactor Physics. Saratoga, United States of America (2009).

[14] Buldyrev, S.V., Havlin, S., Kazakov, A.Ya., da Luz, M.G.E., Raposo, E.P., Stanley, H.E., and Viswanathan, G.M. *Average Time Spent by Levy Flights and Walks on an Interval with Absorbing Boundaries.* Phys. Rev. E **64**, 041108 (2001).

[15] Case, K.M., DeHoffmann, F., and Placzek, G. *Introduction to the Theory of Neutron Diffusion.* U.S. Government Printing Office, Washington, 1953.

[16] Case, K.M. and Zweifel, P.F. *Linear Tranport Theory.* Addison-Wesley, Massachusetts, 1967.

[17] Cecchi-Pestellini, C., Barletti, L., Bellini-Morante, A., and Aiello, S. *Radiative Transfer in the Stochastic Interstellar Medium.* Transport Th. Statist. Phys. **28**, 199 (1999).

[18] Cogliati, J.J. and Ougouag, A.M. *Pebbles: A Computer Code for Modeling Packing, Flow, and Re-Circulation of Pebbles in a Pebble Bed Reactor.* 3rd International Topical Meeting on High Temperature Reactor Technology. Johannesburg, South Africa (2006).

[19] Conway, J.H. and Sloane, N.J.H. *Sphere Packings, Lattices and Groups.* Springer-Verlag, New York, 1998.

[20] Davis, A.B. *Effective Propagation Kernels in Structured Media with Broad Spatial Correlations, Illustration with Large-Scale Transport of Solar Photons Through Cloudy Atmospheres;* **in** *Computational Methods in Transport.* Springer, New York, 2004.

[21] Davis, A.B., Polonsky, I.N., and Marshak, A. *Space-Time Green Functions for Diffusive Radiation Transport, in Application to Active and Passive Cloud Probing;* **in** *Light Scattering Reviews (Vol. 4).* Springer-Verlag, Heidelberg, 2009.

[22] Davis, A.B. and Marshak, A. *Photon Propagation in Heterogeneous Optical Media with Spatial Correlations: Enhanced Mean-Free-Paths and Wider-Than-Exponential Free-Path Distributions.* J. Quant. Spectrosc. Radiat. Transfer **84**, 3 (2004).

[23] Davis, A.B. and Mineev-Weinstein, M. *Radiation Transport Through Random Media Represented as Measurable Functions: Positive versus Negative Spatial Correlations.* International Conference on Advances in Mathematics, Computational Methods, and Reactor Physics. Saratoga, United States of America (2009).

[24] Davis, I.M., Palmer, T.S., and Larsen, E.W. *A Comparison of Binary Stochastic Media Transport Models in "Solid-Void" Mixtures.* PHYSOR 2004 - The Physics of Fuel Cycles and Advance Nuclear Systems: Global Developments. Chicago, United States of America (2004).

[25] Duderstadt, J.J. and Hamilton, L.J. *Nuclear Reactor Analysis.* John Wiley & Sons, New York, 1976.

[26] Duderstadt, J.J. and Martin, W.R. *Transport Theory.* Wiley-Interscience, New York, 1979.

[27] Dumas, L. and Golse, F. *Homogenization of Transport Equations.* SIAM J. Appl. Math. **60**, 1447 (2000).

[28] El-Wakil, M-M. *Nuclear Energy Conversion.* International Textbook Company, American Nuclear Society, 1982.

[29] Gerwin, H. and Scherer, W. *Treatment of the Upper Cavity in a Pebble-Bed High-Temperature Gas-Cooled Reactor by Diffusion Theory.* Nucl. Sci. Eng. **97**, 9 (1987).

[30] Grimmett, G. and Stirzaker, D. *Probability and Random Processes.* Oxford University Press, Oxford, 2001.

[31] Habetler, G.J. and Matkowsky, B.J. *Uniform Asymptotic Expansions in Transport Theory with Small Mean Free Paths, and the Diffusion Approximation.* J. Math. Phys. **16**, 846 (1975).

[32] Hales, T.C., et al. *Multiple papers on the proof of Kepler's conjecture.*
See
http://sites.google.com/site/thalespitt/ **and** http://code.google.com/p/flyspeck/.

[33] Jullien, R. and Meakin, P. *Simple Three-Dimensional Models for Ballistic Deposition with Restructuring.* Europhys. Lett. **4**, 1385 (1987).

[34] Jullien, R., Pavlovitch,A., and Meakin, P. *Random Packings of Spheres Built with Sequential Models.* J. Phys. A: Math. Gen. **25**, 4103 (1992).

[35] Kadak, A.C. *MIT Pebble-Bed Reactor Project.* Nucl. Eng. Tech. **39**, 95 (2007).

[36] Koster, A., Matzner, H.D., and Nicholsi, D.R. *PBMR Design for the Future.* Nucl. Eng. Design **222**, 231 (2003).

[37] Kostinski, A.B. and Shaw, R.A. *Scale-Dependent Droplet Clustering in Turbulent Clouds.* J. Fluid Mech. **434**, 389 (2001).

[38] Kostinski, A.B. *On the Extinction of Radiation by a Homogeneous but Spatially Correlated Random Medium.* J. Opt. Soc. Am. A **18**, 1929 (2001).

[39] Kostinski, A.B. *On the Extinction of Radiation by a Homogeneous but Spatially Correlated Random Medium: Reply to Comment.* J. Opt. Soc. Am. A **19**, 2521 (2002).

[40] Lamarsh, J.R. *Introduction to Nuclear Reactor Theory.* Addison-Wesley, Massachusetts, 1966.

[41] Larsen, E.W., Morel, J.E., and McGhee, J.M. *Asymptotic Derivation of the Multigroup P_1 and Simplified P_N Equations with Anisotropic Scattering.* Nucl. Sci. Eng. **123**, 328 (1996).

[42] Larsen, E.W. and Keller, J.B. *Asymptotic Solution of Neutron Transport Problems for Small Mean Free Paths.* J. Math. Phys. **15**, 75 (1974).

[43] Larsen, E.W. *Diffusion Theory as an Asymptotic Limit of Transport Theory for Nearly Critical Systems with Small Mean Free Paths.* Ann. Nucl. Energy **7**, 249 (1980).

[44] Larsen, E.W., Vasques, R., and Vilhena, M.T. *Particle Transport in the 1-D Diffusive Atomic Mix Limit.* International Topical Meeting on Mathematics and Computation, Supercomputing, Reactor Physics and Nuclear and Biological Applications. Avignon, France (2005).

[45] Larsen, E.W. *A Generalized Boltzmann Equation for "Non-classical" Particle Transport.* Joint International Topical Meeting on Mathematics & Computation and Supercomputing in Nuclear Applications. Monterey, United States of America (2007).

[46] Larsen, E.W. *Why is a Pebble Bed Reactor Like a Cloud?.* Seminar given at Texas A&M University. College Station, Texas, United States of America (2008).

[47] Lewis, E.E. and Miller, Jr., W.F. *Computational Methods of Neutron Transport.* American Nuclear Society, La Grange Park, 1993.

[48] Lieberoth, J. and Stojadinović, A. *Neutron Streaming in Pebble Beds.* Nucl. Sci. Eng. **76**, 336 (1980).

[49] Malvagi, F., Byrne, R.N., Pomraning, G.C., and Somerville, R.C.J. *Stochastic Radiative Transfer in a Partially Cloudy Atmosphere.* J. Atmos. Sci. **50**, 2126 (1993).

[50] Malvagi, F. and Pomraning, G.C. *Stochastic Atmospheric Radiative Transfer.* Atmos. Ocean Optics **6**, 610 (1993).

[51] Mathews, D., Thibulsky, V., and Chawla, R. *Anisotropic Diffusion Effects in Deterministic Pebble-Bed Lattices.* Trans. Am. Nucl. Soc. **68**, 20 (1993).

[52] Maxwell, J.C. *Illustrations of the Dynamical Theory of Gases.* Phil. Mag. **[4]**: **19**, 19 and **20**, 21 (1860).

[53] Meakin, P. and Jullien, R. *Simulation of Small Particle Penetration in a Random Medium* J. Phys. **51**, 2673 (1990).

[54] Meakin, P. and Jullien, R. *Two-Dimensional Defect-Free Random Packing.* Europhys. Lett. **14**, 667 (1991).

[55] Meyer, P.L. *Introductory Probability and Statistical Applications.* Addison-Wesley, Massachusetts, 1965.

[56] Miller, D.S. *A Stochastic Method for Brownian-like Optical Transport Calculations in Anisotropic Biosuspensions and Blood.* J. Math. Phys. **39**, 1534 (1998).

[57] Miller, D.S., Graziani, F., and Rodrigue, G. *Benchmark and Models for Time-Dependent Grey Radiation Transport with Material Temperature in Binary Stochastic Media.* J. Quant. Spectrosc. Radiat. Transfer **70**, 115 (2001).

[58] Neef, R. D. *Ausbreitung von Neutronenwellen in statistischen Schüttungen von kugelförmigen Elementen.* **JÜL-1273**, Kernforschungszentrum, Jlich (1974).

[59] Ougouag, A.M. and Terry, W.K. *A Preliminary Study Of The Effect Of Shifts In Packing Fraction On K-Effective In Pebble-Bed Reactors.* International Meeting on Mathematical Methods for Nuclear Applications. Salt Lake City, United States of America (2001).

[60] Ougouag, A.M., Cogliati, J.J., and Kloosterman, J-L. *Methods for modeling the Packing of Fuel Elements in Pebble Bed Reactors.* International Topical Meeting on Mathematics and Computation, Supercomputing, Reactor Physics and Nuclear and Biological Applications. Avignon, France (2005).

[61] Ougouag, A.M., Ortensi, J., and Hiruta, H. *Analysis of an Earthquake-Initiated-Transient in a PBR.* International Conference on Advances in Mathematics, Computational Methods, and Reactor Physics. Saratoga, United States of America (2009).

[62] Pfeilsticker, K. *First Geometrical Path Length Probability Density Function Derivation of the Skylight from High Resolution Oxygen A-Band Spectroscopy. 2. Derivation of the Levy Index for the Skylight Transmitted by Midlatitude Clouds.* J. Geophysical Research **104**, 4101 (1999).

[63] Pomraning, G.C. *Linear Kinetic Theory and Particle Transport in Stochastic Mixtures.* World Scientific Press, Singapore, 1991.

[64] Pomraning, G.C. *The Effect of Random Material Density on Reactor Criticality.* Nucl. Sci. Eng. **108**, 325 (1991).

[65] Pomraning, G.C. and Prinja, A.K. *On the Propagation of a Charged Particle Beam in a Random Medium. II: Discrete Binary Statistics.* Transport Th. Statist. Phys. **24**, 565 (1995).

[66] Pomraning, G.C. *Small Correlation Length Solutions for Planar Symmetry Beam Transport in a Stochastic Medium.* Ann. Nucl. Energy **23**, 843 (1996).

[67] Pomraning, G.C. *Effective Radiative Transfer Properties for Partially Cloudy Atmospheres.* Atmos. Ocean Optics **9**, 7 (1996).

[68] Pomraning, G.C. *The Planar Symmetry Beam Problem in Stochastic Media.* J. Quant. Spectrosc. Radiat. Transfer **55**, 771 (1996).

[69] Prinja, A.K. *Pencil Beam Transport in a Random Medium Using the Fermi Transport Equation.* Transport Th. Statist. Phys. **27**, 667 (1998).

[70] Rycroft, C.H., Bazant, M.Z., Landry, J.W., and Grest, G.S. *Dynamics of Random Packings in Granular Flow.* Phys. Rev. E **73**, 051306 (2006).

[71] Rycroft, C.H., Grest, G.S., Landry, J.W., and Bazant, M.Z. *Analysis of Granular Flow in a Pebble-Bed Nuclear Reactor.* Phys. Rev. E **74**, 021306 (2006).

[72] Shaw, R.A., Kostinski, A.B., and Lanterman, D.D. *Super-Exponential Extinction of Radiation in a Negatively Correlated Random Medium.* J. Quant. Spectrosc. Radiat. Transfer **75**, 13 (2002).

[73] Scherer, W., Gerwin, H., and Neef, R.D. *Theoretische Analyse des Kritischen HTR-Experiments KAHTER.* **JÜL-1136-RG**, Kernforschungszentrum, Jlich (1974).

[74] Song, C., Wang, P., and Makse H.A. *A Phase Diagram for Jammed Matter.* Nature **453**, 629 (2008).

[75] Stephens, G.L., Gabriel, P.M., and Tsay, S-C. *Statistical Radiative Transport in One-Dimensional Media and its Application to the Terrestrial Atmosphere.* Transport Th. Statist. Phys. **20**, 139 (1991).

[76] Strieder, W.C. and Prager, S. *Knudsen Flow through a Porous Medium.* Phys. Fluids **11**, 2544 (1968).

[77] Su, B. and Pomraning, G.C. *Benchmark Results for Particle Transport in Binary Non-Markovian Mixtures.* J. Quant. Spectrosc. Radiat. Transfer **50**, 211 (1993).

[78] Su, B. and Pomraning, G.C. *A Stochastic Description of a Broken Cloud Field.* J. Atmos. Sci. **51**, 1969 (1994).

[79] Su, B. and Pomraning, G.C. *The Fermi-Eyges Beam Analysis for a Heterogeneous Absorbing Stochastic Medium.* Ann. Nucl. Energy **23**, 1153 (1996).

[80] Szpiro, G.G. *Kepler's Conjecture.* John Wiley & Sons, New York, 2003.

[81] Titov, G.A. *Statistical Description of Radiation Transfer in Clouds.* J. Atmos. Sci. **47**, 24 (1990).

[82] Torquato, S. *Random Heterogeneous Materials: Microstructure and Macroscopic Properties.* Springer-Verlag, New York, 2002.

[83] Torquato, S., Truskett, T.M., and Debenedetti, P.G. *Is Random Close Packing of Spheres Well Defined?* Phys. Rev. Lett. **84**, 2064 (2000).

[84] Vasques, R., Vilhena, M.T., Thompson, M., and Larsen, E.W. *State of Art of Particle Transport Theory in Stochastic Media.* XXV Iberian Latin American Congress on Computational Methods in Engineering. Recife, Brazil (2004).

[85] Vasques, R. *A Review of Particle Transport Theory in a Binary Stochastic Medium.* Masters Thesis - PPGMAp/Universidade Federal do Rio Grande do Sul. Porto Alegre, Brazil (2005).

[86] Vasques, R. and Larsen, E.W. *Anisotropic Diffusion in Model 2-D Pebble-Bed Reactor Cores.* International Conference on Advances in Mathematics, Computational Methods, and Reactor Physics. Saratoga, United States of America (2009).

[87] Valentyuk, A.N. and Tsymbarevich, E.G. *Stochastic Propagation of Radiation in the Atmosphere and Ocean.* Atmospheric & Oceanic Phys. **35**, 52 (1999).

[88] Williams, M.M.R. *The Effect of Random Geometry on the Criticality of a Multiplying System.* Ann. Nucl. Energy **27**, 143 (2000).

[89] Williams, M.M.R. *The Effect of Random Geometry on the Criticality of a Multiplying System II: Extension to Resonance Absorption.* Ann. Nucl. Energy **27**, 517 (2000).

[90] Williams, T., Rosselet, M., and Scherer, W. (editors), *Critical Experiments and Reactor Physics Calculations for Low-Enriched High Temperature Gas Cooled Reactors.* **IAEA-TECDOC-1249** (advance eletronic version), Vienna, Austria (2001).

[91] Wu, Z., Lin, D., and Zhong, D. *The Design Features of the HTR-10.* Nucl. Eng. Design **218**, 25 (2002).

[92] Zhang, Z., Wu, Z., Xu, Y., Sun, Y., and Li, F. *Design of Chinese Modular High-Temperature Gas-Cooled Reactor HTR-PM.* 2nd International Topical Meeting on High Temperature Reactor Technology. Beijing, China (2004).

[93] Zuchuat, O., Sanchez, R., Zmijarevic, I., and Malvagi, F. *Transport in Renewal Statistical Media: Benchmarking and Comparisons with Models.* J. Quant. Spectrosc. Radiat. Transfer **51**, 689 (1994).

[94] Zuev, V.E. and Titov, G.A. *Radiative Transfer in Cloud Fields with Random Geometry.* J. Atmos. Sci. **52**, 176 (1995).

[95] From the molecular physics correspondent: *What is Random packing.* Nature **239**, 488 (1972).